Aus dem Institut für Klinische Chemie und Pathobiochemie
der medizinischen Fakultät
der Otto-von-Guericke-Universität Magdeburg

Activated protein C reverses epigenetically sustained $p66^{Shc}$ expression in plaque-associated macrophages in diabetes mellitus

Dissertation

zur Erlangung des Doktorgrades

(Dr. rer. medic.)
Doctor rerum medicarum

an der Medizinischen Fakultät
der Otto-von-Guericke-Universität Magdeburg

vorgelegt von Ihsan-Ur-Rehman Khan Gadi

geb. am 01.01.1981 in Muzaffargarh, Punjab, Pakistan

Magdeburg, 2021

Bibliographical description

Ihsan-Ur-Rehman Khan Gadi; DVM, M.Phil. Activated protein C reverses epigenetically sustained $p66^{Shc}$ expression in plaque-associated macrophages in diabetes

Abstract

Impaired activated protein C (aPC) generation is associated with atherosclerosis and diabetes mellitus. Diabetes-associated atherosclerosis is characterized by the hyperglycaemic memory, e.g. failure of disease improvement despite attenuation of hyperglycaemia. Therapies reversing the hyperglycaemic memory are lacking. Here we demonstrate that hyperglycaemia, but not hyperlipidaemia, induces the redox-regulator $p66^{Shc}$ and reactive oxygen species (ROS) in macrophages. $p66^{Shc}$ expression, ROS generation, and a proatherogenic phenotype are sustained despite restoring normoglycemic conditions. Inhibition of $p66^{Shc}$ abolishes this sustained proatherogenic phenotype, identifying $p66^{Shc}$-dependent ROS in macrophages as a key mechanism conveying the hyperglycaemic memory. The $p66^{Shc}$-associated hyperglycaemic memory can be reversed by aPC *via* protease-activated receptor-1 signalling. aPC reverses glucose-induced CpG hypomethylation within the $p66^{Shc}$ promoter by induction of the DNA methyltransferase-1 (DNMT1). Thus, epigenetically sustained $p66^{Shc}$ expression in plaque-macrophages drives the hyperglycaemic memory, which – however – can be reversed by aPC. This establishes that reversal of the hyperglycaemic memory in diabetic atherosclerosis is feasible.

Keywords: Atherosclerosis, Cardiovascular diseases, Diabetes, aPC, $p66^{Shc}$, ROS, Macrophages

Zusammenfassung

Die Hauptursache für Mortalität und Morbidität bei Diabetespatienten ist die Atherosklerose und die damit verbundenen Komplikationen wie Myokardinfarkt, Schlaganfall und periphere arterielle Verschlusskrankheit. Während der aggressivere Krankheitsverlauf der Atherosklerose bei diabetischen Patienten bekannt ist, bleiben die zugrundeliegenden Mechanismen unklar. Daher fehlen spezifische Ansätze zur Therapie der Atherosklerose bei diabetischen Patienten.

Diabetes-assoziierte Atherosklerose ist gekennzeichnet durch eine Verschleterung der Atherosklerose trotz deutlicher Verbesserung des Blutzuckerspiegels. Dieses Phänomen, welches als hyperglykämisches Gedächtnis bezeichnet wird, - ist für Patienten und Ärzte gleichermaßen enttäuschend.

Es ist uns nun gelungen, einen neuen Mechanismus aufzuklären, der dem hyperglykämischen Gedächtnis zugrunde liegt. Wir konnten nachweisen, dass Makrophagen (Entzündungszellen), die sich in den atherosklerotischen Plaques anreichern, bei Patienten mit Diabetes mellitus vermehrt das Redox-Protein $p66^{Shc}$ exprimieren und daher auch vermehrt reaktive Sauerstoffspezies (ROS, oxidativer Stress) erzeugen. Wichtig ist, dass $p66^{Shc}$ spezifisch in den Makrophagen von diabetischen Mäusen oder Diabetes-Patienten exprimiert wird. Die Expression von $p66^{Shc}$ und damit die Bildung von reaktiven Sauerstoffspezies bleibt auch nach Normalisierung der Blutglukosespiegel hoch. Mechanistisch korrigiert aktiviertes Protein C (aPC) die Glukose-induzierte CpG-Hypomethylierung innerhalb des $p66^{Shc}$-Promotors. Mittels aPC-Behandlung kann *in vivo* in DNMT1-abhängiger Weise die $p66^{Shc}$-Expression, ROS-Erzeugung und IL-6-Expression in Plaques nach Normalisierung des Blutzuckerspiegels normalisiert werden. Somit konnten wir zeigen, dass das hyperglykämische Gedächtnis mit einer epigenetisch anhaltenden $p66^{Shc}$-Expression in Plaque-Makrophagen assoziiert ist, welche durch aPC normalisiert werden kann. Diese Ergebnisse legen nahe, dass eine Umkehrung des hyperglykämischen Gedächtnisses bei diabetischer Atherosklerose möglich ist. Diese Erkenntnisse geben neue Einblicke in ein mögliches Therapiekonzept für Diabetiker mit Atherosklerose legen.

Schlüsselwörter

Atherosklerose, Herz-Kreislauf-Erkrankung, Diabetes, aPC, $p66^{Shc}$, ROS, Makrophage

Contents

Table of Figures

List of tables

List of abbreviations

aPC	activated protein C
ApoE	apolipoprotein E
ADA	american diabetes association
AZA	5-aza-2'-deoxycytidine
BMDM	bone marrow derived macrophages
BSA	bovine serum albumin
CCL-2	C–C motif chemokine ligand 2
cDNA	complementary deoxyribonucleic acid
CD36	cluster of differentiation 36
Cont	control
CVD	cardiovascular disease
Dapa	dapagliflozin
DAPI	4', 6-diamidino-2-phenylindole (fluorescent stain)
ddH_2O	double distilled water
dH_2O	distilled water
DEPC	diethyl pyrocarbonate
DM	diabetes mellitus
DMSO	dimethyl sulfoxide
DNA	deoxyribonucleic acid
DNMT	DNA methyl transferase
$dNTP_s$	deoxy nucleotide triphosphates
EDTA	ethylene diamine tetra acetic acid
EPCR	endothelial cell protein C receptor
FBS	foetal bovine serum
g	gravitational acceleration
GDM	gestational diabetes mellitus
GOT	glutamate-oxaloacetate transaminase
GPT	glutamate pyruvate transaminase
HDL	high density lipoprotein
HFD	high fat diet, western type diet

HG	high glucose
HUVECs	human umbilical vein endothelial cells
H_2O_2	hydrogen peroxide
IL-6	interleukin 6
JMJD2C	Jumonji domain-containing protein 2C
Kb	kilobase(s)
LDL	low density lipoprotein
LMWH	low molecular weight heparin
MnSOD	manganese superoxide dismutase
$MgCl_2$	magnesium chloride
mtDNA	mitochondrial DNA
MO	morpholino
MOMA-2	monocyte/macrophage marker-2
mRNA	messenger ribonucleic acid
MMP	matrix metalloproteinase
NADPH	nicotinamide adenine dinucleotide phosphate
ND	normal diet
NG	normoglycemia
Nitro	nitrotyrosine
NF-κB	nuclear factor kappa B
8-oxo-2dG	8-Oxo-2'-deoxyguanosine
PAR	protease-activated receptor
PARP-1	poly [ADP-ribose] polymerase 1
PBS	phosphate buffered saline
PCR	polymerase chain reaction
PFA	paraformaldehyde
ROS	reactive oxygen specie
rpm	revolutions per minute
RT-PCR	reverse transcription polymerase chain reaction
SDS	sodium dodecyl sulfate
s.e.m.	standard error of the mean
SMC	smooth muscle cells

STE	sodium chloride Tris-HCL EDTA
STZ	streptozotocin
TAT	thrombin anti-thrombin
TBE	tris borate EDTA
TE	tris-HCL EDTA
TM	thrombomodulin
U	units
UV	ultra violet
VCAM-1	vascular cell adhesion molecule 1
W	weeks

1. Introduction

1.1. Diabetes Mellitus (DM)

Globally, the number of people with diabetes mellitus (DM) has increased four-fold in the past three decades, and DM has emerged as the ninth major cause of death [1].

According to a WHO report from 2016, diabetes mellitus accounted for a total of 3.7 million deaths globally. Amongst these, 43% of the deaths were under the age of 70 [2, 3]. This number is estimated to double by 2030 [4].

Diabetes mellitus refers to group of metabolic disorders characterized by chronic hyperglycaemia that over time can leads to serious damage of vital organs including heart, blood vessels, eyes, kidneys, feet's and nerves (Figure 1)[3]. Chronic hyperglycaemia results from defects in insulin secretion, insulin action or both. Abnormalities in carbohydrates, lipids, and protein metabolism results from the defective action of insulin on target tissues. The severity of symptom is due to the type and duration of diabetes mellitus and the quality of blood glucose control and other therapies (e.g. for associated lipid disorders) [5, 6].

1.1.1. Classification of DM

The standard classification of diabetes mellitus as proposed by the American Diabetes Association (ADA) in 1997 as type 1, type 2, other types, and gestational diabetes mellitus (GDM) broad categories are still the most accepted classification and adopted by the ADA [5].

1.1.1.1. Type 1 DM (T1DM)

Diabetes mellitus type 1 (T1DM), is an autoimmune disease where the beta cells of pancreas are slowly destroyed by the body's own immune system and hence insulin production is hampered. Both environmental and genetic factors have been linked with T1DM, however their exact contribution to disease development is still not completely known [7, 8]. Daily insulin therapy with multiple injections is currently the only method of treatment regime for T1DM patients.

1.1.1.2. Type 2 DM (T2DM)

More than 90-95 % of patients with diabetes mellitus are adults and belong to the type 2 diabetes cluster [9]. A sedentary life style and over consumption of unhealthy food increases the incidence of type 2 diabetes already during youth. Obesity is the major reason for insulin resistance which ultimately results in type 2 diabetes [10]. In type 2 diabetic patients insulin resistance increases the demand for insulin in insulin-target tissues. In addition to insulin resistance, the increased demand for insulin cannot be met by the pancreatic β cells due to ensuing defects in the function of these cells [11]. As a result, insulin secretion decreases with the increased demand for insulin over time due to the gradual destruction of β cells (Figure 2)[12, 13].

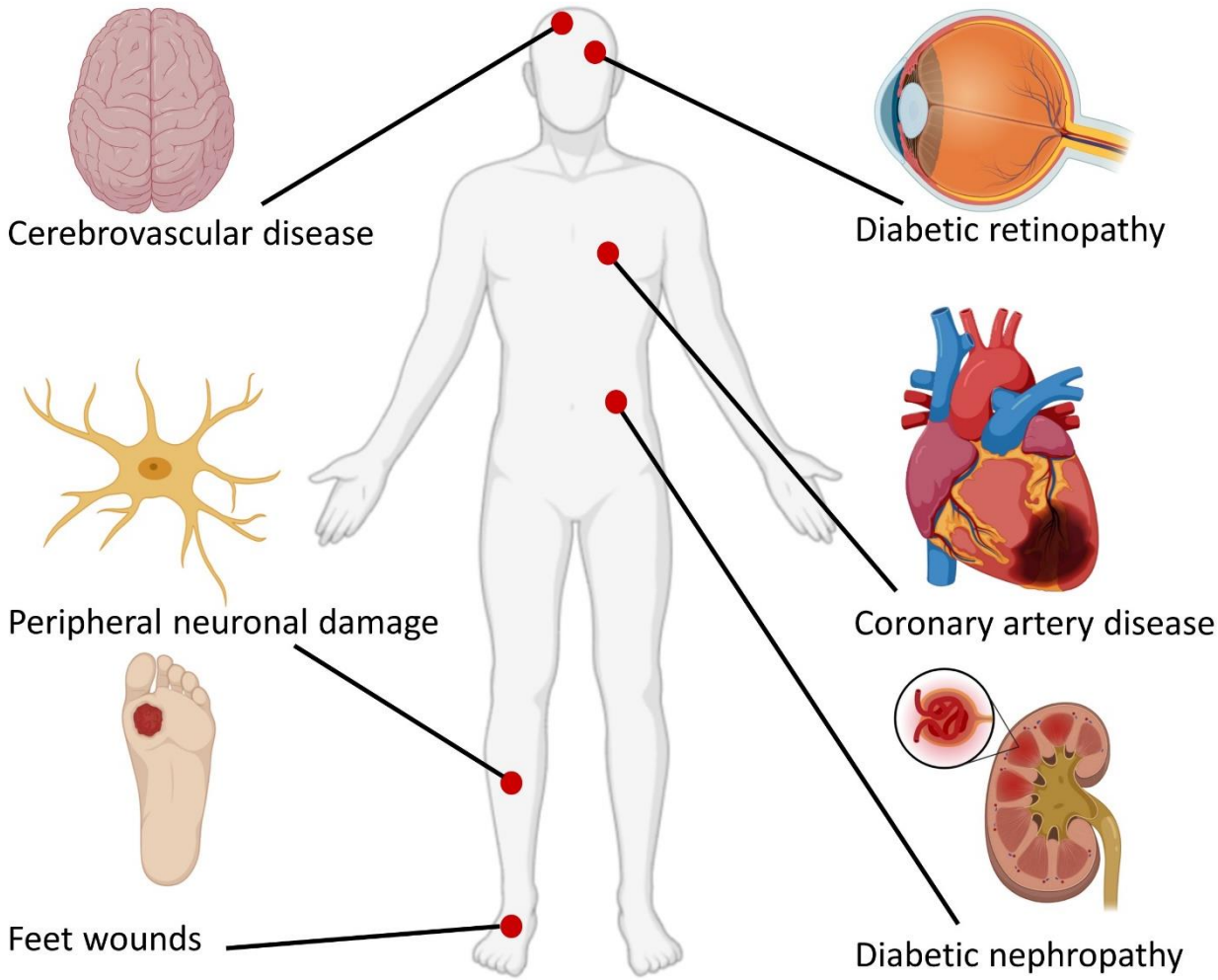

Figure 1: Major organs affected by diabetes mellitus.

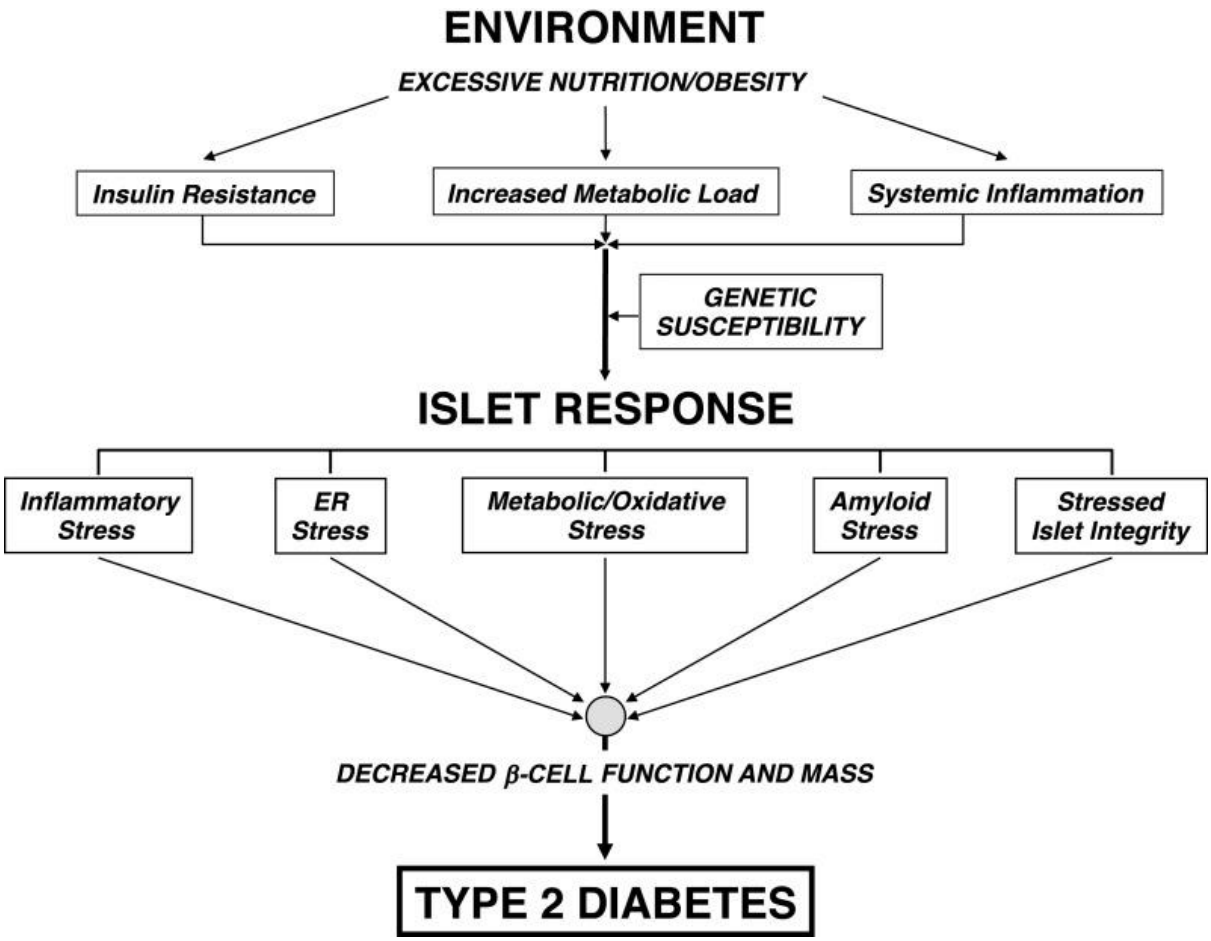

Figure 2: Stressors on the β-cell in the pathogenesis of T2DM

Pathological conditions like hyperglycemia and hyperlipidemia develop increasing metabolic load coupled with concurrent insulin resistance and chronic low grade sterile inflammation. The pancreatic islet cellular response to this new pathological micro environment is likely variable among individuals with differing genetic susceptibility but may include inflammatory stress, ER stress, metabolic and oxidative stress (e.g., glucotoxicity, lipotoxicity, and glucolipotoxicity), causing loss of islet cell integrity and promoting β-cell dysfunction [11, 14, 15].

1.2. Cardiovascular disease

Atherosclerotic cardiovascular disease (CVD), including coronary artery disease (CAD) and its complications, is a leading cause of death and disability worldwide. CVD is a general term for pathological conditions affecting the heart or blood vessels and is most prevalent cause of mortality worldwide [16]. The major causes of mortality worldwide are cardiovascular diseases [17]. CVDs as principal cause of mortality resulted in deaths of 17.7 million people which represents 31% of all global deaths. Furthermore, this number is expected to grow to

approximately 23.6 million in 2030. Cardiovascular diseases include coronary heart disease like myocardial infarction along with other disorders like cerebrovascular disease, peripheral arterial disease, deep vein thrombosis and pulmonary embolism [18]. CVD, in particular myocardial infarction which is a complication of atherosclerosis, becomes a serious ailment and leading cause of death in diabetic patients [19].

1.3. Atherosclerosis

Atherosclerosis, the main cause of ischaemic heart or coronary artery disease (heart attack) and cerebrovascular disease (stroke), is leading cause of death and morbidity worldwide [20]. Atherosclerosis is an inflammatory disease which results in thickening of the blood vessel walls and is characterized by progressive accumulation of lipids and inflammatory cells with intima of blood vessels which with time initiates the formation of plaque inside the lumen of the blood vessels. Over time plaque growth narrows the arteries, obstructing blood flow through the vessels and causing damage to organs like heart and brain, causing eventually heart attack or stroke respectively [21, 22]. The plaque or atheroma is composed of mainly cells, lipids and debris. Along with vascular endothelial and smooth muscle cells, the significant constituents are immune and inflammatory cells in particular macrophages [22-25].

The causes of atherosclerosis can be multifactorial and the stimulus can be either systemic or local factors that deteriorate vascular function. Hyperglycaemia and hyperlipidaemia are the most prevalent metabolic risk factors of atherosclerosis [26, 27].

1.3.1. Role of vascular endothelial cells and macrophages

Endothelium provides a barrier between blood and extravascular space including smooth muscle cells. Endothelial dysfunction primes atherosclerosis and is linked with all stages of atherosclerosis. Macrophages, an essential cellular components of host body's defense system, play a role in atherosclerotic plaque lesion development and thrombogenesis. Monocytes and macrophages play essential roles in all stages of atherosclerosis both in the presence and absence of diabetes mellitus.

The accumulation of monocytes in the artery wall and subsequent maturation of these cells to macrophages propagate a chronic, non-resolving low-grade arterial inflammation. Macrophages express at least six scavenger receptors for modified forms of low-density lipoproteins (LDL) (e.g. oxidized LDL and minimal modified LDL) that contribute to the formation of foam cells in atherosclerosis [28]. Scavenger receptors are the group of receptors which recognize, bind and internalize modified LDL [29]. In response to locally produced chemoattractant molecules, monocytes are recruited to subendothelial space where they differentiate into macrophages which express scavenger receptors to mediate the endocytic uptake of LDL. This inflammatory response transforms the macrophage into a lipid-rich foam cell which is a hallmark feature of atherosclerosis and leads to lesion expansion (Figure 3).

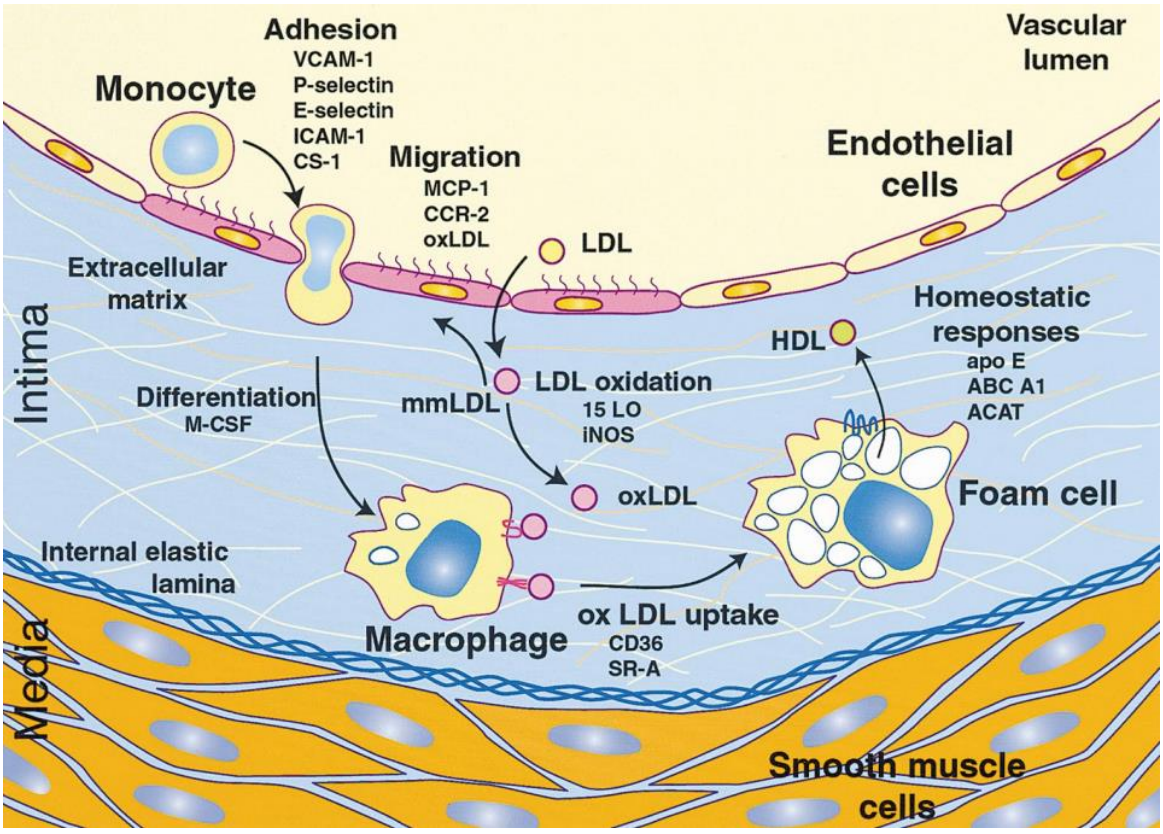

Figure 3: Initiating Events in the Development of atherosclerotic plaques.

LDL is subjected to oxidative modifications in the subendothelial space, progressing from minimally modified LDL (mmLDL), to extensively oxidized LDL (oxLDL). Monocytes under the influence of chemokines are attracted and get attached to mmLDL and / or oxLDL activated endothelial cells. Adherent monocytes migrate into the subendothelial space and differentiate into macrophages. Uptake of oxLDL via scavenger receptors leads to foam cell formation [30].

Which further amplifies the inflammatory response to vascular injury by secreting cytokines including interleukin (IL)-1, IL-6, monocytes chemoattractant protein -1 (MCP-1) and tumor necrosis factor (TNF) and promotes the progression of atherosclerotic plaque to advanced and vulnerable plaques [31].

1.3.2. Diabetes mellitus and atherosclerosis

The leading cause of death among diabetic patients is atherosclerosis and its associated complication like myocardial infarction. Cardiovascular death in diabetic cardiac patients is 2-4-fold higher than in non-diabetic cardiac patients. The risk of CVD is markedly increased in both T1DM and T2DM patients, with cardiac events occurring at younger ages in patients with diabetes mellitus. Optimal glycemic control has been shown to halt microvascular complications of diabetes mellitus, such as kidney disease and eye complications, in at least some patients, but glucose lowering is less effective in preventing major cardiovascular events, especially in patients with established CVD [32] [33, 34]. The underlying mechanism of different disease course in diabetic and non-diabetic heart patients is not clear, although it is evident that monocytes and macrophages are key players at all stages of atherosclerosis both in the absence and presence of diabetes mellitus, and that phenotypes of these cells are altered in a diabetic environment.

Preclinical and clinical data implicate macrophages as a key cell type in atherosclerosis, contribute to the accelerated atherosclerotic lesion progression and impede atherosclerotic plaque regression associated with diabetes mellitus. Thus, disease reversal, e.g. the betterment of already established atherosclerosis, remains an unmet medical need. The persistence of diabetes mellitus-associated complications despite improved blood glucose control is known as the metabolic or hyperglycaemic memory. Several pathomechanisms have been linked with diabetes-associated accelerated atherosclerosis over the last decades, but their potential role for the hyperglycaemic memory remains generally unknown.

1.3.3. Role of mitochondrial ROS in diabetes mellitus-associated atherosclerosis

Mitochondrial dysfunction has been increasingly associated with the initiation and progression of atherosclerosis by elevating the production of reactive oxygen species (ROS) and mitochondrial dynamics dysfunction, and energy supply. Atherosclerotic fibrous cap and core area display significant mitochondrial dysfunction manifested by a reduction in mtDNA

copy number and oxygen consumption [35]. The mtDNA damage accompanied with reduced mtDNA-encoded subunit complexes I, III, IV, and V and impaired mitochondrial function, has been linked with development of atherosclerosis and plaque vulnerability.

The protein $p66^{Shc}$ a redox regulator, which can translocate to the outer mitochondrial space and interact with the electron-transport chain, resulting in increased mitochondrial ROS generation [36, 37] has been linked with glucose-induced excess ROS generation and diabetes mellitus associated vascular complications [38, 39]. Glucose-induced $p66^{Shc}$ expression has been observed in podocytes (renal epithelial cells), endothelial cells, and smooth muscle cells [38, 40]. Expression of $p66^{Shc}$ is epigenetically controlled, suggesting that sustained $p66^{Shc}$ expression may provide a mechanistic link between the hyperglycaemic memory, sustained vascular ROS generation and inflammation, and progressive atherosclerotic disease despite improved blood glucose control [38, 40]. A recent study demonstrated sustained $p66^{Shc}$ expression in peripheral blood monocytes of diabetic patients despite improved blood glucose control [41]. However, whether sustained $p66^{Shc}$ expression likewise occurs in atherosclerotic plaque-associated macrophages remains unknown. Likewise, it remains unknown whether $p66^{Shc}$ expression in macrophages is causatively linked with diabetes mellitus-associated accelerated atherosclerosis and whether targeting $p66^{Shc}$ expression may provide a therapeutic benefit.

1.4. Coagulation proteases:

When an atherosclerotic plaque ruptures, collagen and tissue factor are exposed, and, through the activation of platelets and the coagulation cascade, these trigger atherothrombosis [42]. Human atherosclerotic plaque display coagulation activity [43]. Animal studies establish that the generated thrombin level relates to progression of atherosclerosis, with hypercoagulability producing advanced atherosclerosis in mice with an Apolipoprotein E-deficient $ApoE^{-/-}$ background [44, 45]. Several studies show that administration of direct oral anticoagulants, like dabigatran and rivaroxaban, attenuate atherosclerosis development in $ApoE^{-/-}$ mice [46, 47]. The coagulation cascade has two initiation pathways which result in thrombin activation, which subsequently results in fibrin formation and platelet activation, forming a hemostatic plug and thus stopping bleeding. The initiation pathways are the contact activation pathway (also known as the intrinsic pathway) and the tissue factor pathway (also known as the extrinsic pathway). Both coagulation pathways activate the "final common

pathway" comprising factor X and prothrombin activation. Thrombin then cleaves fibrinogen and activates platelets [2, 48, 49].

Tissue factor and D-dimer levels, the latter reflecting fibrin formation, are increased in diabetic patients with unstable advanced carotid atherosclerosis [50]. Furthermore, plasma fibrinogen levels are upregulated in diabetes mellitus with vascular disease [51, 52], which is considered to be an important risk factor in atherosclerosis. These markers remain elevated for several months after the acute event [53]. Treatment with platelet inhibiting drugs have shown to reduce both the acute and long-term risk of new ischemic events after a myocardial infarction [53, 54] and this is currently standard of care. In the *Acute Coronary Syndrome-Thrombolysis in Myocardial Infarction 51* (ATLAS ACS 2-TIMI 51) trial, the direct oral anticoagulant rivaroxaban reduced the risk of new ischemic events when compared with placebo in patients after myocardial infarction [55, 56], suggesting that inhibition of the coagulation system may provide an additional benefit in patients with an increased risk of an acute coronary event.

Thrombin has a large variety of functions, in addition to the conversion of fibrinogen to fibrin, which is important for the hemostatic plug. Importantly, it activates Factors VIII and V (feedback amplification) and – after binding to thrombomodulin – the anticoagulant protein C (for feedback inhibition), thus adding an additional level of control to the coagulation cascade (Figure 4) [57, 58].

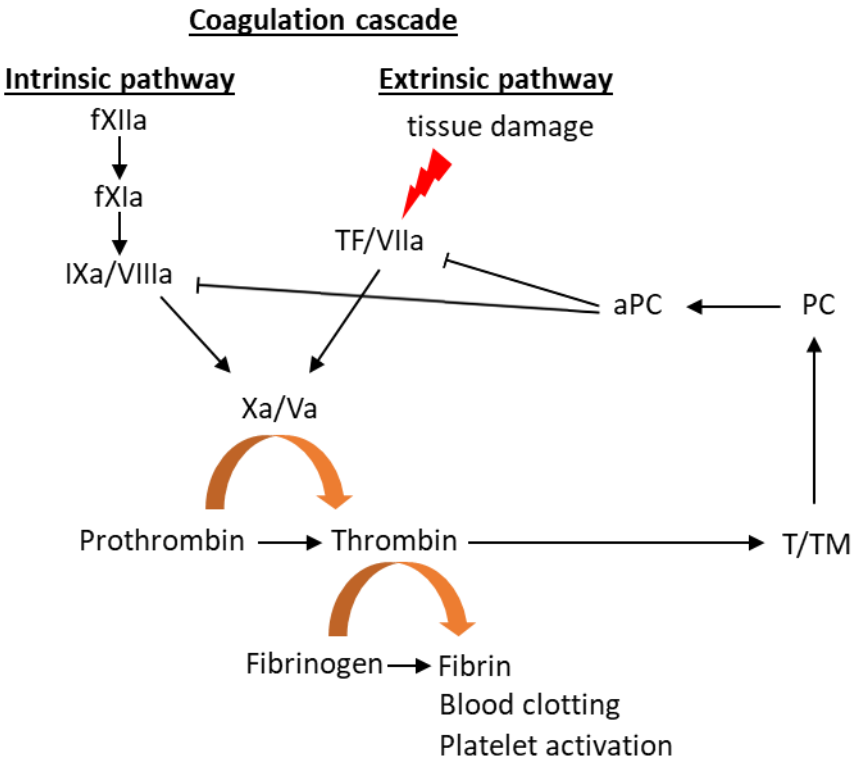

Figure 4: The coagulation cascade

The coagulation cascade comprises two partially interacting activation pathways, the intrinsic and the extrinsic pathway. The intrinsic pathway is initiated by sequential activation of coagulation factors XII, XI and IX. FXIIa converts FXI into FXIa. Factor XIa activates FIX. FIXa interacts with its co-factor FVIIIa, yielding the tenase complex, which activates FX to FXa, thus initiating the common coagulation pathway. The extrinsic pathway is activated following damage to the blood vessel. Upon loss of vascular integrity FVII is able to interact with extravascular tissue factor (TF). Within the TF-FVII complex FVII is activated. The TF-FVIIa complex activates FX to FXa. Within the common coagulation pathways FXa and its co-factor FVa form the prothrombinase complex, which activates prothrombin to thrombin. Thrombin converts fibrinogen to fibrin and activates platelets, which together from a hemostatic plug.

1.5. Role of thrombomodulin - protein C - EPCR system in cardiovascular diseases

Protein C (PC) is a vitamin K-dependent plasma glycoprotein that is synthesized by the liver and circulates as a 2-chain biologically inactive species [59]. PC is transformed to activated protein C (aPC) by thrombin-mediated cleavage of PC at the N-terminus (Figure 5) [57]. Effective activation of PC by thrombin requires the transmembrane glycoprotein, thrombomodulin (TM), as a cofactor for thrombin, amplifying this event ~1000-fold [60]. When in complex with TM, thrombin has lessened pro-coagulant activity. Thus, thrombin's substrate specificity is

efficiently switched by TM. PC activation by the thrombin–TM complex is further enhanced 20-fold when PC is bound to the endothelial cell protein C receptor (EPCR) [61, 62].

aPC, initially characterized as an endogenous anticoagulant, conveys in addition anti-inflammatory, barrier-protective, and pro cell-survival functions [63-66]. Indeed, it became increasingly apparent that aPC controls cellular function largely independent of its anticoagulant effects through cell- and context-specific receptor complexes and intracellular signalling pathways [63, 64]. Thrombomodulin-mediated PC activation is impaired in both acute diseases and chronic diseases [44, 67-72]. Coronary endothelial TM and EPCR expressions inversely correlates with the severity of atherosclerosis [73]. Furthermore, human and mouse plasma levels of TM and aPC declines in atherosclerosis, myocardial infarction and diabetes mellitus [74-76]. Genetically superimposed loss of PC activation aggravates experimental diabetic nephropathy (dNP) [70] and exogenous aPC treatment protects murine dNP and renal ischemia reperfusion-injury. The pathological relevance of loss of TM and aPC for accelerated atherosclerosis in diabetes mellitus remains unknown.

aPC exerts pleiotropic cytoprotective and anti-inflammatory effects on immune and tissue resident cells of a variety cell populations [59, 77].

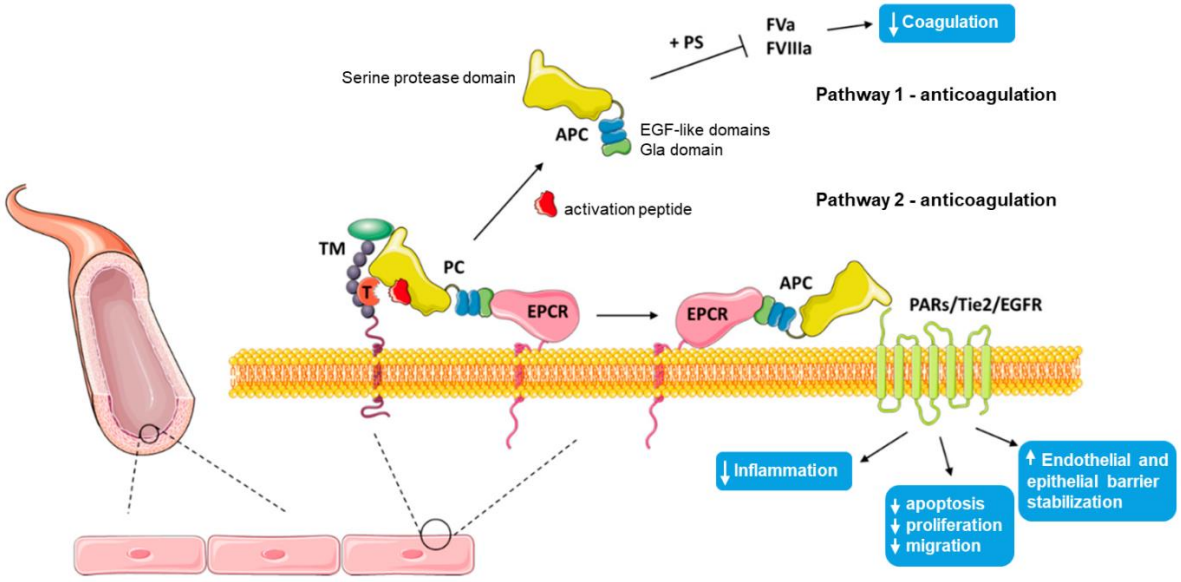

Figure 5: Mechanism of protein C activation and actions on the surface of human endothelial cells.

Protein C (PC) is bound to an endothelial protein C receptor (EPCR) on the surface of endothelial cells, where it is activated by thrombin (complexed with thrombomodulin) cleavage of its activation peptide. Activated protein C (APC) is then either released, where it participates in negative feedback of the coagulation cascade (pathway 1), or presented to cleave PARs/Tie2/EGFR in order to exert its

cytoprotective effects (pathway 2). Pathway 2 also occurs on the surface of keratinocytes. EGFR: endothelial growth factor receptor; FVa: activated factor V; FVIIIa: activated factor VIII; PAR: protease-activated receptor; PS: protein S; T: thrombin; TM: thrombomodulin [77].

1.5.1. Cytoprotective and anti-inflammatory function of the aPC

In addition to its anticoagulant function, aPC – frequently in association with EPCR and other co-receptors in a cell specific fashion– conveys cyto-protective signaling through cleavage of protease-activated receptors (PARs). The cyto-protective effects of aPC includes (1) endothelial barrier stabilization, (2) anti-apoptotic properties, (3) anti-inflammatory activity, and (4) alterations of gene expression profile [17, 65, 78]. aPC mediated anti-inflammatory effects include inhibition of NF-kappa B (NF-κB) and reduced expression of cell adhesion molecules (ICAM, VCAM), reduced leukocyte extravasation at site of injury, inhibition of the release of inflammatory cytokines (e.g., TNF-α, IL-6) and NLRP3 inflammasome activation (IL-1β, IL-8) [17, 65, 78].

PARs belong to seven transmembrane domain G protein coupled receptors (GPCRs) family and in contrast with classical receptors, PARs are activated by N-terminal proteolytic cleavage [79]. There are four mammalian members of the PAR family PAR1, PAR2, PAR3, and PAR4 are encoded by the genes F2R, F2RL1, F2RL2, and F2RL3, respectively [80]. PARs are cleaved and activated irreversibly by various proteases including thrombin and aPC [81, 82]. Proteases cleave specific N-terminal peptides of PARs. This results in exposure of a new N-terminal peptides, which remains tethered to the receptor and acts as a receptor-activating ligand, named “tethered ligand” [80, 83, 84]. PARs are expressed on endothelial cells, vascular smooth cells and macrophages, relevant to atherosclerosis [85].

Whether aPC prevents diabetes mellitus associated accelerated atherosclerosis and through which receptors it mediates its affects remains to be investigated. As the loss of TM and aPC is observed in both diabetes and atherosclerosis and aPC is known to prevent ROS mediated diabetic microvascular complications like nephropathy, we hypothesize that aPC prevents diabetes mellitus-associated accelerated atherosclerosis by dampening ROS formation.

2. Aim of the study

Plaque morphology differs among diabetic and non-diabetic atherosclerotic disease, indicating at least partially disjunct pathophysiology. In a systematic approach we will first compare atherosclerotic plaques in humans and mice with primarily hyperglycemia or hyperlipidemia associated plaques. We will conduct laser microdissection and isolate fluorescently labelled plaque cells to identify molecular targets which are differentially regulated in diabetic and non-diabetic atherosclerotic disease.

Diabetes mellitus-associated atherosclerosis is perpetuated despite marked improvement of blood glucose control. The sustained disease process despite improved blood glucose is referred to as the hyperglycaemic memory. The hyperglycaemic memory is linked with glucose-induced post-translational modifications and epigenetically sustained gene expression. Loss of thrombomodulin expression and impaired activated protein C (aPC) generation have been associated with atherosclerosis and diabetes mellitus. Approaches to therapeutically reverse the hyperglycaemic memory are lacking. Whether exogenous aPC treatment prevents accelerated atherosclerosis remains obscure. Mechanistically, we will investigate whether aPC prevents diabetes mellitus associated hyperglycemic memory through epigenetic regulation.

To find the translational relevance of our findings we will use *vivo*-morpholino against ROS regulator ($p66^{Shc}$) and employ aPC dependent signalling *in vivo*. This will evaluate whether the hyperglycaemic memory in diabetes mellitus-associated atherosclerosis can be regulated by coagulation protease-dependent signaling and whether it can be pharmacologically targeted. We expect that the current findings will spur efforts to further characterize the effects of coagulation proteases on the epigenetic landscape in plaque-associated cells and the consequences thereof in diabetes mellitus mellitus-associated atherosclerosis.

3. Materials and methods

3.1. Chemicals and reagents

Reagent	Source	Catalogue No.
Agarose, Standard	Carl Roth Gmbh	3810.1
Alcian Blue	Sigma-Aldrich	A5268
Ammonium Hydroxide	Sigma-Aldrich	A6899
Aqueous Mounting medium	ZYTOMED systems	ZY-AMT030
Bovine Serum Albumine, fraction V	Sigma-Aldrich	8076.1
Bouin's Solution	Sigma-Aldrich	HT10
Chloroform	EMD Milllipore	44321
Crocein Scarlett M 003B	Sigma-Aldrich	C8822
Deoxynucleotide triphosphates (dNTPs)	Thermo Fisher Scientific	10216018
Diethylpyrocarbonat (DEPC)	Sigma-Aldrich	4718
Dimethyl Sulfoxide (DMSO)	Carl Roth Gmbh	A994.1
Dihydroethidium (DHE)	Promo Cell, Germany	PK-CA707-10057
DMEM-6429 Medium	Sigma-Aldrich	DMEM6429-500ML
EDTA	Sigma-Aldrich	E9884
Eosin	Sigma-Aldrich	E4009
Ethanol	Carl Roth Gmbh	5054.1
Ethidium Bromide	Carl Roth Gmbh	2218.1
Ferric Chloride Hexahydrate	Sigma-Aldrich	F2877
Formalin, 4% Buffered	Fischar, Saarbrucken	27279
Gelatin from Bovine Skin	Sigma-Aldrich	G9391
Giemsa Stain Solution	Carl Roth Gmbh	T862.1
Glucose	Sigma-Aldrich	G8769
Glycerol Gelatin	Sigma-Aldrich	GG1-15ML
Hematoxylin, Gill's Formula	Carl Roth Gmbh	T864
Isoamylalcohol	Carl Roth Gmbh	8931.1
Isopropanol	Carl Roth Gmbh	9781.1
Magnesium Chloride	Sigma-Aldrich	M8266
Magnesium Sulfate	Sigma-Aldrich	M7506
Mannitol	Sigma-Aldrich	M4125

MassRuler, DNA Ladder, Low Range	Thermo Fisher Scientific	SM0383
Methanol	J.T. Baker, Gliwice, PL	JB8402
2-Mercaptoethanol	Sigma-Aldrich	ROTH4227.1
Oil Red O	Sigma-Aldrich	9755
Paraformaldehyde	Sigma-Aldrich	158127
Phenol	Carl Roth Gmbh	38.1
Phosphotugstic Acid	Sigma-Aldrich	P4006
Potassium Iodide	Sigma-Aldrich	P8256
RNAlater	Invitrogen, Thermo Fisher	AM7021
Roti Histo-Kitt II	Roth, Karlsruhe, Germany	T160.1
RPMI-1640 Medium	Sigma-Aldrich	R388
Saffron	Sigma-Aldrich	9310-4
Sodium Acetate	Sigma-Aldrich	S2889
Sodium Chloride	Sigma-Aldrich	S9888
Sodium Dodecyl Sulfate (SDS)	Carl Roth Gmbh	183.1
Sodium Thiosulfate	Sigma-Aldrich	21.726-3
Streptozotocin	ENZO, Farmingdale, NY	ALX380-010-M100
Tissue Tek, O.C.T. Compound	Sakura, Netherlands	4583
Tris-HCL	Sigma-Aldrich	10812846001
TRIzol	Thermo Fisher Scientific	15596018
Vectashield	Vector Labs, CA, USA	H-1000-10
Xylol	Becton Dickinson, Germany	ROTH9713.1
Yeast Extract	Becton Dickinson, Germany	28860_base

3.2. Antibiotics

Penicillin-Streptomycin Sigma-Aldrich, Steinheim, Germany

3.3. Antibodies and serum

Antibody	Company / Cat NO.	Dilution or Conc.
Anti-^{Shc} Rabbit pAb (p66^{Shc})	Calbiochem / ST1033	1:2000 WB, 1:100 IHC
CD36	Santa Cruz / SC-9154	1:200WB, 1:50 IHC
Nitrotyrosine	Santa Cruz / Sc-32757	1:200WB
8-Oxo-dG	Trevigen / 4354-MC-50	1:1000 IHC

DNMT1	Cell Signaling / 5032S	1:1000WB, 1:100 IHC
DNMT3a	Cell Signaling / 2160S	1:1000WB
DNMT3b	Cell Signaling / 57868S	1:1000WB
MOMA-2	Abcam / ab33451	1:100 IHC
EPCR	Sigma-Ald. / E6280	20µg/ml (cells treatment)
PAR2 (Blocking)	Santa Cruz / Sc13504 L	20µg/ml (cells treatment)
PAR3 (Blocking)	Santa Cruz / Sc5598 L	20µg/ml (cells treatment)
PAR4 (Blocking)	Santa Cruz / Sc8461 L	20µg/ml (cells treatment)
GAPDH	Sigma-Ald. / G9545	1:10000 WB
Anti-rabbit IgG, HRP-Linked	Cell Signalling / 7074S	1:2000 WB
Anti-mouse IgG, HRP-Linked	Cell Signalling / 7076S	1:2000 WB
TRITC (anti-mouse IgG)	Dako /R0156	1:200 IHC
FITC (anti-mouse IgG)	Dako / F0261	1:200 IHC
Fluorescein (anti-rat IgG)	Vector / W1018	1:200 IHC
Taxas Red (anti-mouse IgG)	Vector / X1013	1:200 IHC

3.4. Enzymes

Enzyme	Source
Go Taq G2 flexi DNA Taq polymerase	Promega – Madison USA
Taq polymerase (Phusion)	Theromo scientific Revert Aid first strand
RNase 1 recombinant RNase-free	Theromo scientific Revert Aid first strand
RT Enzyme	Theromo scientific Revert Aid first strand
Ribdock RNase inhibitor	Theromo scientific Revert Aid first strand

3.5. Buffers

3.5.1. Total cell lysate

3.5.2. RIPA buffer (Modified Radioimmunoprecipitation)

3.5.2.1.1. **RIPA Base Ingredients**

- Tris-HCl (buffering agent prevents protein denaturation)
- NaCl (salt prevents non-specific protein aggregation)
- NP-40 (non-ionic detergent to extract proteins; 10% stock solution in H_20)

- Na-deoxycholate (ionic detergent to extract proteins; 10% stock solution in H_2O; protect from light)

  [Note: Do not add Na-deoxycholate when preparing lysates for kinase assays. Ionic detergents can denature proteins, causing them to lose activity.]

3.5.2.1.2. **Procedure (for cells and tissues)**

Prepare 100 ml modified RIPA buffer as follows:

1. Add 790 mg Tris base to 75 ml distilled H_2O. Add 900 mg NaCl and stir the solution until all solids are dissolved. Using HCl, adjust the pH to 7.4.
2. Add 10 ml of 10% NP-40 to the solution.
3. Add 2.5 ml of 10% Na-deoxycholate and stir until solution is clear. (RIPA for tissue add 5ml of 10%)
4. Add 1 ml of 100 mM EDTA to the solution. Adjust the volume of the solution to 100 ml using a graduated cylinder. Store RIPA buffer at 4 C until ready to use.

3.5.3. PBS (10x)

NaCl	= 80g
KCl	= 2g
Na_2HPO_4 ($2H_2O$)	= 14.4g
KH_2PO_4	= 2.4g

Added d.H_2O up to about 900ml, Adjust pH =7.4 by adding NaOH.

3.5.3.1. PBST (Phosphate - buffered saline Tween)

In 1x PBS 0.1% (v/v) tween 20 or triton X-100 was added to make it PBST.

3.5.4. Buffers for SDS-PAGE

Tris-HCL (1.5 M)	= 0.825g
10 % iges SDS (0.4 %)	= 20 ml

Adjust pH:8.8, Make up to 500 ml with d.H_2O

3.5.4.1. Electrophoresis Trenngel-buffer (Resolving buffer)

Tris-HCL (1.5 M)	= 90.825 g
10% iges SDS (0.4 %)	= 20 ml

Adjust pH:8.8, Make up to 500 ml with d.H_2O

3.5.4.2. Sammelgel-buffer (Stacking buffer)

Tris-HCL (1 M) = 30.275 g

10% iges SDS (0.4 %) = 8 ml

Adjust pH:6.8, Make up to 200 ml with d.H_2O

3.5.4.3. Ammoniumpersulfate (APS)

10 % in d.H_2O (1 gm Ammonium per-sulphate in 10ml of H_2O)

3.5.4.4. Resolving-gel 10%

Resolving gel	10 ml (1gel)	20 ml (2gels)	40 ml (3gels)
Tris HCl pH-8.8	2.5ml	5ml	10ml
Acrylamide 30	3.3ml	6.7ml	13.4ml
d. H_2O	4.1ml	8.1ml	16.2ml
APS	100µl	200µl	400µl
TEMED	10µl	20µl	40µl

3.5.4.5. Stacking-gel 6%

Resolving gel	10 ml (1gel)	20 ml (2gels)	40 ml (3gels)
Tris HCl pH-8.8	1000µl	2000µl	4000µl
Acrylamide 30	800µl	1600µl	3200µl
d. H_2O	2160µl	4320µl	8640µl
APS	40µl	80µl	160µl
TEMED	8µl	16µl	32µl

3.5.4.6. Loading Buffer (4x Sample-buffer)

Glycerol (100%) = 20ml

SDS (5%) = 4g

Beta-marceptoethanol = 2.5ml

1 M Tris/HCl pH: 6.8 = 12ml

Bromophenol blue = 20mg Or few drops of Conc. Solution

Add water to make up to 50ml

3.5.4.7. Running Buffer (5x SDS Running-buffer)

Tris (0.125 M) = 15.1 g

Glycine (1.250 M) = 94 g

10 % iges SDS = 50 ml

Make up to 1L with d.H_2O

3.5.4.8. Blot-buffer (5x)

Tris (0.02 M) = 12.125 g

Glycine (1.250 M) = 56.250 g

Make up to 1L with d.H_2O

Note: while preparing working solution (1x); have to add 200ml of methanol, 200ml of 5x blot buffer and 500ml of d.H_2O to make final volume 1L.

3.5.4.9. Blocking buffer

It is either 5% low fat dry milk or it is 5% BSA in PBST or TBST.

3.5.5. Agarose gel electrophoresis

3.5.5.1. TBE (5x)

Tris = 54gm

Boric Acid = 27.5gm

EDTA (0.5 M) = 20ml

Adjust the volume up to 1000ml with DEPEC water (for RNA) or with distilled water (for DNA). For working solution (0.5X TBE) add 100ml of 5X TBE and add DEPEC water (for RNA), Distilled water (for DNA).

3.6. Mice

ApoE-/- (002052), PAR2-/- (024161), PAR3-/- (015230) mice were obtained from the Jackson Laboratory (Bar Harbor, Me, USA). PAR1-/- mice were kindly provided by Eric Camerer (Paris, France) and $p66^{Shc-/-}$ mice has been described previously [35] [82]. Wild type mice (C57BL/6) were obtained from Janvier Lab (S.A.S, St. Berthevin Cedex, France). In the current study we used littermates which have been backcrossed for at least 10 generations on a C57BL/6 or C57BL/6J background, respectively. Only female mice were used throughout this study. All animal experiments were conducted following standards and procedures approved by the local animal care and use committee (Landesverwaltungsamt Halle, Germany).

3.6.1. Atherogenic mouse models

3.6.1.1. Induction of hyperlipidaemia

ApoE$^{-/-}$ mice (age, 6 to 8 weeks) were fed high fat diet "HFD" (Western Type Diet, 43% carbohydrates, 15% proteins and fat 42%) or normal chow diet for 22 weeks.

3.6.1.2. Induction of hyperglycaemia

ApoE$^{-/-}$ mice (age, 6 to 8 weeks) were made as diabetic (DM) by injecting streptozotocin (60 mg/kg) intraperitoneally once per day for five consecutive days [39] [86]. Streptozotocin was freshly dissolved in 0.05 M sodium citrate, pH 4.5. Blood glucose and body weight was measured once in a week. State of diabetes mellitus (minimum 300 mg/dl) was maintained for up to 22 weeks.

3.6.1.3. Measurement of blood glucose level

Two weeks after the last STZ injection, blood was collected from the tail vein and blood glucose was measured with ACCU-CHEK® glucose test strips. Mice with blood glucose levels higher than 400-500 mg/dl received 1-2 units of Insulin (100 U/ml) twice a week subcutaneously, respectively.

3.6.1.4. Mice treatment and groups

Diabetic mice, 16 weeks after the last STZ injection, mice were either treated with SGLT2-inhibitor (SGLT2i) alone to reduce blood glucose levels (Dapagliflozin; 25 mg/kg in the drinking water, DM-NG), or were concomitantly treated with aPC (1 mg/kg intraperitoneally once daily) and SGLT2i (Dapagliflozin, as below, DM-NG-aPC) or were treated concomitantly with aPC, SGLT2i (as below), and 5-azacytidine (0.25mg/kg intraperitoneally on alternative days, DM-NG-aPC-Aza) for additional 6 weeks.

Diabetic mice were then divided into 6 groups. Group1: mice were sacrificed 22 weeks after STZ last injection as baseline (DM, group 1), Group2: after 16 weeks of STZ last injection, mice were treated with SGLT2i- inhibitor (Dapagliflozin; 2.5 mg/kg in drinking water) (DM-NG, group 2) up to 6 weeks, Group3: after 16 weeks of established diabetes mellitus mice were treated with aPC (1 mg/kg i.p. daily intraperitoneally) concomitantly with SGLT2i (Dapagliflozin; 2.5 mg/kg in drinking water) (DM-NG-aPC, group 3) up to 6 weeks, Group4: after 16 weeks of established diabetes mice were treated with aPC concomitantly with 5-Azacytidine (0.25 mg/kg i.p. intraperitoneally on alternative days) and SGLT2i (DM-NG-aPC-AZA, group4) for additional 6 weeks. Group5: after 16 weeks of diabetes mellitus mice were

treated with $p66^{shc}$ or control morpholino (DM-$p66^{shc}$-MO, DM-Cont-MO, group 5) for upto 6 weeks. Group6: after 16 weeks of diabetes mellitus mice were treated either with DNMT1 morpholino and aPC on alternate days or control morpholino (DM-DNMT1-MO+aPC, DM-Cont-MO, group6).

In parallel HFD group was divided into 2 groups. Group1: mice were fed HFD for 22 weeks and were sacrificed (HFD, group1). Group2: after 16 weeks, the diet of high fat diet mice was changed to chow diet for additional 6 weeks.

After 22 weeks of treatment, mice were sacrificed and plaque morphology was analysed as previously described.

3.6.1.4.1. **Vivo-Morpholinos (VM) oligomer treatment**

Morpholinos (MO) were obtained from Gene Tools, LLC, United States. The following oligonucleotides sequence were used: 5'-ATC CCC AGG CCC TTA GCC TAG TCT G-3' against $p66^{Shc}$ (Mus musculus src homology 2 domain-containing transforming protein C1, Shc1, transcript variant 1), blocking the translation of Shc1 transcript variant 1; its mismatch control: 5'- ATC GCC AGG CGC TTA GCG TAG TGT G-3'; the oligonucleotides sequence 5'-CAG GTT GCA GAC GAC AGA ACA GCT C-3' against DNA methyltransferase, DNMT1, transcript variant 1, blocking the translation of DNMT1 transcript variant 1; and its mismatch control 5'-CAG CTT CCA GAC CAC ACA ACA CCT C-3'. MO's were dissolved in PBS (100 µl; 6 mg MO per kg body weight; intraperitoneally) and were injected every other day for 6 weeks into a subset of diabetic $ApoE^{-/-}$ mice.

3.6.2. Analysis of mice

In total after 22 weeks of treatments the body weight was measured, and mice were sacrificed. Blood samples were obtained from the inferior vena cava of anticoagulated mice (500 U unfractionated heparin intraperitoneally). Blood was centrifuged at 2000 x g for 20 minutes at 4°C and plasma (the upper transparent layer) was snap frozen in liquid nitrogen. Mice were perfused with ice-cold PBS for 10 min. The upper heart (containing aortic valve) and brachiocephalic artery was embedded in O.C.T compound and were snap frozen in dry ice. The other aortic arches including thorasic aorta were collected for RNA and were preserved in RNA later at 4°C for 24 hours and then either were proceeded for analysis or

frozen at -80°C. O.C.T embedded brachiocephalic arteries and upper hearts were sectioned from distal to proximal at 6 µm thickness and embedded at glass slides.

3.6.3. Analysis of blood lipids

Blood lipids were measured with the Advia 2400 Chemistry System from Roche (Basel, Switzerland).

3.6.4. Bone marrow transplantation

Donor mice either ApoE$^{-/-}$, or p66$^{Shc\ -/-}$ ApoE$^{-/-}$, were sacrificed via survical dislocation, tibia, and femurs were isolated and then flushed them with medium (RPMI 1640 with 2% FBS, 10 units/ml heparin, penicillin, and streptomycin) using a 25 G needle into 50 ml falcon tube. To remove osseous particles the solution was passed through sterile 100 µm nylon cell strainer and collected in a 50 ml tube. Cells were centrifuged at 2000 rpm (900 x g), 10 min, 4°C. Supernatant was discarded and the cell pellet was washed twice with 50 ml of serum-free RPMI (RPMI 1640 with 20 mM HEPES, penicillin, and streptomycin). Following centrifugation at 2000 rpm (900 x g), 5min, 4°C cells were resuspended in 25 ml of serum-free RPMI. Cell number was determined using a cell counter (TC20^{TM} automated cell counter, Biorad). Cells were suspended in serum-free RPMI to a final concentration of 1 x 10^7 cells/ml. Recipient mice (ApoE$^{-/-}$ 8 weeks old) were lethally irradiated (11 Gy, once) and injected with 5 x 10^6 bone marrow cells (volume 0.2 ml) *via* the tail vein 4-6 hours after irradiation. The mice were kept on antibiotic (sulamethazine; 1 g/L, in the drinking water) for 2 weeks after irradiation and then switched to water without antibiotics. Four weeks after bone marrow transplantation, efficient replacement of bone marrow was ascertained by FACS analysis. Recipient ApoE$^{-/-}$ mice were then divided into 3 groups, mice were either fed western type diet (HFD – high fat diet), normal chow diet (controls) or were made diabetic. After 20 weeks mice were sacrificed and Analysed as above.

3.7. Laser capture microdissection

Lesions macrophages positive for CD68 were laser captured and micro dissected as described elsewhere [87]. Briefly, frozen sections were fixed in clod acetone at 4°C for 10 minutes. Then sections were dried at RT for 10 minutes and washed briefly in, followed by incubation with diluted primary antibody (1:100, rabbit anti-CD68) at RT for 30 minutes. Afterwards, sections

were washed twice with 1x PBS and secondary antibody (1:200, texes red- anti rabbit) was applied on the sections and incubated at RT for 30 minutes. Sections were washed first briefly with 1x PBS, then with RNase-free water and afterwards dried briefly at RT in dark. CD68 positive cells were then captured by using laser capture microdissection microscopy (PixCell II System, Germany), the capture of cells was achieved by placing a specially made cap, lined with a thermos labile film, onto a thinly cut section of tissue, with "pickup" completed by activating the film with a near-infrared laser diode pulse. This melting of the thermoplastic film causes the cells of interest to adhere to the film, which were then isolated from the surrounding tissue when the cap was lifted away from the slide. RNA was isolated by using the Qiagen RNeasy Micro RNA isolation kit. RNA concentration was measured in a nanometer and a 1.8 % agarose gel was run to verify the purity and integrity of RNA. cDNA was synthesized according to manufactur's protocol (Sensiscript First-Strand Sythesis System for RT-PCR from Qiagen).

3.8. Immunoblotting

Proteins were isolated and immunoblotting was performed as described [39, 86, 88-90]. In brief, cell lysates were prepared in RIPA buffer (50 mMTris at pH 7.4, 1% Nonidet P-40, 0.25% sodium deoxycholate, 150 mM NaCl, 1 mM EDTA, 1 mM Na_3VO_4, and 1 mM NaF supplemented with protease inhibitor cocktail). Lysates were centrifuged (10,000 × g for 10 min at 4°C) and insoluble debris was discarded. The protein concentration in supernatants was quantified using BCA reagent. Equal amounts of protein were electrophoretically separated on 10% (vol/vol) or 12.5% (vol/vol) SDS polyacrylamide gels, transferred to PVDF membranes, and probed with the desired primary antibodies overnight at 4°C. Membranes were then washed with TBST and incubated with anti-mouse (1:2,000), anti-rat IgG (1:2,000) or anti-rabbit IgG (1:2000) horseradish peroxidase-conjugated antibodies, as indicated. Blots were developed with the enhanced chemiluminescence system. To compare and quantify levels of proteins, the density of each band was measured by using ImageJ software. Equal loading was confirmed by immuno-blotting with GAPDH antibody.

3.9. Histology and Immunohistochemistry

3.9.1. Oil Red O staining

3.9.1.1. Aorta

Oil Red O staining was conducted on longitudinally opened thoracic aortae. Tissues were stained with Oil Red O for 10 min and rinsed twice with distilled water for 20 sec and once in running tap water for 10 min. Aortae were pinned on a black wax surface by using 0.1 mm diameter stainless steel pins as described previously [44, 91].

3.9.1.2. Brachiocephalic arteries and aortic roots

Cryopreserved sections of the brachiocephalic arteries and aortic roots (4 µm) were fixed in ice cold acetone for 2 min, rinsed twice in ice cold 1x PBS and were stained with Oil Red O using the same protocol, counterstained with haematoxylin for 40 seconds, rinsed in tap water for 10 min, mounted with aqueous mount. Lipid rich areas of the aortae, were Analysed by a blinded investigator using the Image Pro Plus software as described previously [44, 91].

3.9.1.3. Macrophages

Cells grown on glass cover slips were washed with PBS (1x) and were fixed with 4% PFA for 10 minutes. Following washing with PBS, respective staining was performed.

3.9.2. MOVAT's stain

MOVAT's stain was performed on frozen sections of brachiocephalic arteries. Frozen sections (4 µm) were fixed in Bouin's solution at 50°C for 10 min and stained with 5% sodium thiosulfate for 5 min, 1% alcian blue for 15 min, alkaline alcohol for 10 min, Movat's Weigert's solution for 20 min, crocein scarlet acid / fuchsin solution for 1 min, 5 % phosphotungstic acid for 5 min and 1% acetic acid for 5 min. Between every staining step the tissue sections were washed with tap water and with distilled water. Afterwards they were dehydrated in 95 % and 100 % ethanol for 1 min and stained in alcohol saffron for 8 min. Brachiocephalic arteries were washed in 100 % ethanol for 1 min, moved to xylol for 10 min and covered with cytoseal mounting medium. Every 15th section (~90 µm) of the brachiocephalic arteries and aortic roots were Analysed to quantify the plaque area. For histological analysis images were captured with an Olympus Bx43-Microscope (Olympus, Hamburg, Germany). The Image Pro Plus software (version 6.0) software was used for image analysis.

3.9.3. Immunofluorescence

For Immunofluorescence frozen sections of brachiocephalic arteries or aortic valves with maximum plaque size were fixed in ice cold acetone for 8 min, washed twice with ice cold PBS and incubated in 2% BSA in PBST for 1hr and then incubated the sections for overnight at 4°C in either single or mixture of two primary antibodies against $p66^{Shc}$, DNMT1, CD36, MOMA-2 and 8-Oxo-2'-deoxyguanosine. Sections incubated without primary antibodies were used as negative controls for background correction. Decanted the mixture solution and washed the samples three times with 1X PBS five minutes each time followed by Incubation with corresponding fluorescently labelled single or the mixture of two secondary antibodies. After washing nuclear counterstaining was conducted using mounting medium with DAPI and visualized using a fluorescence microscope. All histological analyses were performed by two independent blinded investigators. Immunohistochemistry and immunofluorescence images were captured with an Olympus Bx43-Microscope (Olympus, Hamburg, Gemany). The Image J software was used for image analysis.

3.10. Cell culture

J774.A1 cells were obtained from ATCC and were cultured at 37 C, in a humidified incubator with 5% CO_2 in Dulbecco's Modified Eagle's Medium (DMEM) with 10% fetal bovine serum and 1% Penicillin-Streptomycin as described previously [44, 91]. Bone marrow derived macrophages (BMDM) were isolated and cultured [92, 93]. Briefly, 10 to 12 weeks old mice were sacrificed by cervical dislocation and hind limbs (tibia, femur) were isolated, kept and flushed in RPMI-1640 complete medium containing 15% L929-cell conditioned medium (LCM). Afterwards cells were washed with 1x PBS and resuspended in above culture medium. This procedure was repeated once or twice to remove dead cells. After final washing, pelleted cells were resuspended in conditioned medium (supplemented with 30% of growth supernatant of M-CSF-transduced L929 cells). Finally, after 7-10 days depending on the confluency BMDMs, the purity of cells was confirmed by CD11b+ and it was higher than 90% as measured by FACS analysis and then cells were used for experiments.

3.10.1. Cells treatment

Cells treatment was divided into different groups. Group1: Cells were not treated with any stimuli but were kept in incubator for up to 48 hours (Cont48, group1). Group2: Cells were treated with 25 mM glucose for 48 hours and then were harvested to get protein (HG48,

group2). Group3: cells were treated with high glucose but after 48 hours high glucose treated medium was changed to normal glucose medium (HG48+NG24). Group4: After 48 hours of glucose treatment, aPC (20 nM) was added in the normalized medium for 24 hours (HG48+NG24-aPC. Group5: Cells were treated with glucose for 48 hours, then media was changed to normal, before aPC treatment cells were given an additional treatment of either PAR4 or EPCR blocking antibody for 1hour and then aPC for 24 hours.

3.11. RNA Isolation

We used Precellys® Lysing kit for aortic RNA isolation but to isolate RNA from J774:A1 and BMDMs, 3 ml TRIzol was added to 10 cm^2 dish. The TRIzol-cell-mix was incubated for 5 min at room temperature, 0.2 ml chloroform per 1 ml TRIzol were added, followed by centrifugation at 12,000 x g for 15 min at 4°C to separate phases. The aqueous phase containing the RNA was transferred to a fresh tube and RNA was precipitated by adding 0.5 ml 2-propanol per 1 ml TRIzol reagent. Sample was incubated at room temperature for 10 min and centrifuged at 12,000 rpm for 10 min at 4°C. Supernatant was removed and RNA was washed by adding 1 ml 75% ethanol per 1ml TRIzol. Sample was vortexed and centrifuged at 7,500 x g for 5 min at 4°C. RNA pellet was airdried for 5 min, redissolved in 20 µl DEPC-water and incubated for 10 min at 55 C. RNA concentration was measured in a photometer and a 1.8 % agarose gel was run to verify the purity and integrity of RNA.

3.12. Reverse transcriptase polymerase chain reaction (RT-PCR)

cDNA was synthesized according to manufacturer's protocol (SuperScript First-Strand Synthesis System for RT-PCR from Invitrogen). Primers were custom synthesized by Thermo Fisher Scientific and PCR was performed using the Go Taq Polymerase from Promega. PCR products were separated on a 1.5% (wt/vol) agarose gel and visualized by ethidium bromide staining. Expression was normalized to β-actin. Reactions lacking reverse transcriptase served as negative controls. Primers used in current study are given in table (Table 1).

Target	Primer Sequence
methylated ($p66^{Shc}$)	5'TTTTCGTTTTTTGGGTTC3' 5'TACGTATTCCTACCGAACG3'
unmethylated ($p66^{Shc}$)	5'TAATTTTTGTTTTTTGGGTTT3' 5'TACATATTCCTACCAAACACAA3'
mPAR1	5'CCAGCCAGAATCAGAGAGGA3' 5'TCGGAGATGAAGGGAGGAG3'

mPAR2	5'CCAGGAAGAAGGCAAACATC3'
	5'TGTCCCCCACCAATACCTC3'
mPAR3	5'CATCCTGCTGTT TGTGGTTG3'
	5'TACCCAGTTGTT GCCATTGA3'
mPAR4	5'GCAGACCTTCCGATTAGCTG3'
	5'CACTGCCGAGAACAGTACCA3'
DNMT3b	5'TTCAGTGACCAGTCCTCAGACACGAA3'
	5'TCAGAAGGCTGGAGACCTCCCTCTT3'
β-actin	5'CTAGACTTCGAGCAGGAGATGG3'
	5'GCTAGGAGCCAGAGCAGTAATC3'
TNF-alpha	5'ACAGAAAGCATGATCCGCGA3'
	5'TCCACTTGGTGGTTTGCTACG3'
IL6	5'GCCTTCTTGGGACTGATGCT3'
	5'TGCCATTGCACAACTCTTTTC3'
MCP1	5'GCTGTAGTTTTTGTCACCAAGC3'
	5'AAGGCATCACAGTCCGAGTC3'
CD36	5'TGAATGGTTGAGACCCCGTG3'
	5'CGTGGCCCGGTTCTACTAAT3'
p66^{Shc}	5'ACTACCCTGTGTTCCTTCTTTC3'
	5'TCGGTGGATTCCTGAGATACTGT3'

Table 1: List of primers used in the current study

3.13. DNA Isolation

Cells were centrifuged at 1500 rmp for 5min to get the pellet and were washed with PBS. 1ml lysis buffer was added and suspension was transferred to 2ml microfuge tube. Samples were incubated at 56°C for 2hours while shaking. Equal volume of Phenol: Chloroform:Isoamyl-alcohol (25:24:1) was added and mixed the samples by inverting the tube up and down. Samples were centrifuged at 6500 rpm for 15min to separate the DNA in the upper aqueous layer. Supernatants were transferred into new tube and equal amount of 100% ethanol containing 0.2 volume 10 M ammonium acetate was added. Either the samples were incubated overnight at -20°C or placed at room temperature for 15min until DNA was salted out as white precipitate. Afterwards the tubes were centrifuged at 12000 rpm for 15min to collect DNA precipitates. Pellet was washed with 70% ethanol by centrifuging at 12000 rpm for 5min. Followed by aspiration pellet was air dried for some time. Pellet was resuspended in 50µl water or TE buffer containing 20ug DNAse free RNAse A. Samples were incubated at 60°C for 1hr to dissolve completely. DNA quality was checked on 1% agarose gel.

3.14. Methylation specific PCR

Methylation-specific PCR was performed as described previously described [39]. Briefly, genomic DNA was isolated using the QIAamp DNA Mini Kit (QIAGEN) and treated with sodium bisulfite using the EZ DNA Methylation Kit (Zymo Research) following the manufacturer's instructions. PCR amplification was performed with the EpiTect MSP Kit (Qiagen) using primer pairs designed to specifically detect either methylated or unmethylated CpG sites in the mouse $p66^{Shc}$ promoter. For ratio analyses, amplicons against methylated and unmethylated CpGs were visualized on a 1.8% agarose gel. Universal methylated mouse DNA (Zymo research) was used as a positive control. The sequences of the primers used were as follows: methylated forward, 5'- TTT TTT TGG TTT GTT TAC GTC - 3'; methylated reverse, 5'- GAC GCG AAA AAAAAA TAA AA - 3'; unmethylated forward, 5'- TGT TTT TTT TGG TTT GTT TAT GTT - 3'; and unmethylated reverse, 5'- CCA ACA CAA AAA AAA AAT AAA AA - 3'.

3.15. DNMT activity assay

For DNMTs activity assay, nuclear proteins were extracted from cytoplasmic ones, using two extraction buffers A and C respectively [94]. Briefly medium was removed and cells were washed with 1x PBS. Followed by washing, cells were scrapped in 400µl of cytoplasmic extraction buffer (buffer A) containing protease cocktail inhibitor and kept on ice for 10 minutes. Cells were then briefly first vortexed and then centrifuged at 4°C. Supernatants containing cytoplasmic extractions were discarded; pellet was then re-suspended in 100 µl of nuclear extraction buffer (buffer C or B) and kept for 20 minutes on ice. Followed by centrifugation, supernatants (nuclear lysate) were collected and DNMT activity was measured by using EpiQuik™ DNMT Activity assay ultra kit (EPIGENETEK), following the manufacturer's instructions.

3.16. Preparation of activated protein C

Activated protein C was generated as previously described [17, 71, 95]. Prothrombin complex (Prothromplex NF600), containing all vitamin K dependent coagulation factors, was reconstituted with sterile water and supplemented with $CaCl_2$ at a final concentration of 20 mM. The column for purification of protein C was equilibrated at RT with 1 liter of washing buffer (0.1 M NaCl, 20 mM Tris, pH 7.5, 5 mM benzamidine HCl, 2 mM Ca^{2+}, 0.02% sodium azide). The reconstituted prothrombin complex was gravity eluted on a column filled with

Affigel-10 resin covalently linked to a calcium-dependent monoclonal antibody to PC (HPC4). The column was washed first with two column volumes of washing buffer and then two column volumes with a wash buffer rich in salt (0.5 M NaCl, 20 mM Tris, pH 7.5, mM benzamidine HCl, 2 mM Ca^{2+}, 0.02% sodium azide). Then the benzamidine was washed off the column with a buffer of 0.1 M NaCl, 20 mM Tris, pH 7.5, 2 mM Ca^{2+}, 0.02% sodium azide. To elute PC the column was gravity eluted with elution buffer (0.1 M NaCl, 20 mMTris, pH 7.5, 5 mM EDTA, 0.02% sodium azide, pH 7.5) and 3 ml fractions were collected. The peak fractions were identified by measuring absorbance at 280 nm. The peak fractions were pooled. The recovered PC was activated with human plasma thrombin (5% w/w, 3 hr at 37°C). To isolate activated protein C (aPC) ion exchange chromatography with FPLC (ÄKTAFPLC®, GE Healthcare Life Sciences) was used. First, thrombin was removed with a cation exchange column MonoS (GE Healthcare Life Sciences). Then a MonoQ anion exchange column (GE Healthcare Life Sciences) was equilibrated with 10% of a 20 mM Tris, pH 7.5, 1 M NaCl buffer. After applying the solution that contains aPC a 10-100% gradient of a 20 mM Tris, pH 7.5, 1 M NaCl buffer was run through the column to elute aPC at a flow of 1-2 ml/min under continuous monitoring of OD and conductivity. APC eluted at ~36 mS/cm by conductivity or at 40% of the buffer. Fractions of 0.5 ml were collected during the peak and pooled. Proteolytic activity of purified aPC was ascertained with the chromogenic substrate SPECTROZYME® PCa.

3.17. Analyses of human samples

Diabetes mellitus was diagnosed in patients according to the American Diabetes Association criteria [96, 97]. Diabetic (N=10) and non-diabetic (N=10) patients with atherosclerotic disease were recruited from the cardiology clinic at the University Hospital Magdeburg. All patients and controls were Caucasian. All patients were newly admitted to the university hospital at the Otto-von-Guericke University, Magdeburg, for treatment of ACI-stenosis, which was henceforth the primary diagnosis in all patients. Detailed information about the patient's clinical characteristics is given in Table 2. Tissue biopsies of atherosclerotic plaques were obtained from internal carotid artery during carotid disobliteration. Samples were immediately embedded in O.C.T. compound and snap frozen. Tissue biopsies were sectioned at 6 µm thickness and used for immunofluorescence staining as described above. The study complied with the Declaration of Helsinki and all patients entered the study according to the

guidelines of the local ethics committees after giving informed consent (Ethic-Committee-No: 92/09).

Parameter	Group statistics		*P*-value
	Non-DM (N=10)	**DM** (N=10)	**Non-DM vs DM**
Age (years)	63.39 ± 1.214	62.17 ± 1.341	ns
Sex (M/F)	8/2	7/3	ns
Diabetes duration (years)	-	15.33 ± 1.142	-
HbA1c (%)	4.88 ± 0.053	7.65 ± 0.234	<0.01
CAD (Y/N)	5/5	6/4	ns
RAS (Y/N)	3/7	4/6	ns
HTN (Y/N)	5/5	4/6	ns
Chol (mmol/L)	6.51 ± 0.012	3.56 ± 0.190	0.02
LDL (mmol/L)	4.90 ± 0.571	2.41 ± 0.176	<0.01
BMI (kg/m^2)	32.91 ± 1.096	30.88 ± 0.7462	ns
Smoking (Y/N)	3/7	4/6	ns
Oral antidiabetic medication (Y/N)	-	8/2	-
Insulin treatment (Y/N)	-	6/4	-
Lipid lowering drug (Y/N)	6/4	2/8	<0.01
antihypertensive drug (Y/N)	5/5	4/6	ns
Platelet activation inhibitors (Y/N)	4/6	3/7	ns

Table 2: Clinical characteristics of patients from which plaque biopsies were obtained

Data were obtained at the time of biopsy. Abbreviations: M: Male, F: Female, BMI: body mass index, Y: Yes, N: No, ACI: internal carotid artery, HTN: Hypertension, CAD: Coronary Artery Disease, RAS: Renal Artery Stenosis, Chol: Cholesterol. For statistical analysis of Sex, the Fisher's exact test was used and data are shown as mean ± SEM. For all other parameters analyses were performed using the unpaired two-tailed student's *t*-test. For significant differences the *P*-values are shown (ns: not significant).

4. Results

4.1. Hyperglycaemia promotes plaque instability in ApoE$^{-/-}$ mice

To gain insights into specific pathomechanisms of hyperglycaemia versus hyperlipidaemia induced atherosclerotic plaque development we directly compared hyperglycaemic (induced by low-dose streptozotocin, STZ injection for 5 days, a model of type 1 DM) and hyperlipidaemic (induced by a high fat diet, HFD) ApoE$^{-/-}$ mice with control ApoE$^{-/-}$ mice. Mice were followed up for 22 weeks. As expected, body weight, blood lipids, or blood glucose levels differed among treatment groups (Figure 6).

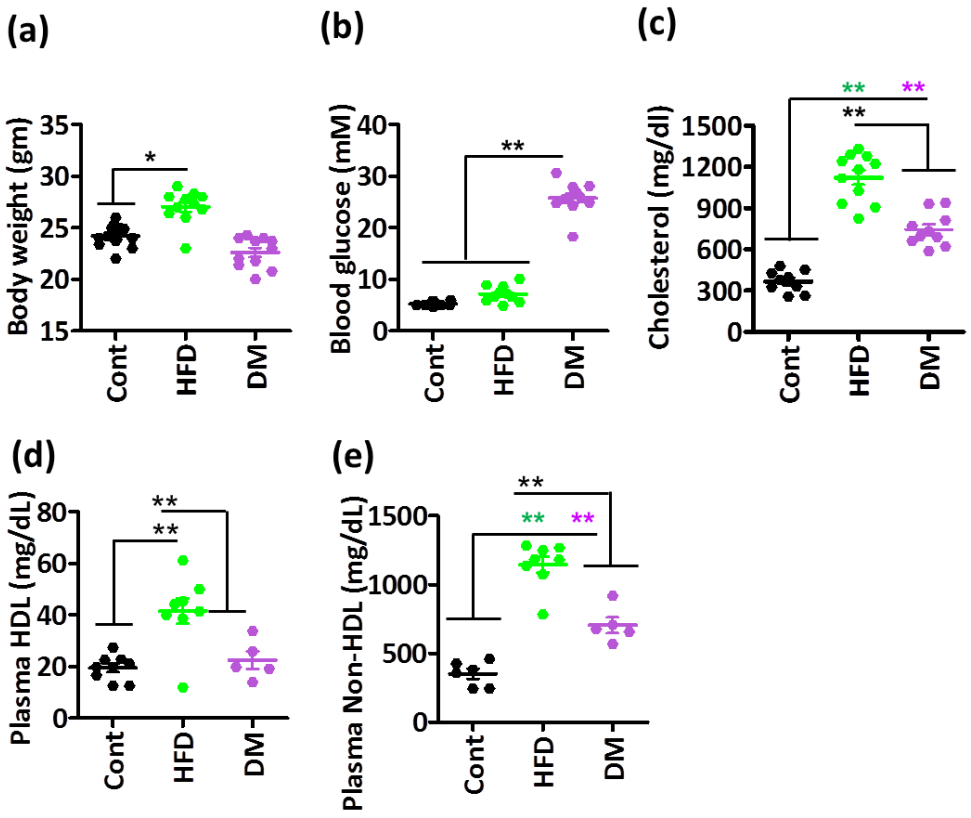

Figure 6: Body weight, blood glucose and blood lipid levels in ApoE$^{-/-}$ HFD versus ApoE$^{-/-}$ DM mice

Body weight (a), blood glucose levels (b), total plasma cholesterol levels (c), plasma HDL (d) and Non-HDL levels (e) in ApoE-/- control mice (Cont, normal chow diet, citrate instead of streptozotocin injections), ApoE-/- HFD mice (high fat diet, no streptozotocin), and ApoE-/- DM mice (normal chow diet, streptozotocin injections). Body weight and total plasma cholesterol levels are increased in ApoE-/- HFD mice as compared to ApoE-/- control mice. In ApoE-/- DM mice body weight is slightly but non-significantly reduced while blood glucose and plasma cholesterol levels are increased.
Data shown as dot-plots represent mean ± SEM of 10-11 mice per group; **P<0.01,* P<0.05; one-way ANOVA with Bonferroni adjusted post-hoc comparison of HFD and DM versus Cont.

Analyses of Oil Red O stained aortae *en face* revealed an increase of lipid-deposits in ApoE$^{-/-}$ HFD mice compared to ApoE-/- DM mice (Figure 7a). Likewise, plaques within the

brachiocephalic artery (Figure 7a,b,c) and the aortic roots (Figure 7b,d) were larger in ApoE-/- HFD than in ApoE-/- DM mice.

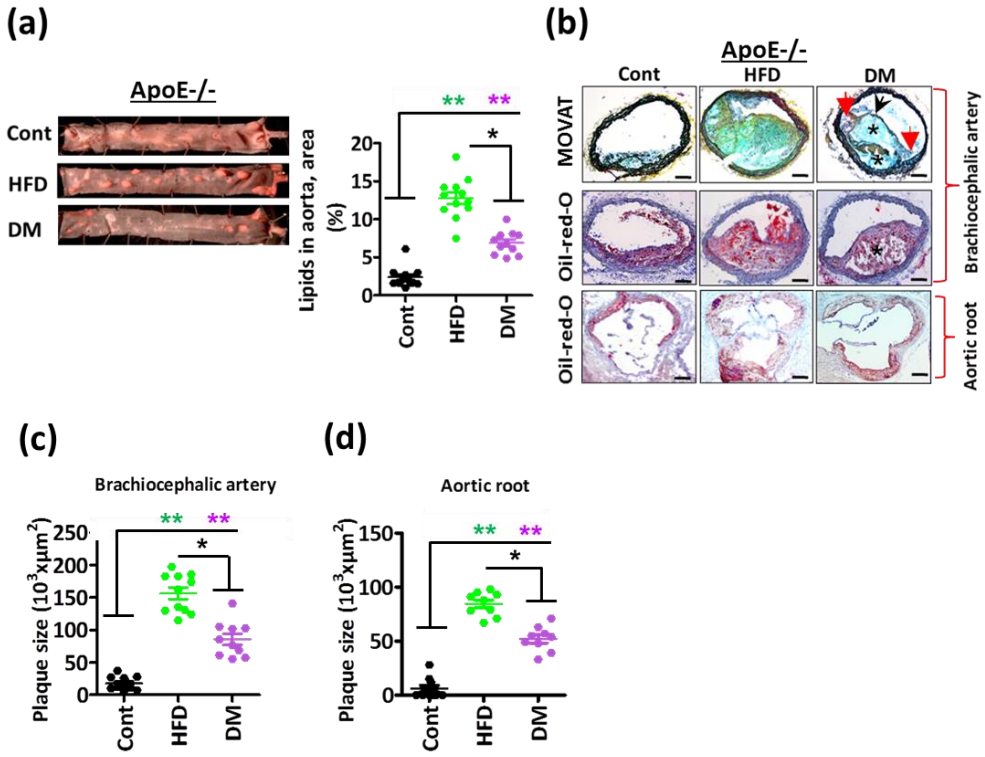

Figure 7: Smaller plaque size in hyperglycaemic versus hyperlipidaemic ApoE$^{-/-}$ mice.

a: Representative images of thoracic aortae showing en face plaques as detected by Oil Red O staining (left panel) and dot-plot summarizing data (total area stained with Oil Red O, right panel) in control (normal chow diet, Cont), hyperlipidaemic (high fat diet, HFD), and diabetic (STZ-induced hyperglycaemia, DM) mice.
b-d: Representative images showing MOVATs staining (b, upper panel) and Oil Red O staining of brachiocephalic arteries (b, middle panel) and aortic roots (b, lower panel). Morphometric analyses of MOVATs and Oil Red O stained images reveal smaller plaques(c,d).
Cont: non-diabetic ApoE-/- mice receiving normal chow diet; HFD: ApoE-/-mice receiving high fat diet (HFD); DM: hyperglycaemic ApoE-/- mice. Data shown as dot-plots represent mean ± SEM of 10-12 mice per group (a,c,d); size bars:20 µm; *P<0.05, **P<0.01; a, c, d: one-way ANOVA with Bonferroni adjusted post-hoc comparison of HFD and DM versus Cont and HFD versus DM.

To evaluate whether the reduced plaque size in hyperglycaemic mice simply reflects the lower total plasma cholesterol levels, we compared a subgroup of ApoE$^{-/-}$ DM and ApoE$^{-/-}$ HFD mice matched for total plasma cholesterol levels (922±52mg dl^{-1} versus 912±46mg dl^{-1} for HFD and DM mice, respectively). Despite matching a subgroup of ApoE$^{-/-}$ HFD and ApoE$^{-/-}$ DM mice for total plasma cholesterol levels lesion size was still smaller in hyperglycaemic ApoE$^{-/-}$ DM mice compared to ApoE$^{-/-}$ HFD mice (Figure 8).

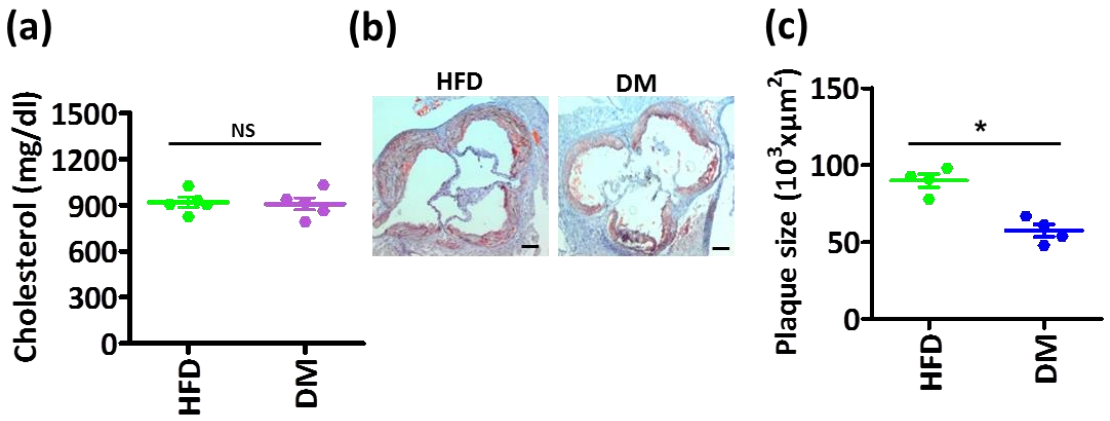

Figure 8: Subgroup analyses of plaque size in hyperlipidaemic vs hyperglycaemic ApoE$^{-/-}$ mice matched for total plasma cholesterol levels.

Total plasma cholesterol levels in selected ApoE-/- HFD (high fat diet, no streptozotocin) and ApoE-/- DM mice (normal chow diet, streptozotocin injections) matched for total plasma cholesterol levels (a). Representative Oil red O staining images of aortic root lesion (b) and dot-plot reflecting plaque size (c) in these selected mice.
Data shown as dot-plots represent mean ± SEM of 4 mice per group; NS: not significant, **P<0.01; a, c: unpaired t-test.

The smaller plaque size in ApoE$^{-/-}$ DM mice suggests that the aggravated disease course of hyperglycaemia related atherosclerosis is not primarily related to an increased plaque size. Hence, we next evaluated cellular composition and other parameters reflecting plaque stability. Indeed, signs of plaque instability were more frequent in ApoE$^{-/-}$ DM mice than in ApoE$^{-/-}$ HFD mice. Thus, plaques in ApoE$^{-/-}$ DM mice had an increased necrotic core area (Figure 9a), thinner fibrous caps (Figure 9b), and an increased frequency of ruptured plaque shoulders (Figure 9c). Plaque morphology and stability depend in part on cellular composition. In plaques of ApoE$^{-/-}$ DM mice macrophages area (immunohistochemically positive for MOMA-2) were increased, while smooth muscle cells (SMC α-actin positive area) were reduced in comparison to plaques of ApoE$^{-/-}$ HFD mice (Figure 9d). The observed shift to more macrophages and less SMC corroborates reduced plaque stability in ApoE$^{-/-}$ DM mice.

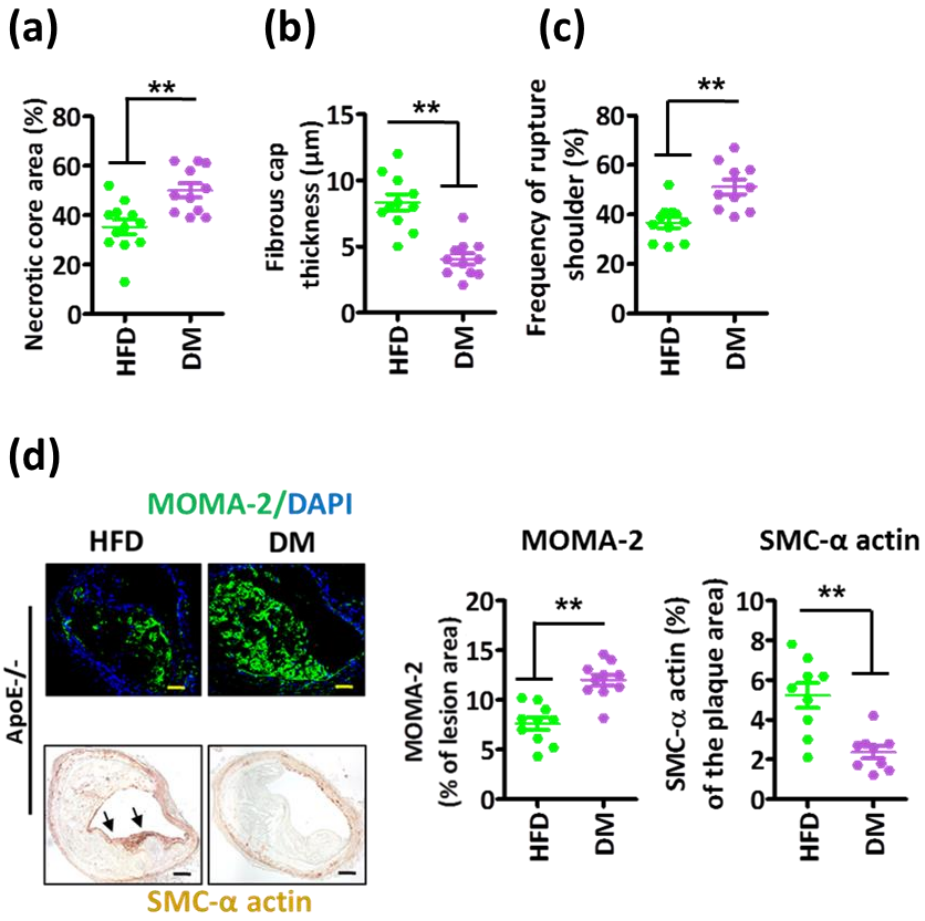

Figure 9: Plaques are less stable in hyperglycaemic versus hyperlipidaemic ApoE$^{-/-}$ mice

a-c: Increased necrotic core area (a), thinner fibrous caps (b), and more ruptured shoulders (c) in ApoE-/- DM mice compared to ApoE-/- HFD. Dot-plots in a-c summarize results obtained from MOVAT-stained brachiocephalic arteries (Figure 8b, top). Necrotic core area within plaque is indicated by a *, fibrous caps thickness by a black arrow, and ruptured shoulders by a red arrow (c).
d: Representative images showing immunofluorescence staining of macrophages (upper panel, MOMA-2, green; DAPI nuclear counterstain, blue) and smooth muscle cells (lower panel, α-actin, positive cells detected by HRP-DAB reaction, brown) within lesions and dot-plot summarizing data.
HFD: ApoE-/-mice receiving high fat diet (HFD); DM: hyperglycaemic ApoE-/- mice. Data shown as dot-plots represent mean ± SEM of 10-12 mice per group (a-d); size bars: d: 20 µm; *P<0.05, **P<0.01; a-d: t-test.

4.2. Hyperglycaemia induces p66^{Shc} and CD36 in macrophages

Plaque-associated macrophages impair plaque stability in part by generating reactive oxygen species (ROS). We therefore Analysed expression of the redox-regulator p66^{Shc} in plaque-associated macrophages of ApoE$^{-/-}$ DM and ApoE$^{-/-}$ HFD mice. Expression of p66^{Shc} was markedly enhanced in CD68 positive laser dissected plaque macrophages of ApoE$^{-/-}$ DM mice

(Figure 10a). Immunohistochemical analyses confirmed increased $p66^{Shc}$ expression and co-localization of $p66^{Shc}$ with MOMA-2, another macrophage marker, in plaques of $ApoE^{-/-}$ DM mice (Figure 10b).

As ROS induces expression of the scavenger receptor CD36, we speculated that enhanced $p66^{Shc}$ expression increases CD36 expression in hyperglycaemic mice. First, we ascertained whether $p66^{Shc}$ conveys glucose-induced CD36 expression. $ApoE^{-/-}$ or $ApoE^{-/-}$ $p66^{Shc}$-deficient ($ApoE^{-/-}$ $p66^{Shc-/-}$) mouse bone marrow derived macrophages (BMDMs) were cultured under normoglycaemic (5 mM glucose plus 20 mM mannitol, NG) or hyperglycaemic (25 mM glucose, HG) conditions for 48 hours. HG-conditions induced CD36 expression in $ApoE^{-/-}$, but not in $ApoE^{-/-}$ $p66^{Shc-/-}$ BMDMs (Figure 10c), demonstrating that $p66^{Shc}$ mediates the glucose-dependent induction of CD36 in macrophages. Consistently, CD36 expression was markedly increased in laser dissected macrophages obtained from plaques of $ApoE^{-/-}$ DM mice (Figure 10a). Immunohistochemical analyses verified an increased expression and co-localization of CD36 in plaque-associated macrophages of $ApoE^{-/-}$ DM versus $ApoE^{-/-}$ HFD mice (Figure 10d).

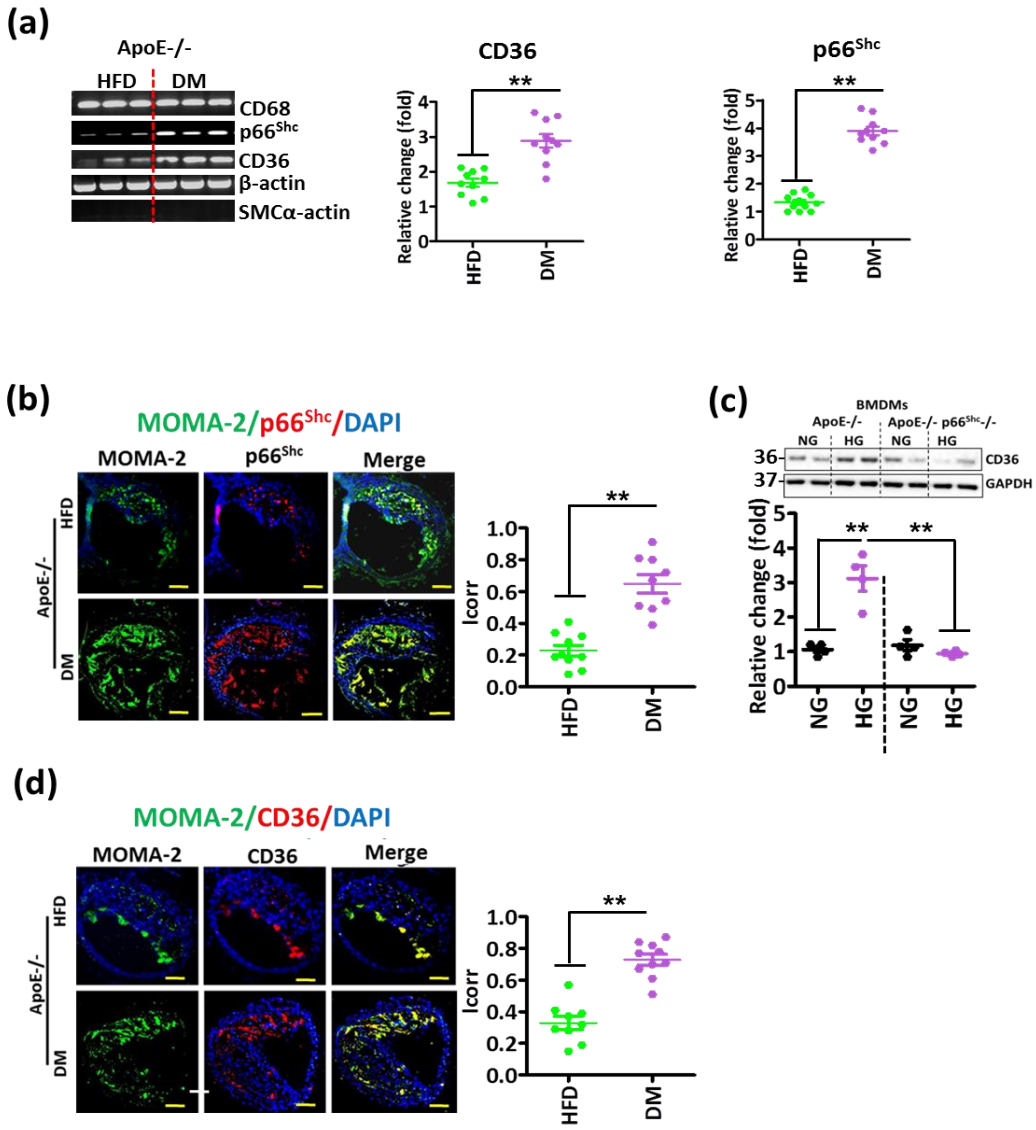

Figure 10: p66^{Shc} and CD36-expressions are increased in plaque-associated macrophages in diabetic mice.

a,b: Representative reverse-transcriptase-PCR gel images showing expression of CD68, p66^{Shc}, CD36, β-actin (loading control), and SMCα-actin (reflecting purity of laser dissected macrophages, a, left panel) and dot-plot summarizing data for CD36 (a, middle panel) and p66^{Shc} (a, right panel). Representative images showing co-immunofluorescence staining for p66^{Shc} (red), MOMA-2 (green), and DAPI nuclear counterstain (blue) within lesions of the brachiocephalic artery (b, left panel) and dot-plot summarizing data using automated digital co-localization analyses, yielding a correlation index (Icorr) (b, right panel).

c: Representative immunoblot images of CD36 (out of 4 independent repeat experiments with two technical replicates each, top) and dot-plot summarizing data (bottom) in ApoE-/- and ApoE-/- p66^{Shc}-/- bone marrow derived macrophages (BMDMs); NG: normal glucose (5 mM); HG: high glucose (25 mM); GAPDH: loading control.

d: Representative co-immunofluorescence images for CD36 (red), MOMA-2 (green), DAPI nuclear counterstain (blue) within lesions of the brachiocephalic artery in ApoE-/- HFD and ApoE-/- DM mice (left panel) and dot-plot summarizing data (Icorr, correlation index, right panel).

DM: hyperglycemic ApoE-/- mice; HFD: ApoE-/-mice with high fat diet (HFD). Data shown as dot-plots represent mean ± SEM of 10 mice per group (a,b,d) or 4 biological distinct replicates (c); size bars: b, d: 20 µm; **P<0.01; a, b, d: t-test; c: two-way ANOVA with Bonferroni adjusted post-hoc comparison of ApoE-/- (NG, HG) versus p66^{Shc}-/- ApoE-/- (NG, HG, respectively) BMDMs.

To investigate the potential translational relevance, we Analysed p66^{Shc} and CD36 expression in atherosclerotic plaques of non-diabetic and diabetic patients. As in mice both p66^{Shc} and CD36 expressions were more abundant in atherosclerotic plaques of diabetic patients compared to those of non-diabetic patients (Figure 11). Again, p66^{Shc} and CD36 expression was predominately observed in macrophages (co-localization of p66^{Shc} and MOMA-2, Figure 11). Thus, in diabetic mice and humans, macrophages within atherosclerotic plaques express more p66^{Shc} and CD36 compared to non-diabetic mice or humans.

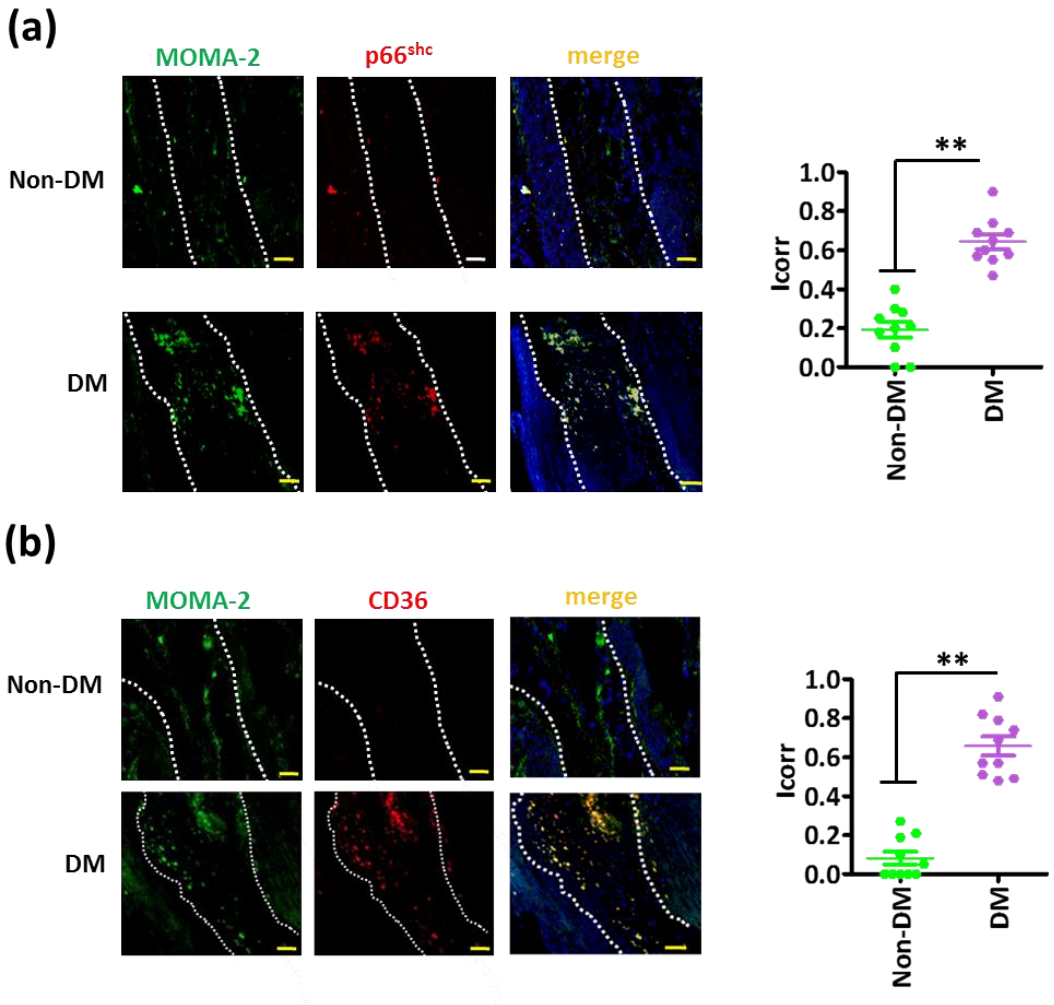

Figure 11: p66^{Shc} and CD36-expressions are increased in plaque-associated macrophages in diabetic patients

Representative co-immunofluorescence images for p66^{Shc} (red, a, left panel), CD36 (red, b, left panel), MOMA-2 (green, a, b, left panels), and DAPI nuclear counterstain (blue) and dot-plot summarizing data (Icorr; correlation index, right panels). Co-localization of p66^{Shc} and CD36 with the macrophage

marker MOMA-2 is increased in diabetic patient's samples (N=10) as compared to non-diabetic patient's samples (N=10).
DM: diabetic patient's samples; non-DM: non-diabetic patient's samples. Data shown as dot-plots represent mean ± SEM of 10 patients per group, size bars: 20 µm; **P<0.01; a: Mann-Whitney U test, b: t-test.

4.3. $p66^{Shc}$ is crucial for hyperglycaemia induced atherosclerosis

To evaluate the pathogenic relevance of $p66^{Shc}$ in myeloid derived cells for hyperglycaemia associated atherosclerosis we conducted bone marrow transplantation experiments. Bone marrow isolated from $ApoE^{-/-}$ or $p66^{Shc-/-}ApoE^{-/-}$ mice was transplanted into lethally irradiated $ApoE^{-/-}$ mice (age 8 weeks, Figure 12a). Control mice were left untreated (control), while in experimental mice hyperglycaemia or hyperlipidaemia were induced at age of 10 weeks. As expected, body weight, total plasma cholesterol or blood glucose levels differed among groups, but transplantation of $ApoE^{-/-}$ or $p66^{Shc-/-}ApoE^{-/-}$ derived bone marrow had no impact on these parameters.

Following transplantation of $p66^{Shc-/-}ApoE^{-/-}$ derived bone marrow plaque size was reduced (Figure 12b). However, the reduction in plaque size was less prominent and only of borderline significance (P=0.052) in the HFD group, while a pronounced reduction of plaque size was apparent in the DM group (Figure 12b). Indeed, plaque size in $p66^{Shc-/-}ApoE^{-/-}$ transplanted $ApoE^{-/-}$ DM mice was comparable to that in the controls (Figure 12b). The markedly reduced plaque size in $p66^{Shc-/-}ApoE^{-/-}$ transplanted $ApoE^{-/-}$ DM mice was associated with a decreased necrotic core area, increased fibrous cap thickness, decreased frequency of rupture shoulder, and less plaque-associated macrophages (Figure 12c, d), reflecting increased plaque stability. Thus, hyperglycaemia associated impaired plaque stability primarily depends on $p66^{Shc}$ expression in myeloid derived cells.

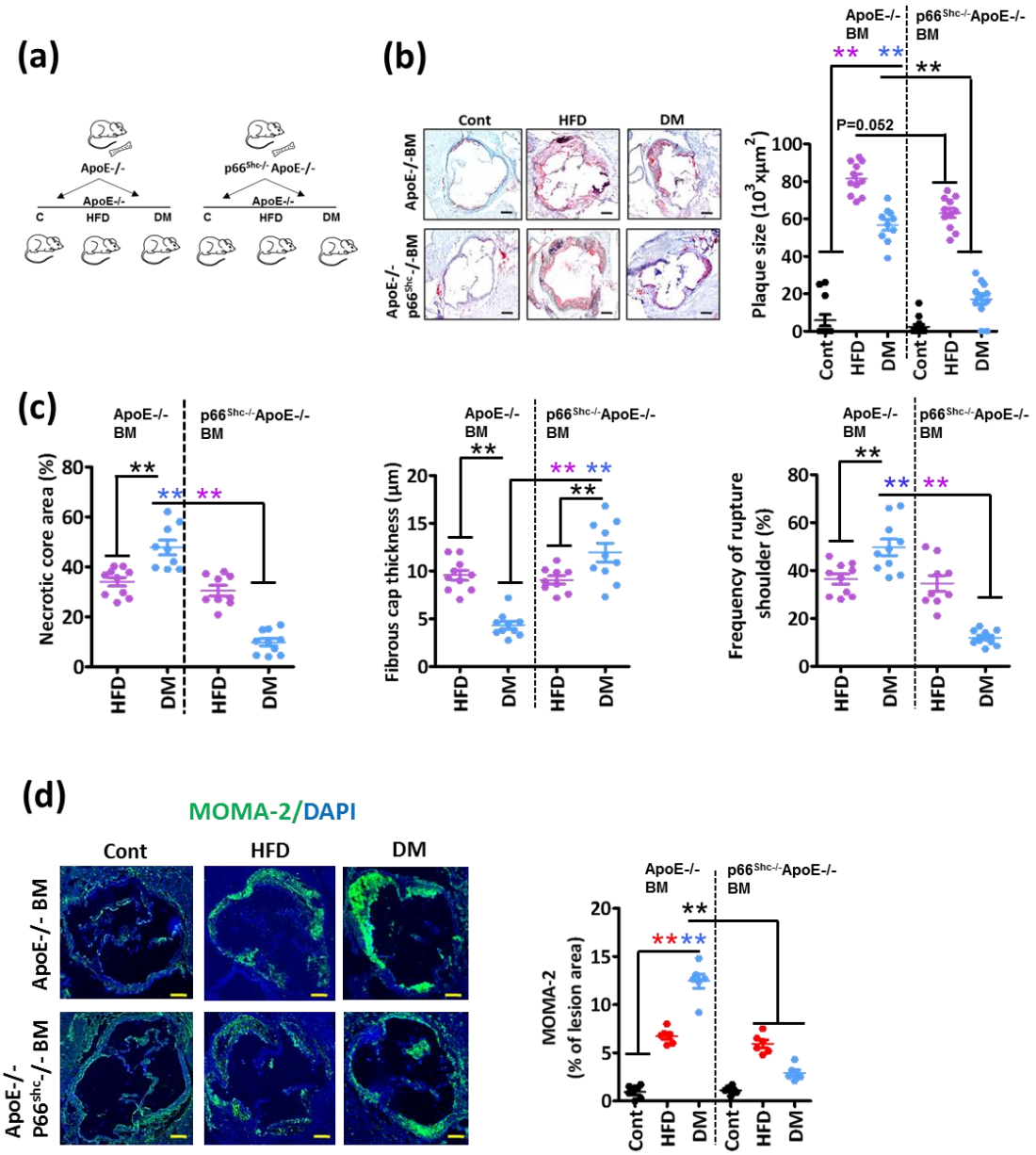

Figure 12: p66^{Shc} has a pivotal function in hyperglycaemia-, but not hyperlipidaemia-induced atherosclerosis

a: Experimental design of bone marrow transplantation experiments.

b: Transplantation of p66^{Shc}-/- deficient bone marrow markedly reduces hyperglycaemia-, but only slightly hyperlipidaemia-induced atherosclerosis. Representative images showing Oil Red O staining of aortic roots (left panel) and dot-plot summarizing plaques size (right panel).

c: Dot plots summarizing results of necrotic core area (left panel), fibrous cap thickness (middle panel), and frequency of ruptured shoulders (right panel).

d: Representative images showing immunofluorescence staining of macrophages (MOMA-2, green; DAPI nuclear counterstain, blue) within lesions (left panel) and dot-plot summarizing data (right panel).

Cont: normoglycaemic ApoE-/- mice with normal chow diet; DM: hyperglycaemic ApoE-/- mice; HFD: ApoE-/- mice with high fat diet (HFD). Data shown as dot-plots represent mean ± SEM of 6-10 mice per group (b, c, d); size bars: b, d: 20 µm; **P<0.01; b, c, d: two-way ANOVA with Bonferroni adjusted

post-hoc comparison of ApoE-/- (Cont, HFD, DM) versus p66^{Shc}-/- ApoE-/- (Cont, HFD, DM, respectively) recipient mice.

To determine whether p66^{Shc} may be a therapeutic target in diabetes mellitus associated atherosclerosis we treated mice with vivo-morpholinos to repress p66^{Shc} expression (p66^{Shc}-MO). After 16 weeks of persistent hyperglycaemia ApoE$^{-/-}$ DM mice were injected with p66^{Shc}-MO (DM-p66^{Shc}-MO) or control-MO (DM-Cont-MO; Figure 13).

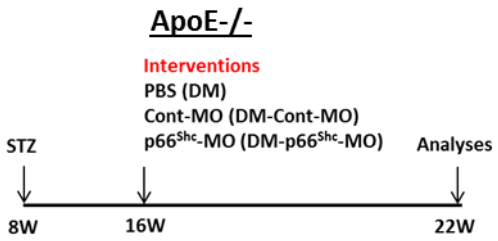

Figure 13: Experimental design of vivo-morpholino p66^{Shc} silencing experiments.

Efficient suppression of p66^{Shc} in the aorta was confirmed by semi-quantitative reverse-transcriptase-PCR (Figure 14a) and immunofluorescence staining (Figure 14b).

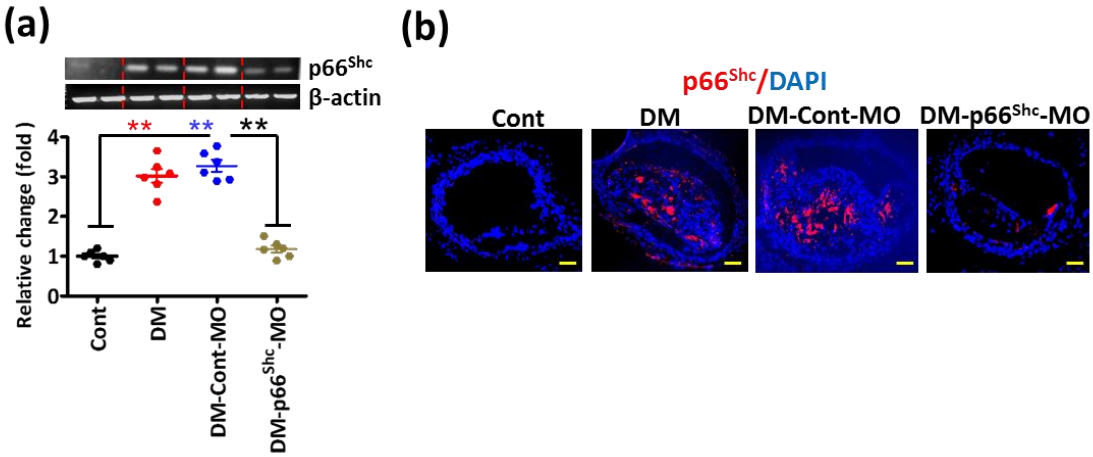

Figure 14: *In vivo* knockdown of p66^{Shc} in diabetic ApoE$^{-/-}$ mice using vivo-morpholinos

In vivo knockdown of p66^{Shc} in diabetic ApoE-/- mice using vivo-morpholinos (p66^{Shc}-MO; mismatched control morpholino: Cont-MO) reduces p66^{Shc} expression in atherosclerotic plaques. Representative reverse-transcriptase-PCR images showing aortic expression of p66^{Shc} (a, top; β-actin: loading control) and dot-plot summarizing data (a, bottom). Representative co-immunofluorescence images for p66^{Shc} (red) and DAPI counterstain (blue) within brachiocephalic artery lesions (b).
Cont: normoglycaemic ApoE-/- mice with normal chow diet; DM: hyperglycaemic ApoE-/- mice; DM-Cont-MO: DM mice treated with mismatch control morpholinos; DM-p66^{Shc}-MO: ApoE-/- DM mice treated with p66^{Shc} vivo-morpholinos. Data shown as dot-plots represent mean ± SEM of 6 mice per group; **P<0.01; one-way ANOVA with Bonferroni adjusted post-hoc comparison of DM and DM-Cont-MO versus Cont and DM-p66^{Shc}-MO versus DM-Cont-MO.

Treatment with vivo-morpholinos had no impact on body weight, blood glucose, or blood lipid levels. Following suppression of $p66^{Shc}$ plaques within aortic roots (Figure 15a) and brachiocephalic arteries (Figure 15b) were smaller in $p66^{Shc}$-MO as compared to Cont-MO treated $ApoE^{-/-}$ DM mice.

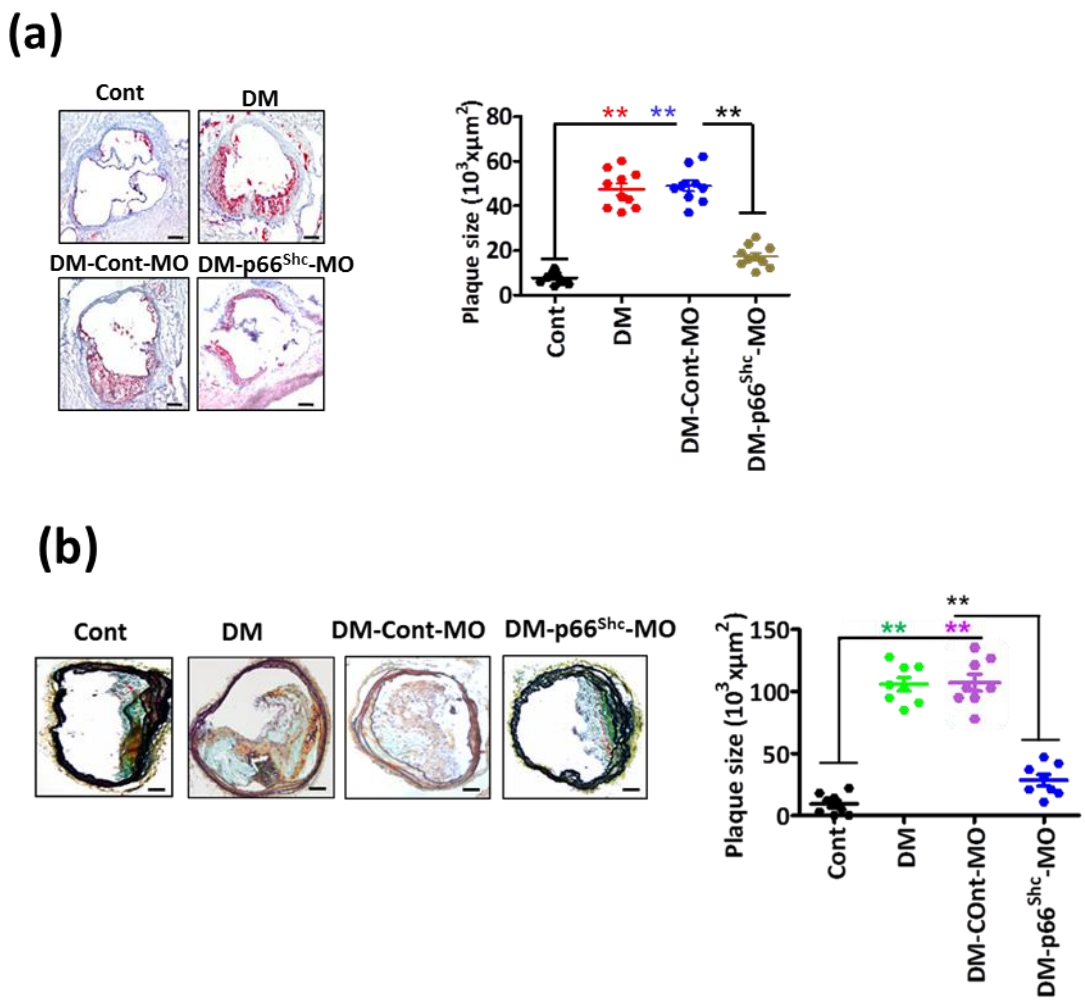

Figure 15: *In vivo* silencing of $p66^{Shc}$ by vivo-morpholino reduces hyperglycaemia-induced atherosclerosis

a: Representative images of Oil Red-O staining of the aortic root lesions (left panel) and dot-plot summarizing plaque size (right panel).
b: *In vivo* knockdown of $p66^{Shc}$ using vivo-morpholinos ($p66^{Shc}$-MO; mismatched control morpholino: Cont-MO) induces atherosclerotic plaques regression in hyperglycaemic mice. Representative images of MOVAT stained brachiocephalic artery (left) and dot-plot summarizing data (right).
Cont: normoglycaemic ApoE-/- mice with normal chow diet; DM: hyperglycaemic ApoE-/- mice. DM-Cont-MO: ApoE-/- DM mice treated with mismatch control morpholinos; DM-$p66^{Shc}$-MO: ApoE-/- DM mice treated with $p66^{Shc}$ vivo-morpholinos; mean ± SEM of 8 mice per group; **P<0.01; one-way ANOVA with Bonferroni adjusted post-hoc comparison of DM and DM-Cont-MO versus Cont and DM-$p66^{Shc}$-MO versus DM-Cont-MO.

This was associated with increased signs of plaque stability as reflected by decreased necrotic core area, increased fibrous cap thickness, decreased frequency of rupture shoulder and less plaque-associated macrophages in p66^{Shc}-MO as compared to Cont-MO treated ApoE$^{-/-}$ DM mice (Figure 16a,b). These results demonstrate that p66^{Shc} expression in macrophages promotes diabetes mellitus-accelerated atherosclerosis and that targeting p66^{Shc} may be a feasible therapeutic approach in diabetes mellitus-associated atherosclerosis.

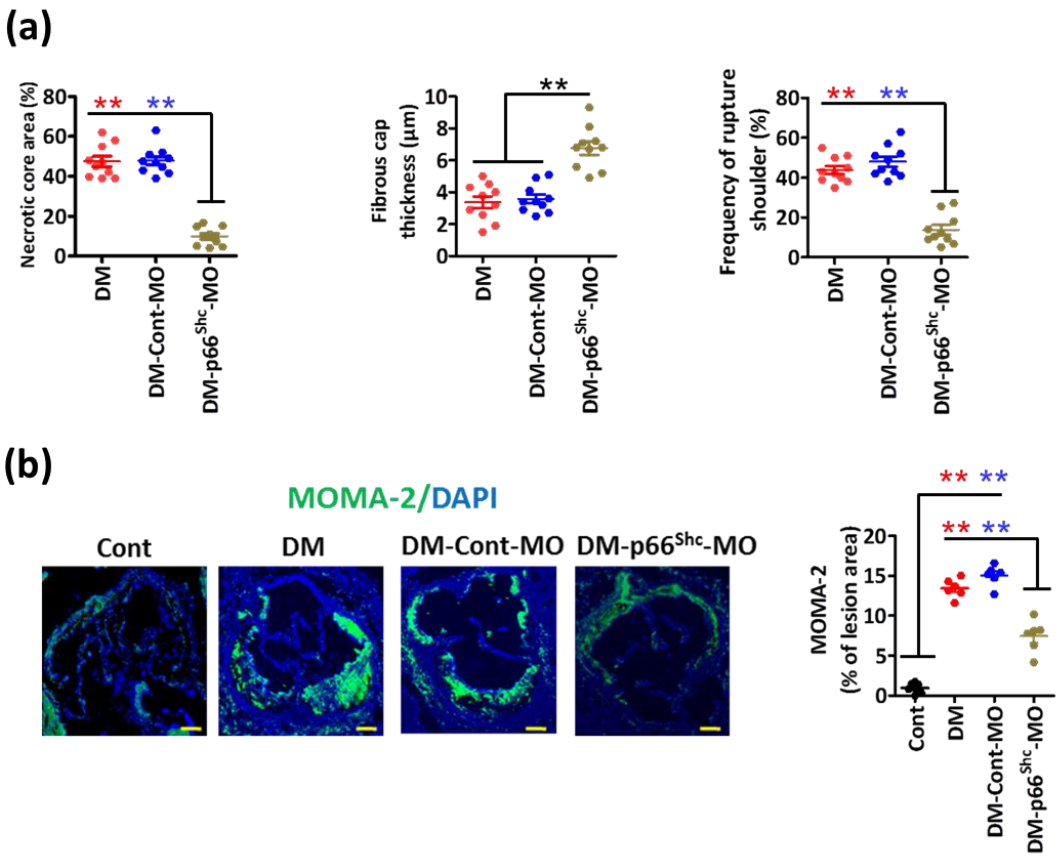

Figure 16: *In vivo* knock down of p66^{Shc} improves plaque stability and reduces macrophage enrichment in hyperglycaemia-induced atherosclerosis.

a: Dot plots summarizing result of necrotic core area (left panel), fibrous cap thickness (middle panel), and frequency of ruptured shoulders (right panel).
b: Representative images showing immunofluorescence staining of macrophages (MOMA-2, green; DAPI nuclear counterstain, blue) within lesions (left panel) and dot-plot summarizing data (right panel).
Cont: normoglycaemic control mice; DM: hyperglycaemic ApoE-/- mice treated with PBS; Cont-MO: hyperglycaemic ApoE-/- mice treated with control vivo morpholino; p66^{Shc}-MO: hyperglycaemic ApoE-/- mice treated with p66^{Shc} specific vivo morpholino. Data shown as dot-plots represent mean ± SEM of 6-10 mice per group (a, b); size bars: d: 20 µm; **P<0.01; one-way ANOVA with Bonferroni adjusted post-hoc comparison of DM and DM-Cont-MO versus Cont and DM-p66^{Shc}-MO versus DM-Cont-MO (b) or DM-p66^{Shc}-MO versus DM-Cont-MO and DM (a).

4.4. Sustained p66^{Shc} and CD36 expression in macrophages

To evaluate whether glucose induces persistent p66^{Shc} expression in macrophages we exposed mouse BMDMs to high LDL (50 µg/ml, HL) or high glucose (25 mM, HG) for 48 hr *in vitro*. High LDL (but not low LDL, Figure 17a) induced p66^{Shc} and CD36 expression. Similarly, high glucose (but not mannitol, Figure 17b) induced p66^{Shc} and CD36 expression. We then ascertained whether normalization of glucose or lipid concentration reverses elevated p66^{Shc} and CD36 expression in BMDMs. Following normalization of LDL for additional 24 hr (HL-NL) p66^{Shc} and CD36 expression returned to baseline (Figure 17a). In contrast, despite normalization of glucose concentration for the last 24 hr (HG-NG) p66^{Shc} and CD36 expression remained elevated in BMDMs (Figure 17b). Thus, high glucose causes a sustained induction of p66^{Shc} and CD36 expression in macrophages in vitro.

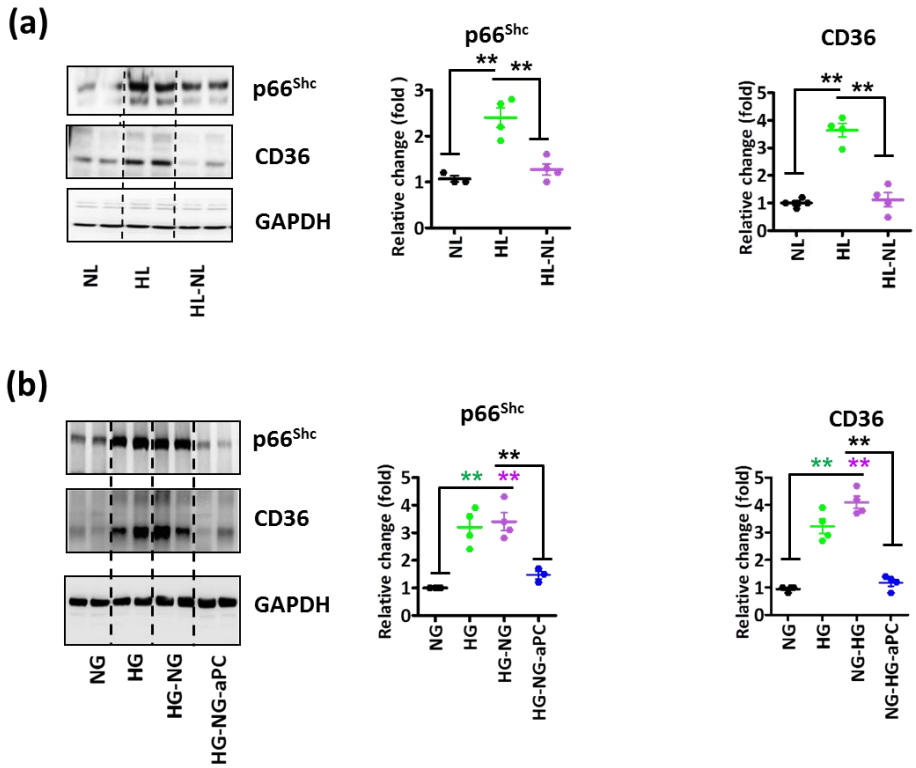

Figure 17: aPC reverses glucose-induced sustained p66^{Shc} expression and the pro-atherogenic phenotype of macrophages

a,b: Representative immunoblot images (out of 4 independent repeat experiments with two technical replicates each, left) and dot-plot summarizing relative expression levels (right panels) of p66^{Shc}, CD36, and GAPDH (loading control) in mouse bone marrow derived macrophages (BMDMs) exposed to different lipid (a) or glucose (b) concentrations without or with additional aPC treatment.
NL: normal LDL; HL: high LDL (50 µg/ml, 48 hr); HL-NL: 50 µg/ml LDL, 48 hr, followed by NL, , 24 hr); NG: normal glucose (5 mM glucose plus 20 mM mannitol, NG, 48 hr); HG: high glucose (25 mM, 48 hr); HG-NG: high glucose followed by normal glucose (25 mM glucose, 48 hr, followed by 5 mM glucose,

24 hr), HG-NG-aPC: HG-NG treated in addition with aPC (20 nM for the last 24 hr); Data shown as dot-plots represent mean ± SEM of at least 3 independent repeat experiments with at least two technical replicates each; **P<0.01; one-way ANOVA with Bonferroni adjusted post-hoc comparison of HL versus NL and HL-NL versus HL (a), HG and HG-NG versus NG and HG-NG-aPC versus HG-NG (a,b).

4.5. aPC reverses sustained $p66^{Shc}$ expression *via* PAR-1

We next determined whether aPC reverses $p66^{Shc}$ expression in glucose stressed macrophages *in vitro*. BMDMs were left untreated or exposed for 48hr to high glucose concentrations, followed by normal glucose concentrations for 24hr (HG-NG). Concomitant aPC treatment (20 nM, HG-NG-aPC) during the 24 hr period of normalized glucose concentrations markedly reduced $p66^{Shc}$ expression as compared to PBS-treated controls (HG-NG, Figure 17b). Parallel changes were observed for CD36 expression, indicating that glucose-induced persistent CD36 expression depends on $p66^{Shc}$, but can be normalized by aPC (Figure 17b).

To evaluate the *in vivo* relevance of these findings we analysed freshly isolated BMDMs, which were *in vivo* conditioned using different treatment schemes: (A) control mice (Cont., no hyperglycaemia), (B) diabetic mice (DM, 22 weeks of persistent hyperglycaemia), and (C) diabetic mice, in which blood glucose levels were normalized for 6 weeks after 16 weeks of persistent hyperglycaemia using the SGLT2-inhbitor dapagliflozin (DM-NG). The DM-NG group was randomly assigned to receive either PBS (DM-NG-PBS) or aPC (DM-NG-aPC) parallel to the treatment with the SGLT2-inhbitor (Figure 1Figure 18a). aPC treatment had no impact on blood glucose levels (Figure 18b).

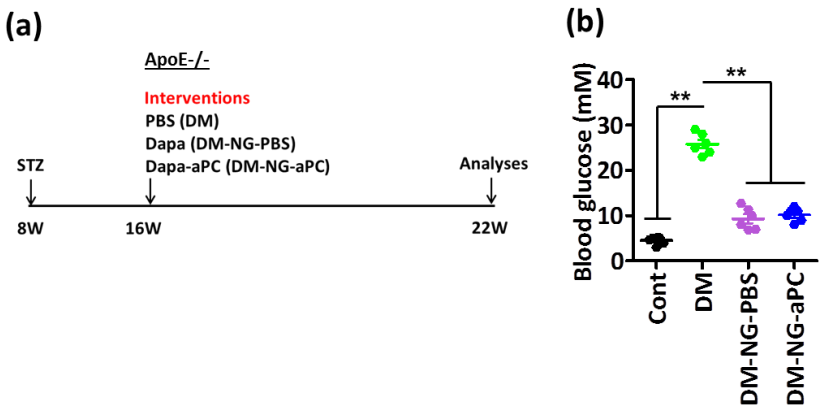

Figure 18: Effect of dapagliflozin and aPC treatment on blood glucose levels in $ApoE^{-/-}$ DM mice

a: Experimental scheme.

b: SGLT2 inhibitor treatment (dapagliflozin) for 6 weeks after 16 weeks of persistent hyperglycaemia (DM-NG-PBS) markedly reduces blood glucose levels. Additional treatment with aPC (DM-NG-aPC) has no further effect on blood glucose levels.
Cont: normoglycaemic ApoE-/- mice with normal chow diet; DM: hyperglycaemic ApoE-/- mice; DM-NG-PBS: SGLT2 inhibitor and PBS treated ApoE-/- DM mice; DM-NG-aPC: DM-NG mice with concomitant aPC and SGLT2 inhibitor treatment. Data shown as dot-plots represent mean ± SEM of 6-8 mice per group (b); **P<0.01; b, one-way ANOVA with Bonferroni adjusted post-hoc comparison of DM versus Cont and DM-NG-aPC and DM-NG-PBS versus DM mice.

Expression of p66^{Shc} was high in BMDMs derived from DM and DM-NG-PBS mice, but markedly reduced in DM-NG-aPC mice (Figure 19a), demonstrating that aPC normalizes glucose-induced sustained p66^{Shc} expression not only *in vitro*, but also *in vivo*.

To identify the receptors through which aPC reduces p66^{Shc} expression in glucose stressed BMDMs we first determined the expression of protease activated receptors (PARs) and endothelial protein C receptor (EPCR) in BMDMs. Expression of PAR1, PAR2, PAR3, PAR4, and EPCR was readily detectable in BMDMs. To determine the functional relevance of these receptors we isolated BMDMs from PAR1$^{-/-}$, PAR2$^{-/-}$, or

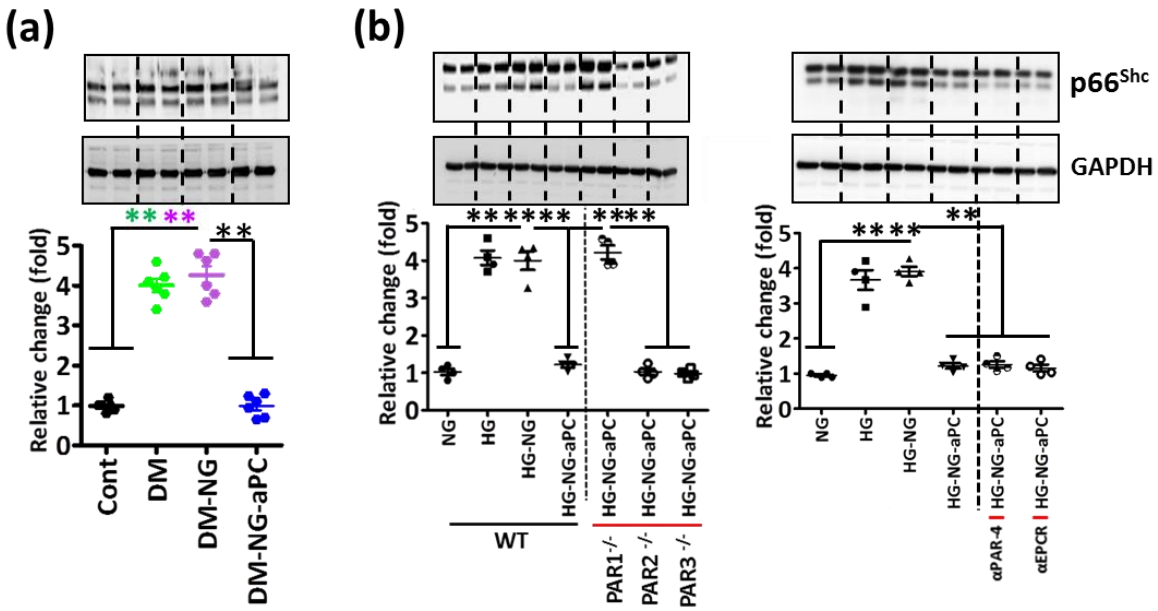

Figure 19: aPC reverses glucose-induced sustained p66^{Shc} expression via PAR1

a: Representative immunoblot images (out of 6 independent repeat experiments with two technical replicates each, top) and dot-plot summarizing data (bottom) of p66^{Shc} and GAPDH (loading control) in BMDMs isolated from non-hyperglycaemic (control, Cont), hyperglycaemic (DM, 22 weeks persistent hyperglycaemia), transiently hyperglycaemic (DM-NG, 16 weeks of sustained hyperglycaemia followed by 6 weeks of SGLT2-inhbitor treatment), or DM-NG-aPC (DM-NG mice with aPC treatment parallel to SGLT2-inhibitors treatment).

b: Representative immunoblot images of p66^{Shc} (out of 4 independent repeat experiments with two technical replicates each) and GAPDH (loading control) in wild-type (WT), PAR1-/-, PAR2-/-, or PAR3-/- BMDMs (b, left panel) and in WT-BMDMs exposed to inhibitory antibodies of PAR4 or EPCR (b, right panels).
DM: hyperglycaemic ApoE-/- mice; DM-NG-PBS: SGLT2 inhibitor and PBS treated ApoE-/- DM mice; DM-NG-aPC: DM-NG mice with concomitant aPC and SGLT2 inhibitor treatment. DM and DM-NG versus Cont and DM-NG-aPC versus DM-NG (a), HG-NG-aPC (αPAR-4 and αEPCR-4 BMDMs) versus HG-NG-aPC (b, right panel) BMDMs. One-way ANOVA with Bonferroni adjusted post-hoc comparison of WT (HG and HG-NG versus NG and HG-NG-aPC versus HG-NG) and HG-NG-aPC (PAR3-/-and PAR2-/-BMDMs) versus HG-NG-aPC (PAR1-/- BMDMs) (b, left panel).

PAR3$^{-/-}$ mice, while PAR4 or EPCR function was blocked in wild-type BMDMs using inhibitory antibodies. PAR1 deficiency efficiently abolished p66^{Shc} inhibition by aPC, whereas PAR2, PAR3 deficiency or PAR4 and EPCR inhibition had no effect (Figure 19). Hence, PAR-1 is required for the aPC-dependent inhibition of glucose-induced sustained p66^{Shc} expression in BMDMs.

4.6. aPC reverses the sustained atherogenic macrophage phenotype

To determine whether aPC modulates p66^{Shc} dependent functional consequences in macrophages we analysed ROS and inflammatory markers. In HG exposed BMDMs 8-Oxo-dG (8-Oxo-2'-deoxyguanosine) and nitrotyrosine, both reflecting ROS generation, were induced and remained high despite normalization of glucose levels (HG-NG, Figure 20a,b). The sustained expression of these ROS-markers was reversed by concomitant aPC treatment (HG-NG-aPC, Figure 20a,b).

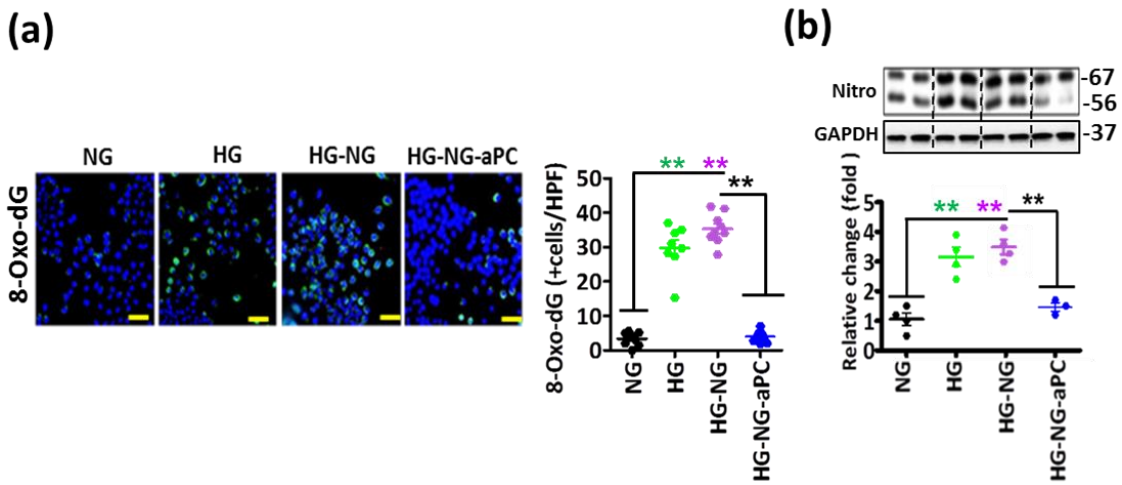

Figure 20: aPC reverses the glucose-induced ROS in macrophages

a,b: Representative co-immunofluorescence images (a, left panel) for 8-Oxo-dG (green; DAPI nuclear counterstain, blue) and immunoblots images (out of 3 independent repeat experiments with two technical replicates each) for nitrotyrosine (Nitro, b, top; GAPDH: loading control) of BMDMs with treatment as indicated and dot-plot summarizing data (a, right panel, b, bottom).
NG: normal glucose (5 mM glucose plus 20 mM mannitol, 48 hr), HG: high glucose (25 mM, 48 hr), HG-NG: HG (48 hr) followed by NG (24 hr) condition; HG-NG-aPC: HG-NG conditions with additional exposure to aPC (20 nM) during the last 24 hr). Data shown as dot-plots represent mean ± SEM of at least 3 independent repeat experiments with at least two technical replicates each; **P<0.01 (one-way ANOVA with Bonferroni adjusted post-hoc comparison of HG and HG-NG versus NG and HG-NG-aPC versus HG-NG).

In parallel, IL-6, TNF-α, and NF-κB p65 expression were induced in BMDMs and remained high despite normalization of glucose levels, but were reversed by concomitant aPC treatment (HG-NG-aPC, Figure 21a-e).

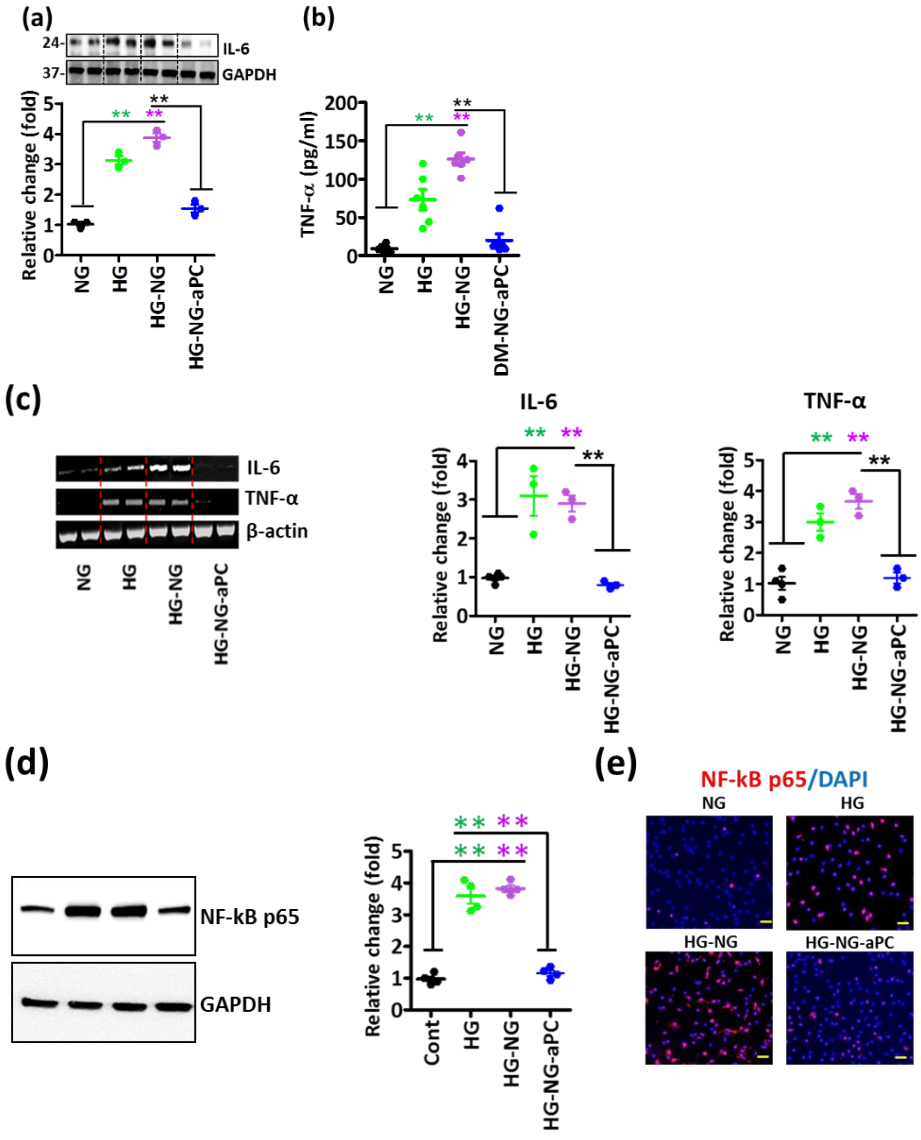

Figure 21: aPC reverses glucose induced and sustained expression of pro-inflammatory markers in macrophages

a: Representative immunoblot images of IL-6 (a, out of 3 independent repeat experiments each with two technical replicates, top; GAPDH: loading control) and dot-plot summarizing data representing of three independent experiments (a, bottom).
b: Dot-plot summarizing data of TNF-α level determined by ELISA representing six independent experiments.
c: Representative reverse-transcriptase-PCR gel images (out of 3 independent repeat experiments with two technical replicates each) for IL-6 and TNF-α (right panel; β-actin: loading control) and dot-plot summarizing data (middle and right panels, respectively).
d: Representative immunoblot images (out of 4 independent repeat experiments with two technical replicates each) for NF-κB p65 (top panel; GAPDH: loading control) and dot-plot summarizing data (bottom).
e: Representative co-immunofluorescence images (out of 3 independent repeat experiments) for NF-κB p65 (red) and DAPI counterstain (blue).
NG: normal glucose (5 mM glucose plus 20 mM mannitol, 48 hr), HG: high glucose (25 mM, 48 hr), HG-NG: HG (48 hr) followed by NG (24 hr) condition; HG-NG-aPC: HG-NG conditions with additional exposure to aPC (20 nM) during the last 24 hr). Data shown as dot-plots represent mean ± SEM of at least 3 independent repeat experiments with at least two technical replicates each; **P<0.01 (one-way ANOVA with Bonferroni adjusted post-hoc comparison of HG and HG-NG versus NG and HG-NG-aPC versus HG-NG).

In agreement with the observed CD36 expression pattern lipid uptake by BMDMs was increased by HG and remained high despite normalization of glucose levels (HG-NG, Figure 22), but was normalized by aPC (HG-NG-aPC, Figure 22). Thus, glucose induces sustained pro-inflammatory and pro-atherogenic effects in macrophages *in vitro*, which can be efficiently reversed by aPC.

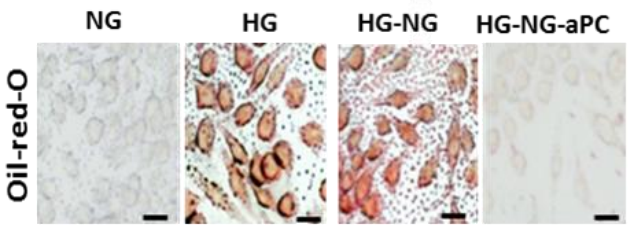

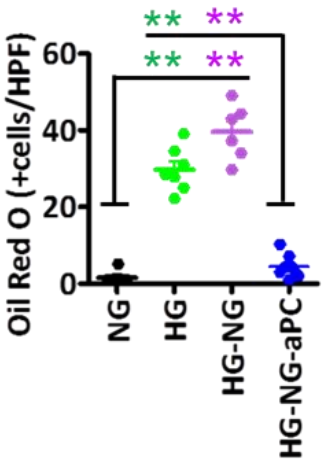

Figure 22: Oil Red O images reflecting lipid uptake into BMDMs

Representative Oil Red O images reflecting lipid uptake into BMDMs (left panel) and dot-plot summarizing data (right panel).

4.7. aPC epigenetically inhibits sustained p66^{Shc} expression

We next analysed p66^{Shc} promoter methylation in macrophages. Compared to control BMDMs (normal glucose, NG) CpG dinucleotides within the p66^{Shc} promoter were hypomethylated in BMDMs maintained under hyperglycaemic conditions (HG, Figure 23a). The p66^{Shc} promoter remained hypomethylated despite normalization of glucose levels for 24 hr (HG-NG, Figure 23a). However, concomitant aPC treatment restored p66^{Shc} promoter methylation (Figure 23a). Corresponding changes were observed for p66^{Shc} mRNA levels (Figure 23b).

To gain further mechanistic insights we determined DNMTs expression parallel to p66^{Shc} expression in BMDMs. The expression pattern of DNMT1 was opposite to that of p66^{Shc} (Figure 23c), while DNMT3a and DNMT3b expression remained unchanged. We observed concomitant changes in DNMT-activity (Figure 23d). Of note, the DNMTs-inhibitor 5-azacytidine (Aza) abolished the inhibitory effect of aPC on glucose sustained p66^{Shc} expression (HG-NG-aPC-Aza, Figure 23c). This suggests that the induction of DNMT1 by aPC is required for aPC-mediated repression of sustained p66^{Shc} expression.

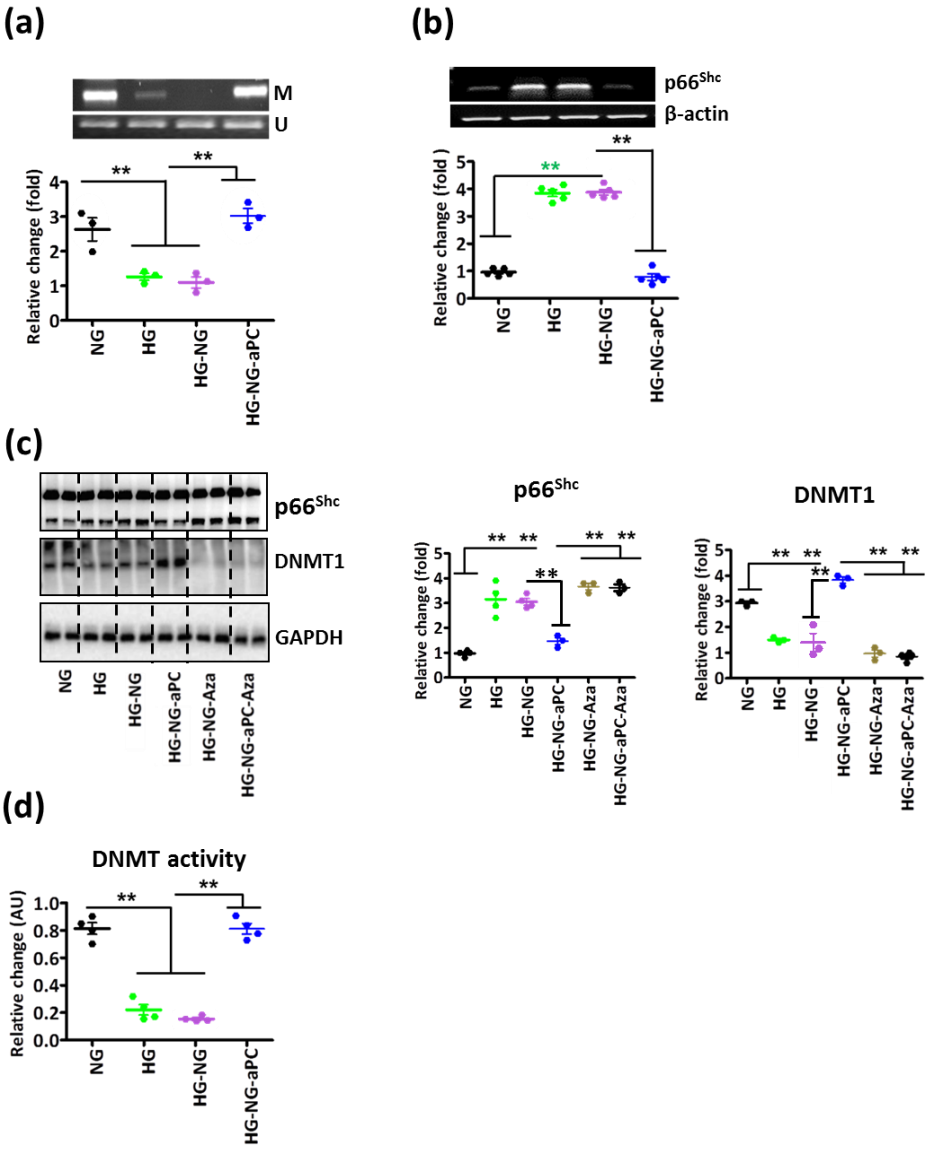

Figure 23: aPC epigenetically inhibits glucose-induced sustained p66^{Shc} expression

a: Representative reverse-transcriptase-PCR gel images (out of 3 independent repeat experiments, top) showing methylated (M) and unmethylated (U) p66^{Shc} promoter DNA in BMDMs with treatment

as indicated and dot-plot summarizing the ratio of methylated to unmethylated $p66^{Shc}$ promoter DNA (bottom).
b: Glucose-induced sustained $p66^{Shc}$ mRNA expression is prevented by aPC (20 nM) in BMDMs cells. Representative RT-PCR gel image (out of 5 independent repeat experiments, top; β-actin: loading control) and dot-plot summarizing data (bottom).
c: Representative immunoblot images (out of 3 independent repeat experiments with two technical replicates each) for $p66^{Shc}$ and DNMT1 expression in BMDMs with treatment as indicated (left panel; GAPDH: loading control) and dot-plot summarizing data (middle and right panels).
d: dot-plot summarizing DNMT activity in BMDMs with treatment as indicated.
NG: normal glucose (5 mM glucose plus 20 mM mannitol, 48 hr), HG: high glucose (25 mM, 48 hr). HG-NG: HG (24 hr) followed by NG (24 hr) condition; HG-NG-aPC: HG-NG conditions with additional exposure to aPC (20 nM) during the last 24 hr); HG-NG-Aza: HG-NG conditions with additional exposure to the DNMT-inhibitor 5-azacytidine (Aza, 5μM) during the last 24 hr; HG-NG-aPC-Aza: HG-NG conditions with additional and concomitant exposure to aPC (20 nM) and 5-azacytidine (5μM) during the last 24 hr. Data shown represent mean ± SEM of at least three independent experiments each with at least two technical replicates (a-d); **P<0.01; one-way ANOVA with Bonferroni adjusted post-hoc comparison of HG and HG-NG versus NG, HG-NG-aPC versus HG-NG (a,b,d), and HG-NG, HG-NG-Aza, HG-NG-aPC-Aza versus DM-NG-aPC).

4.8. Sustained p66^{Shc} impairs atherosclerosis regression

We next evaluated whether glucose-induced epigenetic p66^{Shc} expression contributes to the hyperglycaemic memory in macrovascular disease and whether this can be reversed by aPC. First, we established a "memory effect" in glucose, but not in lipid exposed ApoE$^{-/-}$ mice (see experimental scheme, Figure 24a). Aortic root plaque size was prominently reduced following lowering of blood lipid levels in HFD-adeno hApoE versus HFD-adeno LacZ mice (Figure 24b-e). Conversely, the size of atherosclerotic plaques remained unchanged following restoration of normoglycaemia (Figure 24b-e), reflecting sustained plaques size secondary to the hyperglycaemic memory.

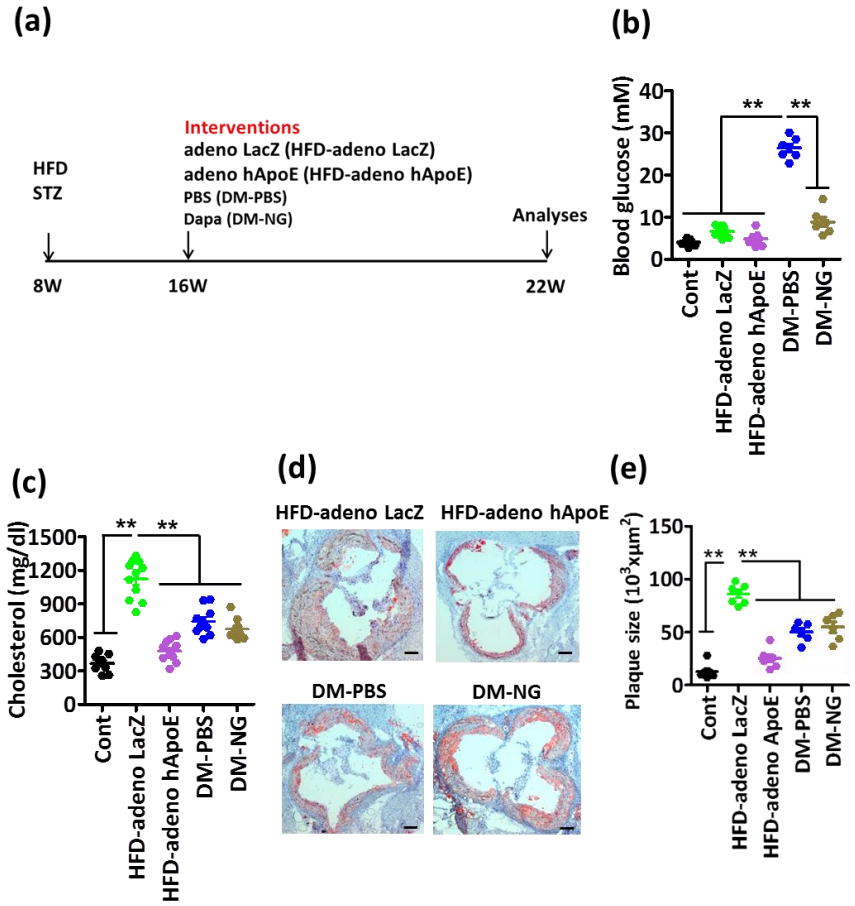

Figure 24: Atherosclerotic plaque regression is impaired in diabetic, but not hyperlipidaemic mice

a: Experimental scheme.
b,c: Dot-plot summarizing blood glucose (b) and total plasma cholesterol levels in experimental mice.
d,e: Plaque size regressed in HFD-adenohApoE versus HFD-adenoLacZ mice but remained stable in DM-NG versus DM-PBS mice. Representative Oil Red O staining of aortic roots lesion (d) and dot-plot summarizing results (e).

Cont: normoglycaemic ApoE-/- mice with normal chow diet; HFD-adeno LacZ: HFD ApoE-/- mice treated with control LacZ adenovirus; HFD-adeno hApoE: HFD ApoE-/- mice treated with human ApoE expressing adenovirus; DM-NG: ApoE -/- DM mice treated with SGLT2 inhibitor weeks 16 to 22; DM-PBS: DM mice treated with PBS. Data shown represent mean ± SEM of 6-10 mice per group (b, c, e); **P<0.01; one-way ANOVA with Bonferroni adjusted post-hoc comparison of DM-PBS versus Cont, HFD-adeno LacZ, HFD-adeno ApoE, and DM-NG (a), HFD-adeno LacZ versus Cont, DM-PBS, DM-NG, HFD-adeno ApoE (c,e).

Using this model, we were able to determine whether aPC reverses the hyperglycaemic memory effect in the context of atherosclerosis in vivo. Indeed, concomitant aPC treatment in addition to blood-glucose reduction markedly reduced the size of aortic root plaques when compared to mice in which only blood glucose levels were normalized (DM-NG-aPC versus DM-NG-PBS, Figure 25).

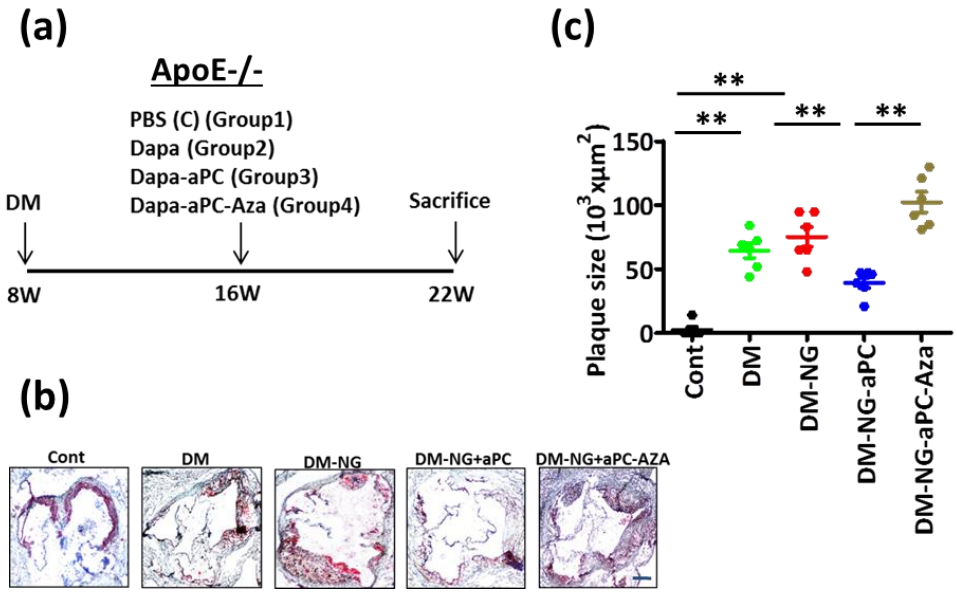

Figure 25: aPC promotes atherosclerotic plaque regression in mice

Experimental design (a) and representative Oil Red O stained images of aortic roots (b) and dot-plot summarizing data (c).

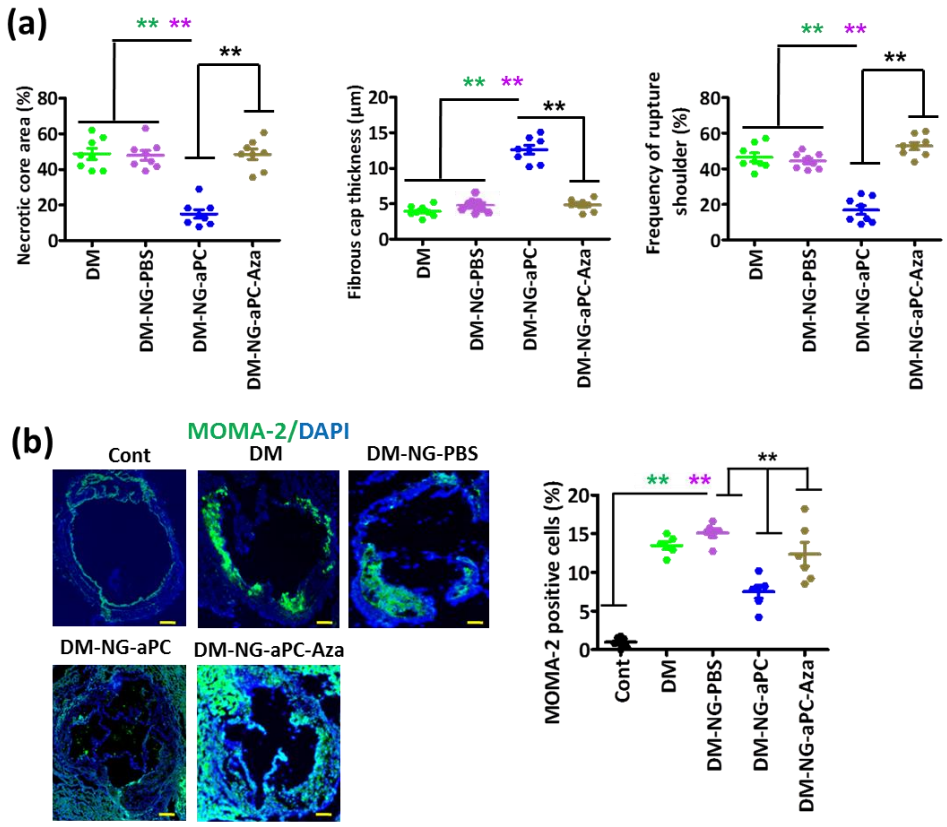

Figure 26: aPC reverses hyperglycaemia-induced plaque instability

a: Morphometric analyses of haematoxylin and eosin stained images showing necrotic core area (left panel), fibrous cap thickness (middle panel), and frequency of ruptured shoulders (right panel). b: Representative images showing immunofluorescence staining of macrophages (MOMA-2, green; DAPI nuclear counterstain, blue) within lesions (left panel) and dot-plot summarizing data (right panel).

Importantly, concomitant aPC treatment reduced $p66^{Shc}$ expression, ROS-generation (8-Oxo-dG) and IL-6 expression, while normalization of blood glucose levels alone had no impact on these parameters (Figure 27a-d). Treatment of mice with 5-azacytidine in addition to aPC-treatment and blood glucose normalization (DM-NG-aPC-Aza) abolished aPC's effects (Figure 27a-d).

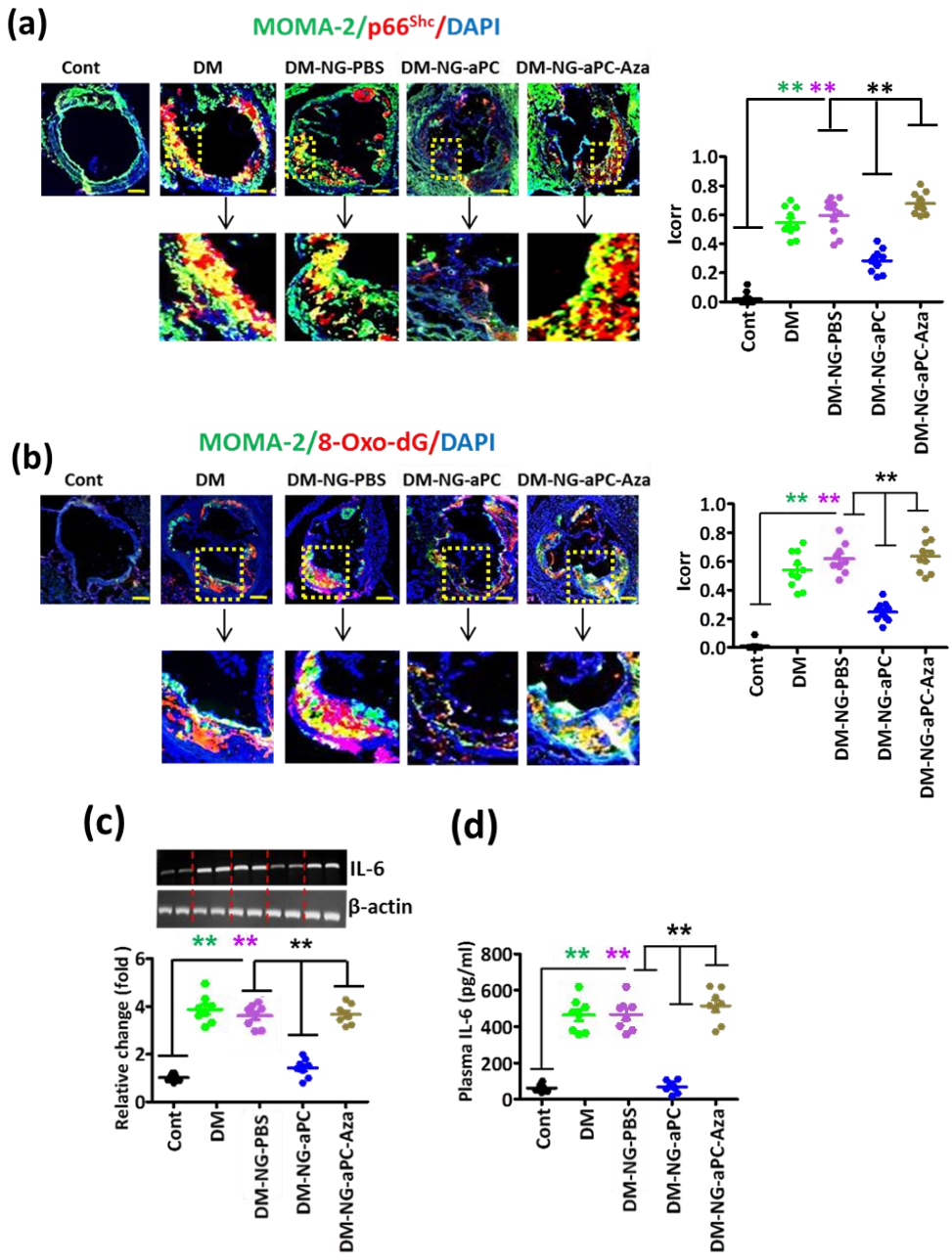

Figure 27: aPC reverses hyperglycaemic induced and epigenetically sustained p66^{Shc} expression, ROS-generation and persistent IL-6 expression

a,b: Representative co-immunofluorescence images for p66^{Shc} (a, red), 8-Oxo-dG (b, red), macrophages (MOMA-2, a,b, green), and DAPI nuclear counterstain (a,b, blue; boxed areas shown at higher magnification in the lower panel). Dot-plot summarize data for p66^{Shc}-MOMA-2 (a) and 8-Oxo-dG-MOMA-2 co-localization (b, both Icorr, correlation index).

c, d: Representative reverse-transcriptase-PCR gel images (c, top, β-actin as loading control) and dot-plot summarizing for IL-6 protein expression (c). Dot-plot summarizing data of plasma IL-6 levels (d).

Cont: normoglycaemic ApoE-/- mice with normal chow diet; DM: hyperglycaemic ApoE-/- mice; DM-NG-PBS: ApoE-/- DM mice receiving the SGLT2 inhibitor and PBS from week 16 to week 22; DM-NG-aPC: ApoE-/- DM mice with concomitant SGLT2 inhibitor and aPC treatment from week 16 to week 22; DM-NG-aPC-Aza: DM-NG mice with concomitant SGLT2 inhibitor, aPC, and 5-azacytidine. Data shown as dot-plots represent mean ± SEM of 8-10 mice per group (a, c); size bars: a-c: 20 µm; **P<0.01 (one-way ANOVA with Bonferroni adjusted post-hoc comparison of DM and DM-NG-aPC versus control and DM-NG-PBS and DM-NG-aPC-Aza versus DM-NG-aPC).

Treatment with aPC or 5-azacytidine had no impact on body weight, blood glucose levels, or total plasma cholesterol levels (Figure 28a-c).

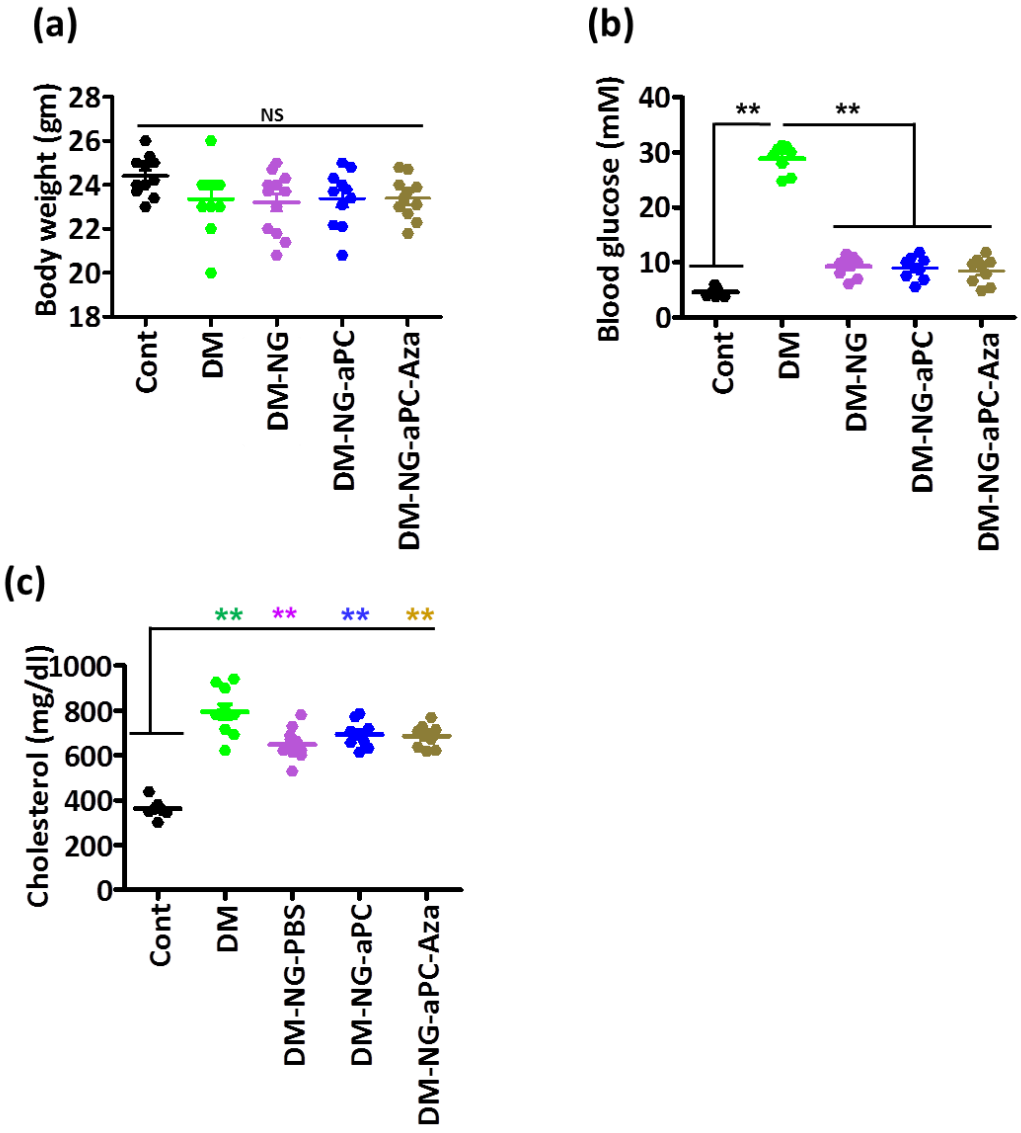

Figure 28: Effect of 5-azacytidine on body weight, blood glucose, and total plasma cholesterol levels in ApoE$^{-/-}$ DM mice

Treatment of mice with 5-azacytidine (Aza) in addition to aPC and blood glucose normalization (DM-NG-aPC-Aza) has no impact on body weight (a, compared to all other groups), blood glucose levels (b,

compared to DM-NG-PBS and DM-NG-aPC) or total plasma cholesterol levels (c, compared to DM, DM-NG-PBS and DM-NG-aPC).
Cont: normoglycaemic ApoE-/- mice with normal chow diet; DM: hyperglycaemic ApoE-/- mice; DM-NG-PBS: SGLT2 inhibitor and PBS treated ApoE-/- DM mice; DM-NG-aPC: SGLT2 inhibitor and aPC treated ApoE-/- DM mice; DM-NG-aPC-Aza: SGLT2 inhibitor, aPC and 5-azacytidine treated ApoE-/- DM mice. Data shown as dot-plots represent mean ± SEM of 8-10 mice per group; NS: not significant, **P<0.01; one-way ANOVA with Bonferroni adjusted post-hoc comparison of DM, DM-NG-PBS, DM-NG-aPC and DM-NG-aPC-Aza versus Cont (a,c), DM versus Cont, DM-NG-PBS, DM-NG-aPC and DM-NG-aPC-Aza (b).

Taken together, these data demonstrate that aPC in addition to normalization of blood glucose levels reverses the high glucose-induced sustained $p66^{Shc}$ expression and atherosclerotic plaque phenotype in $ApoE^{-/-}$ mice.

4.9. aPC reverses diabetes mellitus-associated atherosclerosis via DNMT1

We next determined the *in vivo* relevance of DNMT1 for the aPC-mediated reversion of sustained $p66^{Shc}$ expression in macrophages. Expression of DNMT1 was reduced in the aorta of diabetic (DM) animals and remained low despite normalization of blood glucose levels for 6 weeks after 16 weeks of persistent hyperglycaemia (DM-NG, Figure 29). Concomitant treatment with aPC restored DNMT-1 expression (DM-NG-aPC, Figure 29).

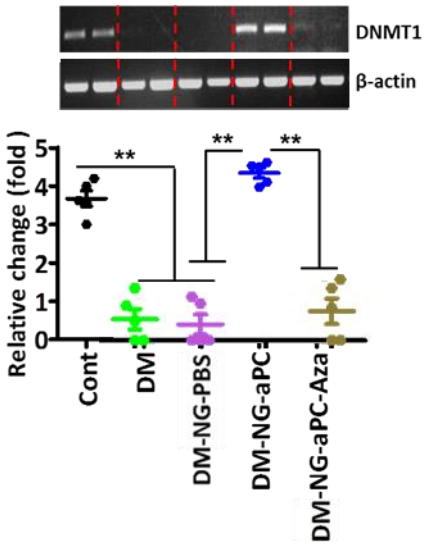

Figure 29: DNMT1 mRNA expression in aorta

Representative semi-quantitative reverse-transcriptase-PCR gel image of DNMT1; β-actin as loading control.
Cont: normoglycaemic ApoE-/- mice with normal chow diet; DM: hyperglycaemic ApoE-/- mice; DM-NG-PBS: SGLT2 inhibitor and PBS treated ApoE-/- DM mice; DM-NG-aPC: SGLT2 inhibitor and aPC treated ApoE-/- DM mice; DM-NG-aPC-Aza: SGLT2 inhibitor, aPC and 5-azacytidine treated ApoE-/- DM mice. Data shown as dot-plots represent mean ± SEM of 6 mice per group; **P<0.01; one-way

ANOVA with Bonferroni adjusted post-hoc comparison of DM and DM-NG-PBS versus Cont and DM-NG-aPC versus DM-NG-aPC-Aza and DM-NG-PBS.

Since constitutive genetic DNTM1 deficiency is lethal in mice, we inhibited DNMT1 expression in diabetic ApoE$^{-/-}$ mice using vivo morpholinos (DNMT1-MO, Figure 30a).

ApoE$^{-/-}$ mice with hyperglycaemia (DM) for 16 weeks followed by 6 weeks of normoglycaemia (NG, achieved by SGLT2 inhibitor treatment) and concomitant aPC treatment were injected with a DNMT1 specific morpholinos (DM-NG-aPC-DNMT1-MO) or a non-specific control morpholino (DM-NG-aPC-Cont-MO, Figure 30a). The DNMT1 specific morpholino sufficiently reduced DNMT1 expression in the aorta (DM-NG-aPC-DNMT1-MO), while a control morpholino (DM-NG-aPC-Cont-MO) had no impact (Figure 30a).

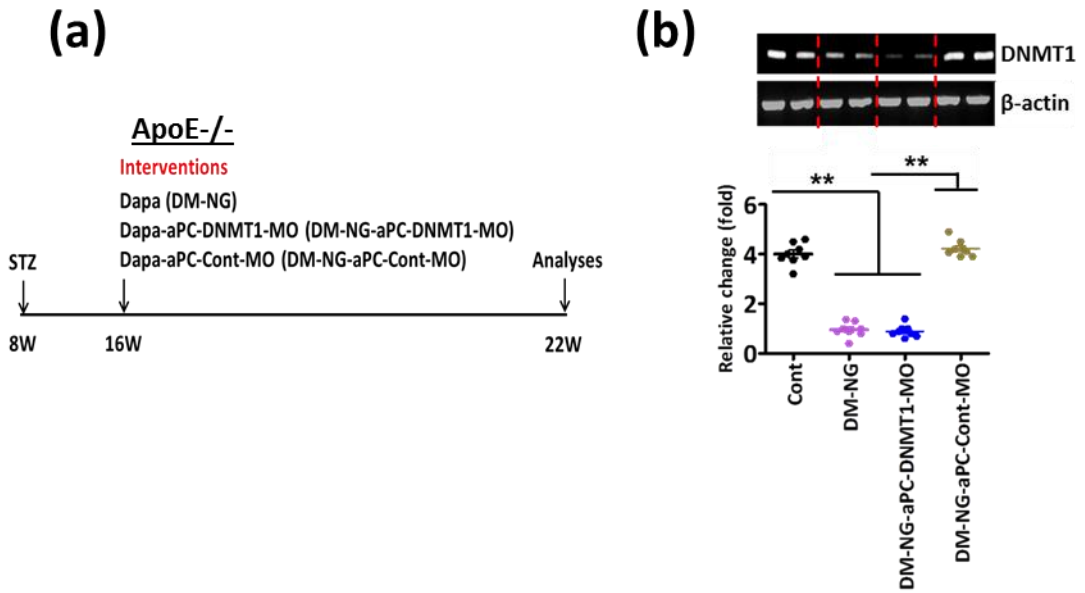

Figure 30: Experimental design and effects of aPC treatment in mice following DNMT1 in vivo silencing

a: Experimental design.
b: Representative reverse-transcriptase-PCR gel images for DNMT1 expression (b, β-actin as loading control, top) and dot-plot summarizing data (b, bottom).

Suppression of DNMT1 expression abolished the effect of aPC, as reflected by a failure of aPC to reduce plaque size (Figure 31a) or to improve plaque stability, as reflected by an unchanged necrotic core area, fibrous cap thickness, frequency of rupture shoulder (Figure 31b), and frequency of plaque-associated macrophages (Figure 31c) in DM-NG-aPC-DNMT1-MO mice as compared to DM-NG mice. (Figure 31b,c). Likewise, aPC failed to reduce 8-Oxo-dG levels,

p66^{Shc} expression, and IL-6 expression in the aorta (Figure 31d-f). Treatment with vivo-morpholinos had no impact on body weight, blood glucose, or total plasma cholesterol levels. Thus, the aPC-mediated reversal of the hyperglycaemic memory phenotype in hyperglycaemic ApoE$^{-/-}$ mice depends on DNMT1.

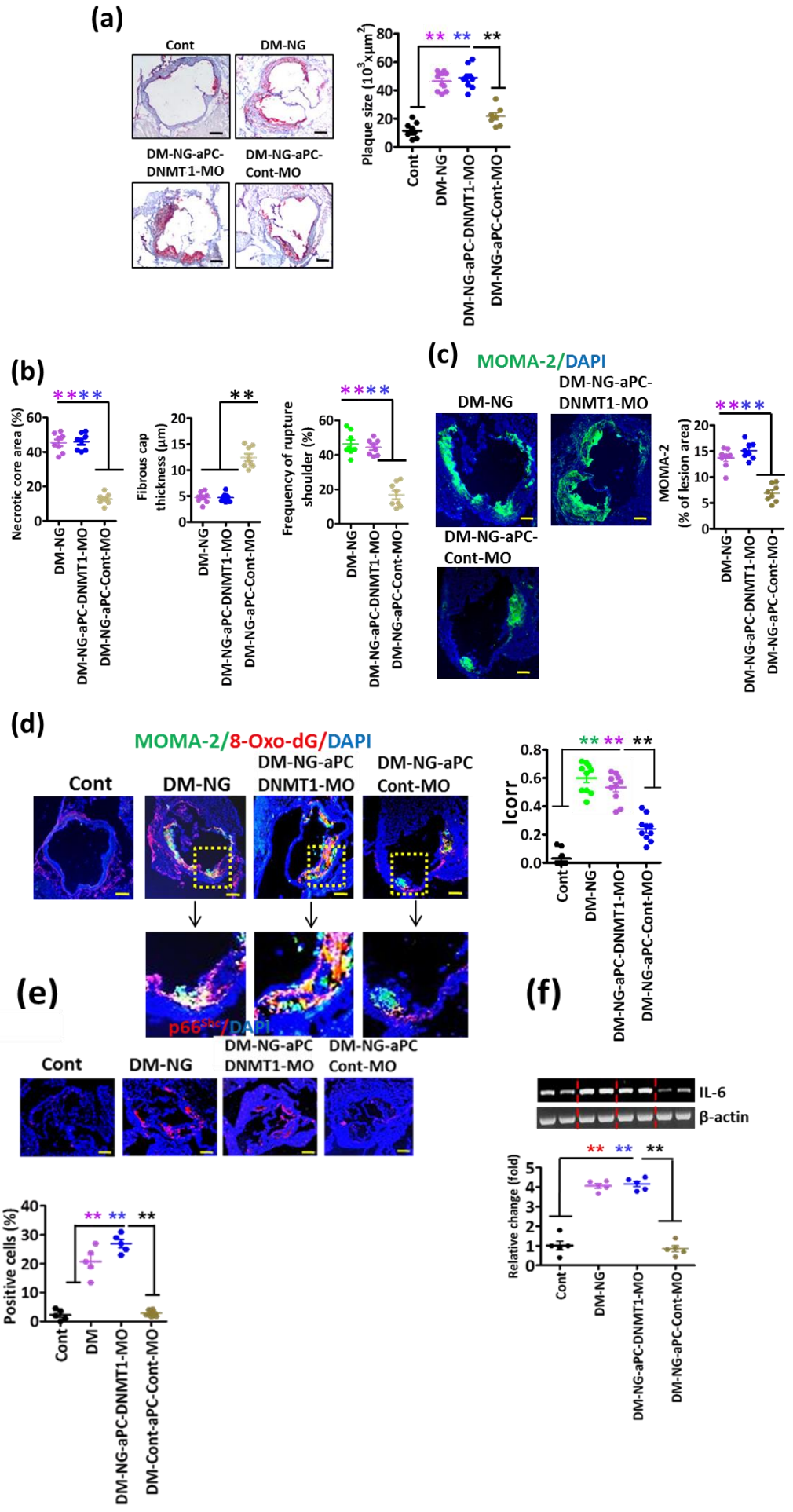
(a)
Cont
DM-NG
DM-NG-aPC-DNMT1-MO
DM-NG-aPC-Cont-MO
Plaque size (10^3xμm^2)
Cont
DM-NG
DM-NG-aPC-DNMT1-MO
DM-NG-aPC-Cont-MO
(b)
Necrotic core area (%)
Fibrous cap thickness (μm)
Frequency of rupture shoulder (%)
(c)
MOMA-2/DAPI
DM-NG
DM-NG-aPC-DNMT1-MO
DM-NG-aPC-Cont-MO
MOMA-2 (% of lesion area)
(d)
MOMA-2/8-Oxo-dG/DAPI
Cont
DM-NG
DM-NG-aPC DNMT1-MO
DM-NG-aPC Cont-MO
Icorr
(e)
p66Shc/DAPI
Positive cells (%)
(f)
IL-6
β-actin
Relative change (fold)

Figure 31: aPC mediated reversal of hyperglycaemia-induced persistent p66^{Shc} expression and plaque instability depends on DNMT1

a: Representative images of Oil Red O stained aortic root lesions (left panel) and dot-plot summarizing data (right panel).
b: Dot-plots summarizing morphometric analyses of necrotic core area (left panel), fibrous cap thickness (middle panel), and frequency of ruptured shoulders (right panel).
c: Representative images showing immunofluorescence staining of macrophages within lesions (MOMA-2, green; DAPI nuclear counterstain, blue; left panel) and dot-plot summarizing data (right panel).
d: Representative co-immunofluorescence images for 8-Oxo-dG (red), macrophages (MOMA-2, green), and DAPI nuclear counterstain (blue) within aortic root lesions (left, 10 x magnified images shown in lower panel) and dot-plot summarizing data (Icorr, correlation index, right).
e: Representative co-immunofluorescence images (top panel) for p66Shc (red), DAPI nuclear counterstain (blue), and dot-plot summarizing data (bottom panel).
f: Representative reverse-transcriptase-PCR gel images for IL-6 expression (β-actin as loading control, top) and dot-plot summarizing data (bottom).
Cont: normoglycaemic ApoE-/- mice with normal chow diet; DM-NG: ApoE-/- DM mice receiving the SGLT2 inhibitor and PBS from week 16 to week 22; DM-NG-aPC-DNMT1-MO: DM-NG mice with concomitant SGLT2 inhibitor, aPC, and DNMT1-MO treatment; DM-NG-aPC-Cont-MO: DM-NG mice with concomitant SGLT2 inhibitor, aPC, and control morpholino treatment. Data shown as dot-plots represent mean ± SEM of 8-10 mice per group; size bars: a, c, d: 20 µm; **P<0.01; b-e: one-way ANOVA with Bonferroni adjusted post-hoc comparison of DM-NG and DM-NG-aPC-DNMT1-MO versus DM-NG-aPC-Cont-MO).

5. Discussion

Reduced thrombomodulin expression and aPC plasma levels have been clinically associated with diabetes mellitus and its vascular complications [70, 73, 98-100]. While impaired thrombomodulin-dependent protein C activation has been mechanistically linked with diabetic microangiopathy[39, 70, 101, 102] the role of aPC in diabetic macroangiopathy remained unknown. Here we demonstrate that aPC reverses the hyperglycaemic memory by correcting glucose-induced p66^{Shc} promoter hypomethylation in macrophages *via* a DNMT1 dependent mechanism. Thus, aPC in addition to blood glucose normalization reduces the atherosclerotic plaque burden, signs of plaque instability, and associated inflammation. Importantly, the current data do not only identify a new mechanism contributing to the hyperglycaemic memory in atherosclerosis (glucose induced and DNMT1 dependent sustained p66^{Shc} expression in macrophages), but also identifies a potential therapeutic approach to the atherosclerosis-associated hyperglycaemic memory. The current data suggest that targeting p66^{Shc} expression in macrophages either directly (as demonstrated by the vivo morpholino approach) or indirectly by employing aPC-based therapies is a feasible approach to combat the hyperglycaemic memory in atherosclerosis [63, 103].

By directly comparing hyperglycaemic ApoE-/- (ApoE-/- DM) mice to non-diabetic ApoE-/- mice on a high fat diet (ApoE-/- HFD) we first show that the expression of the redox regulator p66^{Shc} in bone marrow derived cells is a major determinant of plaque development and instability in hyperglycaemic conditions. While normalization of blood glucose levels alone fails to reduce glucose-induced and epigenetically sustained p66^{Shc} expression in macrophages, aPC in addition to blood glucose normalization reverses glucose-induced p66^{Shc} promoter hypomethylation, p66^{Shc} expression in macrophages and associated ROS generation. These aPC-mediated consequences are congruent with aPC's anti-oxidant effects and its effect on p66^{Shc} expression in glucose stressed podocytes (renal epithelial cells) [39, 104].

We specifically addressed the consequences of persistently elevated glucose level and associated changes for the hyperglycaemic memory in the current manuscript. The results show that hyperglycaemia *per se* drives plaque instability in murine models of hyperglycaemia-associated atherosclerosis. These findings add to previous important work, demonstrating that insulin-resistance promotes unstable plaques through chronic inflammation [105-107]. Hence, we propose that insulin resistance and hyperglycaemia both

promote plaque instability, and that the concurrence of insulin resistance and hyperglycaemia in insulin-resistance type 2 diabetic patients may synergistically promote plaque instability. Accordingly, we cannot exclude that other metabolic changes, such as obesity, increased insulin levels, or impaired insulin signaling, contribute to a "memory" effect in type 2 diabetic patients. Indeed, epigenetic control of $p66^{Shc}$ in association with obesity has been recently reported [108]. Here the methyltransferase SUV39H1 was identified as a key regulator modulating $p66^{Shc}$ expression by orchestrating recruitment of JMJD2C (a demethylase) and SRC-1 (an acetyltransferase) to the $p66^{Shc}$ promoter [108]. Intriguingly, SUV39H1 forms a complex with DNMT1 [109], suggesting that SUV39H1 and DNMT1 coordinately modulate the epigenetic landscape controlling $p66^{Shc}$ expression. Further characterization of the complex modulating the $p66^{Shc}$-associated epigenetic landscape and thus $p66^{Shc}$ expression may identify additional therapeutic targets. This may lay ground for individualized treatment strategies in the context of diabetes mellitus-associated atherosclerosis, as recently proposed [110].

The translational relevance of the current finding is supported by a recent clinical study which demonstrated that $p66^{Shc}$ expression is epigenetically increased in peripheral blood monocytes of type 2 diabetic patients[41]. In agreement with these clinical results we observed increased $p66^{Shc}$ expression in plaque-associated macrophages of diabetic, but not of non-diabetic patients and mice. The concordant observation in human peripheral blood monocytes[41], human plaque associated macrophages (Figure 11), and the murine data presented within this manuscript argue against sustained $p66^{Shc}$ expression in ApoE-/-DM mice as a consequence of toxic streptozotocin effects[111]. Congruently, we were not able to detect increased cell death, markers of the DNA damage response, or liver toxicity in STZ-injected ApoE-/- mice. Taken together, these studies identify $p66^{Shc}$ as an epigenetically controlled gene modulating the phenotype of monocytes and macrophages in diabetes mellitus. We speculate that the $p66^{Shc}$ dependent modulation of the macrophage phenotype constitutes a diabetes mellitus-specific facet of trained innate immunity [112, 113]. aPC-based approaches may allow modulation of trained innate immunity in the context of diabetes mellitus.

The pivotal role of p66^{Shc} in bone marrow derived cells, the co-localization of p66^{Shc} with macrophages, and the expression of pro-atherogenic (CD36) and pro-inflammatory (NF-κB p65, IL-6, and TNFα) genes in hyperglycaemia-associated macrophages are entirely congruent with the previously proposed pathogenetic function of macrophages in diabetes mellitus-associated atherosclerosis in animal [114-116] and clinical studies [117]. In extension of previous work, we thus identify p66^{Shc} as a specific regulator of diabetes mellitus-associated atherosclerosis [118]. Different pathways through which increased and sustained p66^{Shc} expression may impair plaque stability, such as increased macrophages cell death, enhanced ROS-induced inflammasome activation, or impaired efferocytosis may contribute to impaired plaque stability in hyerglycaemic mice. Similar to p66^{Shc}, ACSL-1 (long-chain acyl-CoA synthetase 1, an enzyme that catalyzes the thioesterification of fatty acids) promotes atherosclerotic plaque development specifically in a diabetic milieu [119]. Collectively, these studies support the concept of a specific pathophysiology underlying diabetes mellitus-associated atherosclerosis, thus providing a rationale for "individualized" therapeutic strategies in patients with diabetes mellitus-associate atherosclerosis.

Hyperglycaemia is thought to cause mitochondrial dysfunction, thus promoting diabetes mellitus-associated vascular complications [120]. The role of p66^{Shc} for diabetic vascular complications, as shown here and previously [38, 39, 120], supports a pivotal role of mitochondrial ROS generation. Excess ROS-generation activates the redox-sensitive transcription factor NF-κB, promoting a pro-inflammatory micromilieu-characterized by increased IL-6, TNFα, CCL2, or VCAM-1 expression [121]. Intriguingly, inhibition of pro-inflammatory NF-κB signalling by aPC has been demonstrated before [86, 122] but the underlying mechanism remained unknown. Given the current insights we propose that aPC restricts p66^{Shc}-mediated ROS generation and thus NF-κB signalling. Additionally, increased ROS-generation promotes NO-uncoupling and inflammasome activation, which are closely linked with diabetic vascular complications [123]. The observed induction of IL-6 and TNFα in glucose stressed macrophages is entirely congruent with these observations and with the perception of diabetic vascular complications as inflammation driven diseases [89, 124]. The current data indicate that endothelial dysfunction with impaired thrombomodulin protein C activation accelerates and perpetuates the

hyperglycaemia-induced vascular inflammation by unrestrained p66^{Shc}-mediated ROS-generation in macrophages.

Other mechanisms of increased ROS-generation have been linked with diabetes mellitus associated accelerated atherosclerosis [125]. Intriguingly, enhanced p66^{Shc} expression induces NADPH oxidase activity, while repressing manganese superoxide dismutase (MnSOD) expression, resulting in increased ROS-generation in peripheral blood monocytes [126]. Accordingly, enhanced p66^{Shc} expression may be a common pathomechanism inducing mitochondrial and other mechanisms of increased ROS-generation, thus generating a pro-inflammatory and pro-atherogenic micromilieu.

Mitochondrial dysfunction in bone marrow derived cells promotes unstable plaques [119]. Here we show that p66^{Shc} (a mitochondrial redox-regulator) promotes CD36 expression and lipid uptake in glucose-stimulated macrophages. As excess lipid uptake promotes cell death and thus the evolution of an unstable acellular – or necrotic – core, increased and perpetuated p66^{Shc} expression may contribute to the impaired plaque stability observed in diabetic patients [127].

While providing novel insights, the current study has potential limitations. We aimed to directly compare mice with hyperlipidaemia and hyperglycaemic associated atherosclerosis. However, due to the study design total plasma cholesterol levels and plasma HDL-levels were not comparable between groups. While a subgroup analyses of ApoE-/-DM and ApoE-/-HFD mice gave similar results, we cannot exclude an impact of different plasma levels of lipid species such as HDL cholesterol. Yet, we are confident that the observed changes largely reflect hyperglycaemia-dependent effects as the endpoints analysed (e.g. p66^{Shc} expression and its sequelae: ROS-generation, CD36, IL-6, TNFα-expression) were increased in the hyperglycaemic milieu compared to the hyperlipidaemic milieu despite lower total cholesterol levels in the hyperglycaemic milieu.

Of note, the mixed phenotype in diabetic ApoE-/- mice, characterized by hyperglycaemia and hyperlipidaemia, reflects the situation in diabetic patients, in which likewise both risk factors are increased. Accordingly, some consider the ApoE-/- streptozotocin model to be the most appropriate mouse model to study accelerated diabetes mellitus-associated atherosclerosis [126]. The recent clinical observation showing epigenetically sustained p66^{Shc} expression in diabetic patients [41] and the increased p66^{Shc} expression in atherosclerotic lesions from

diabetic as compared to non-diabetic patients in the current study supports the translational relevance of the model used.

Finally, the question arises how the current finding may be taken further. Approaches to directly target $p66^{Shc}$ may be appropriate in addition to exploiting aPC-based signalling. In the current study morpholinos targeting $p66^{Shc}$ efficiently restricted hyperglycaemia induced lesion development. Targeting morpholinos to relevant cell-types, e.g. macrophages, through a receptor-dependent mechanism, e.g. *via* CD36, may constitute an approach to enable a targeted therapy, thus avoiding unwanted site-effects. Alternatively, biased PAR-1 agonists may be suitable to restrict $p66^{Shc}$ expression in plaque macrophages. These questions need to be addressed in future studies.

6. Conclusion:

The major cause of mortality and morbidity among diabetic patients is atherosclerosis and its associated complications like myocardial infarction, stroke, and peripheral vascular disease. While the more aggressive disease progression of atherosclerosis in diabetic patients is established, the underlying mechanisms remain obscure, hampering specific therapeutic approaches to atherosclerosis in diabetic patients.

A hallmark of diabetes mellitus-associated atherosclerosis is the perpetuated disease progression despite marked improvement of blood glucose. The sustained disease progression despite improved blood glucose is known as the hyperglycaemic memory – a phenomenon that is equally disappointing and discouraging for patients and doctors.

We unravelled a new mechanism underlying the hyperglycaemic memory. We establish that in macrophages, inflammatory cells accumulating in the atherosclerotic plaques, more reactive oxygen species are generated as a consequence of increased expression of a redox regulator protein known as $p66^{Shc}$. Importantly, this $p66^{Shc}$ is specifically expressed in diabetic atherosclerotic lesions, but not in patients or mice without diabetes mellitus. Furthermore, despite normalization of blood glucose levels expression of $p66^{Shc}$ and hence generation of reactive oxygen species remained high. Mechanistically, aPC corrects glucose-induced CpG hypomethylation within the $p66^{Shc}$ promoter. *In vivo*, aPC – but not normalization of blood glucose levels – reverses in a DNMT1-dependent fashion $p66^{Shc}$ expression, ROS-generation, and IL-6 expression in plaques. Thus, the hyperglycaemic memory is linked with epigenetically sustained $p66^{Shc}$ expression in plaque-macrophages, which can be reversed by aPC. These findings suggest that reversal of the hyperglycaemic memory in diabetic atherosclerosis is feasible. These insights will lay ground to an individualized therapeutic concept for diabetic mellitus patients with atherosclerosis.

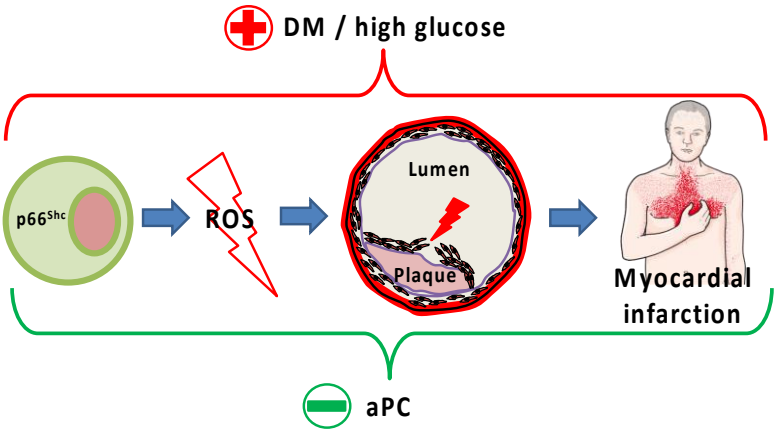

Figure 32: cytoprotective effect of aPC in DM and associated hyperglycemia

Diabetes mellitus (DM) and the associated hyperglycaemia cause an increase of the redox-protein p66Shc and reactive oxygen species (ROS) in macrophages, causing instable plaques, which predisposes diabetic patients to myocardial infarction. These effects are counteracted by the cytoprotective effects of the coagulation protease activated protein C (aPC).

7. Future Outlook

While providing new insights into the cytoprotective effects of aPC, the current study also raises questions.

1) We demonstrate that hyperglycaemia-induced and "memorised" (epigenetically sustained) $p66^{Shc}$ expression worsens diabetes mellitus associated accelerated atherosclerosis. However, whether **endothelial dysfunction** with impaired thrombomodulin protein C activation accelerates and perpetuates the hyperglycaemia-induced vascular inflammation by unrestrained $p66^{Shc}$-mediated ROS-generation remains to be evaluated using cell-specific approaches.
2) We demonstrate enhanced $p66^{Shc}$ expression impairs diabetes associated plaque stability. $p66^{Shc}$ is known to induce NADPH oxidase activity, while repressing manganese superoxide dismutase (MnSOD) expression in pheripheral blood monocytes. Whether enhanced $p66^{Shc}$ expression is a common pathomechanism inducing mitochondrial and other mechanisms of increased ROS-generation, thus generating a pro-inflammatory and pro-atherogenic micromilieu, remains unknown.
3) The mechanisms controlling $p66^{Shc}$ activation, e.g. the molecular signatures of the chromatin architectures (histone acetylation or methylation epigenetic modifications) that sensitize the genome to hyperglycaemic metabolites and whether other co-receptors (e.g. PAR3, Apolipoprotein E receptor 2 / LDL Receptor Related Protein 8, or integrin CD11b/CD18) in addition to PAR-1 are required for aPC- mediated $p66^{Shc}$ suppression, remain to be uncovered. Deciphering the specific co-receptors and signaling pathways involved may allow further optimization of a molecular targeted therapy to reverse hyperglycemia memory-induced plaque instability. Alternatively, biased PAR-1 agonists mimicking the effect of aPC may be suitable to restrict $p66^{Shc}$ expression in plaque macrophages. These questions need to be addressed in future studies.
4) ROS induced NLRP3 inflammasome activation has been linked with atherosclerosis and myocardial infarction. It is not known whether the hyperglycemia induced memorised $p66^{Shc}$ expression activates inflammasome activation and contributes to accelerated atherosclerosis.

The delineation of these questions is expected to provide novel insights into the relevance of $p66^{Shc}$ activation and its contribution to accelerated atherosclerosis.

8. References

1. Zheng, Y., S.H. Ley, and F.B. Hu, *Global aetiology and epidemiology of type 2 diabetes mellitus and its complications.* Nat Rev Endocrinol, 2018. **14**(2): p. 88-98.
2. Guerrero, B. and M. Lopez, *Global report on diabetes.* Invest Clin, 2016. **56**(4): p. 432-54.
3. Roglic, G. and World Health Organization, *Global report on diabetes*. 2016, Geneva, Switzerland: World Health Organization. 86 pages.
4. Danaei, G., et al., *National, regional, and global trends in fasting plasma glucose and diabetes prevalence since 1980: systematic analysis of health examination surveys and epidemiological studies with 370 country-years and 2.7 million participants.* Lancet, 2011. **378**(9785): p. 31-40.
5. Association, A.D., *Diagnosis and classification of diabetes mellitus.* Diabetes Care, 2014. **37 Suppl 1**: p. S81-90.
6. Craig, M.E., A. Hattersley, and K.C. Donaghue, *Definition, epidemiology and classification of diabetes in children and adolescents.* Pediatr Diabetes, 2009. **10 Suppl 12**: p. 3-12.
7. Giloyan, A., T. Harutyunyan, and V. Petrosyan, *The prevalence of and major risk factors associated with diabetic retinopathy in Gegharkunik province of Armenia: cross-sectional study.* BMC Ophthalmol, 2015. **15**: p. 46.
8. de Barros Pimentel Villaca, C., et al., *Beneficial effects of physical exercise for beta-cell maintenance in a Type 1 Diabetes mellitus animal model.* Exp Physiol, 2021.
9. Dabelea, D., et al., *Prevalence of type 1 and type 2 diabetes among children and adolescents from 2001 to 2009.* Jama, 2014. **311**(17): p. 1778-86.
10. Ginsberg, H., et al., *Demonstration of insulin resistance in untreated adult onset diabetic subjects with fasting hyperglycemia.* J Clin Invest, 1975. **55**(3): p. 454-61.
11. Halban, P.A., et al., *beta-cell failure in type 2 diabetes: postulated mechanisms and prospects for prevention and treatment.* Diabetes Care, 2014. **37**(6): p. 1751-8.
12. Druet, C., et al., *Characterization of insulin secretion and resistance in type 2 diabetes of adolescents.* J Clin Endocrinol Metab, 2006. **91**(2): p. 401-4.
13. Buse, J.B., et al., *2019 Update to: Management of Hyperglycemia in Type 2 Diabetes, 2018. A Consensus Report by the American Diabetes Association (ADA) and the European Association for the Study of Diabetes (EASD).* Diabetes Care, 2020. **43**(2): p. 487-493.
14. Kaludercic, N. and F. Di Lisa, *Mitochondrial ROS Formation in the Pathogenesis of Diabetic Cardiomyopathy.* Front Cardiovasc Med, 2020. **7**: p. 12.
15. Shyr, Z.A., et al., *The role of membrane excitability in pancreatic beta-cell glucotoxicity.* Sci Rep, 2019. **9**(1): p. 6952.
16. Virani, S.S., et al., *Heart Disease and Stroke Statistics-2020 Update: A Report From the American Heart Association.* Circulation, 2020. **141**(9): p. e139-e596.
17. Ritchie, H., et al., *Causes of Death.* Our World in Data, 2018. **130**(24): p. 2664-2677.
18. Benjamin, E.J., et al., *Heart Disease and Stroke Statistics-2017 Update: A Report From the American Heart Association.* Circulation, 2017. **135**(10): p. e146-e603.
19. Alvarez, C.A., et al., *Cardiovascular Risk in Diabetes Mellitus: Complication of the Disease or of Antihyperglycemic Medications.* Clin Pharmacol Ther, 2015. **98**(2): p. 145-61.

20. Thomas, H., et al., *Global Atlas of Cardiovascular Disease 2000-2016: The Path to Prevention and Control.* Glob Heart, 2018. **13**(3): p. 143-163.
21. Torres, N., et al., *Nutrition and Atherosclerosis.* Arch Med Res, 2015. **46**(5): p. 408-26.
22. Badimon, L., G. Vilahur, and T. Padro, *Lipoproteins, platelets and atherothrombosis.* Rev Esp Cardiol, 2009. **62**(10): p. 1161-78.
23. Hellings, W.E., et al., *Composition of carotid atherosclerotic plaque is associated with cardiovascular outcome: a prognostic study.* Circulation, 2010. **121**(17): p. 1941-50.
24. Stary, H.C., et al., *A definition of advanced types of atherosclerotic lesions and a histological classification of atherosclerosis. A report from the Committee on Vascular Lesions of the Council on Arteriosclerosis, American Heart Association.* Circulation, 1995. **92**(5): p. 1355-74.
25. Stary, H.C., et al., *A definition of initial, fatty streak, and intermediate lesions of atherosclerosis. A report from the Committee on Vascular Lesions of the Council on Arteriosclerosis, American Heart Association.* Circulation, 1994. **89**(5): p. 2462-78.
26. Yusuf, S., et al., *Global burden of cardiovascular diseases: part I: general considerations, the epidemiologic transition, risk factors, and impact of urbanization.* Circulation, 2001. **104**(22): p. 2746-53.
27. de Ferranti, S.D., et al., *Type 1 diabetes mellitus and cardiovascular disease: a scientific statement from the American Heart Association and American Diabetes Association.* Diabetes Care, 2014. **37**(10): p. 2843-63.
28. Greaves, D.R. and S. Gordon, *Thematic review series: the immune system and atherogenesis. Recent insights into the biology of macrophage scavenger receptors.* J Lipid Res, 2005. **46**(1): p. 11-20.
29. Prabhudas, M., et al., *Standardizing scavenger receptor nomenclature.* J Immunol, 2014. **192**(5): p. 1997-2006.
30. Glass, C.K. and J.L. Witztum, *Atherosclerosis. the road ahead.* Cell, 2001. **104**(4): p. 503-16.
31. Lane, A., et al., *Cytokine production by cholesterol-loaded human peripheral monocyte- macrophages: the effect on fibrinogen mRNA levels in a hepatoma cell-line (HepG2).* Biochim Biophys Acta, 1991. **1097**(3): p. 161-5.
32. Bebu, I., et al., *Mediation of the Effect of Glycemia on the Risk of CVD Outcomes in Type 1 Diabetes: The DCCT/EDIC Study.* Diabetes Care, 2019. **42**(7): p. 1284-1289.
33. Bebu, I., et al., *The relationship of blood glucose with cardiovascular disease is mediated over time by traditional risk factors in type 1 diabetes: the DCCT/EDIC study.* Diabetologia, 2017. **60**(10): p. 2084-2091.
34. Patel, A., et al., *Intensive blood glucose control and vascular outcomes in patients with type 2 diabetes.* N Engl J Med, 2008. **358**(24): p. 2560-72.
35. Peng, W., et al., *Mitochondrial Dysfunction in Atherosclerosis.* DNA Cell Biol, 2019. **38**(7): p. 597-606.
36. Giorgio, M., et al., *Electron transfer between cytochrome c and p66Shc generates reactive oxygen species that trigger mitochondrial apoptosis.* Cell, 2005. **122**(2): p. 221-33.
37. Gertz, M. and C. Steegborn, *The Lifespan-regulator p66Shc in mitochondria: redox enzyme or redox sensor?* Antioxid Redox Signal, 2010. **13**(9): p. 1417-28.
38. Paneni, F., et al., *Gene silencing of the mitochondrial adaptor p66(Shc) suppresses vascular hyperglycemic memory in diabetes.* Circ Res, 2012. **111**(3): p. 278-89.

39. Bock, F., et al., *Activated protein C ameliorates diabetic nephropathy by epigenetically inhibiting the redox enzyme p66Shc.* Proc Natl Acad Sci U S A, 2013. **110**(2): p. 648-53.
40. Xi, G., et al., *Hyperglycemia-induced p66shc inhibits insulin-like growth factor I-dependent cell survival via impairment of Src kinase-mediated phosphoinositide-3 kinase/AKT activation in vascular smooth muscle cells.* Endocrinology, 2010. **151**(8): p. 3611-23.
41. Costantino, S., et al., *Impact of Glycemic Variability on Chromatin Remodeling, Oxidative Stress, and Endothelial Dysfunction in Patients With Type 2 Diabetes and With Target HbA1c Levels.* Diabetes, 2017. **66**(9): p. 2472-2482.
42. Loeffen, R., H.M. Spronk, and H. ten Cate, *The impact of blood coagulability on atherosclerosis and cardiovascular disease.* J Thromb Haemost, 2012. **10**(7): p. 1207-16.
43. Crawley, J., et al., *Expression, localization, and activity of tissue factor pathway inhibitor in normal and atherosclerotic human vessels.* Arterioscler Thromb Vasc Biol, 2000. **20**(5): p. 1362-73.
44. Seehaus, S., et al., *Hypercoagulability inhibits monocyte transendothelial migration through protease-activated receptor-1-, phospholipase-Cbeta-, phosphoinositide 3-kinase-, and nitric oxide-dependent signaling in monocytes and promotes plaque stability.* Circulation, 2009. **120**(9): p. 774-84.
45. ten Cate, H., *Tissue factor-driven thrombin generation and inflammation in atherosclerosis.* Thromb Res, 2012. **129 Suppl 2**: p. S38-40.
46. Posthuma, J.J., et al., *Targeting Coagulation Factor Xa Promotes Regression of Advanced Atherosclerosis in Apolipoprotein-E Deficient Mice.* Sci Rep, 2019. **9**(1): p. 3909.
47. Bea, F., et al., *Melagatran reduces advanced atherosclerotic lesion size and may promote plaque stability in apolipoprotein E-deficient mice.* Arterioscler Thromb Vasc Biol, 2006. **26**(12): p. 2787-92.
48. Achneck, H.E., et al., *Pathophysiology of bleeding and clotting in the cardiac surgery patient: from vascular endothelium to circulatory assist device surface.* Circulation, 2010. **122**(20): p. 2068-77.
49. Dahlback, B., *Vitamin K-Dependent Protein S: Beyond the Protein C Pathway.* Semin Thromb Hemost, 2018. **44**(2): p. 176-184.
50. Krupinski, J., et al., *Increased tissue factor, MMP-8, and D-dimer expression in diabetic patients with unstable advanced carotid atherosclerosis.* Vasc Health Risk Manag, 2007. **3**(4): p. 405-12.
51. Lipinski, B., *Pathophysiology of oxidative stress in diabetes mellitus.* J Diabetes Complications, 2001. **15**(4): p. 203-10.
52. Corti, R., et al., *Evolving concepts in the triad of atherosclerosis, inflammation and thrombosis.* J Thromb Thrombolysis, 2004. **17**(1): p. 35-44.
53. Testa, L., et al., *Re: early decrease in coagulation activity after myocardial infarction is associated with lower risk of new ischaemic events: observations from the ESTEEM trial.* Eur Heart J, 2007. **28**(14): p. 1782-3; author reply 1783.
54. Dockendorff, C., et al., *Discovery of 1,3-Diaminobenzenes as Selective Inhibitors of Platelet Activation at the PAR1 Receptor.* ACS Med Chem Lett, 2012. **3**(3): p. 232-237.

55. Atar, D., et al., *Anticoagulants for secondary prevention after acute myocardial infarction: lessons from the past decade.* Fundam Clin Pharmacol, 2014. **28**(4): p. 353-63.
56. Cavender, M.A., et al., *The effect of rivaroxaban on myocardial infarction in the ATLAS ACS 2 - TIMI 51 trial.* Eur Heart J Acute Cardiovasc Care, 2015. **4**(5): p. 468-74.
57. Van de Wouwer, M., D. Collen, and E.M. Conway, *Thrombomodulin-protein C-EPCR system: integrated to regulate coagulation and inflammation.* Arterioscler Thromb Vasc Biol, 2004. **24**(8): p. 1374-83.
58. Esmon, C.T., *Coagulation and inflammation.* J Endotoxin Res, 2003. **9**(3): p. 192-8.
59. Esmon, C.T., *Inflammation and the activated protein C anticoagulant pathway.* Semin Thromb Hemost, 2006. **32 Suppl 1**: p. 49-60.
60. Stearns-Kurosawa, D.J., et al., *The endothelial cell protein C receptor augments protein C activation by the thrombin-thrombomodulin complex.* Proc Natl Acad Sci U S A, 1996. **93**(19): p. 10212-6.
61. Esmon, C.T., *Structure and functions of the endothelial cell protein C receptor.* Crit Care Med, 2004. **32**(5 Suppl): p. S298-301.
62. Taylor, F.B., Jr., et al., *Endothelial cell protein C receptor plays an important role in protein C activation in vivo.* Blood, 2001. **97**(6): p. 1685-8.
63. Griffin, J.H., B.V. Zlokovic, and L.O. Mosnier, *Activated protein C: biased for translation.* Blood, 2015. **125**(19): p. 2898-907.
64. Griffin, J.H., B.V. Zlokovic, and L.O. Mosnier, *Protein C anticoagulant and cytoprotective pathways.* Int J Hematol, 2012. **95**(4): p. 333-45.
65. Shahzad, K., et al., *Cell biology of activated protein C.* Curr Opin Hematol, 2019. **26**(1): p. 41-50.
66. Griffin, J.H., B.V. Zlokovic, and L.O. Mosnier, *Activated protein C, protease activated receptor 1, and neuroprotection.* Blood, 2018. **132**(2): p. 159-169.
67. Bock, F., et al., *Activated protein C based therapeutic strategies in chronic diseases.* Thromb Haemost, 2014. **111**(4): p. 610-7.
68. Lattenist, L., et al., *Activated protein C protects against renal ischaemia/reperfusion injury, independent of its anticoagulant properties.* Thromb Haemost, 2016. **116**(1): p. 124-33.
69. Neyrinck, A.P., et al., *Protective mechanisms of activated protein C in severe inflammatory disorders.* Br J Pharmacol, 2009. **158**(4): p. 1034-47.
70. Isermann, B., et al., *Activated protein C protects against diabetic nephropathy by inhibiting endothelial and podocyte apoptosis.* Nat Med, 2007. **13**(11): p. 1349-58.
71. Ranjan, S., et al., *Activated protein C protects from GvHD via PAR2/PAR3 signalling in regulatory T-cells.* Nat Commun, 2017. **8**(1): p. 311.
72. Shahzad, K. and B. Isermann, *The evolving plasticity of coagulation protease-dependent cytoprotective signalling.* Hamostaseologie, 2011. **31**(3): p. 179-84.
73. Laszik, Z.G., et al., *Down-regulation of endothelial expression of endothelial cell protein C receptor and thrombomodulin in coronary atherosclerosis.* Am J Pathol, 2001. **159**(3): p. 797-802.
74. Zorio, E., et al., *Circulating activated protein C is reduced in young survivors of myocardial infarction and inversely correlates with the severity of coronary lesions.* J Thromb Haemost, 2006. **4**(7): p. 1530-6.

75. Zorio, E., et al., *Thrombin-activatable fibrinolysis inhibitor in young patients with myocardial infarction and its relationship with the fibrinolytic function and the protein C system.* Br J Haematol, 2003. **122**(6): p. 958-65.
76. Fellner, B., et al., *Activated protein C levels and outcome in patients with cardiogenic shock complicating acute myocardial infarction.* Eur Heart J Acute Cardiovasc Care, 2017. **6**(4): p. 348-358.
77. Zhao, R., et al., *Activated Protein C in Cutaneous Wound Healing: From Bench to Bedside.* Int J Mol Sci, 2019. **20**(4).
78. Yamashita, A., et al., *C-terminal residues of activated protein C light chain contribute to its anticoagulant and cytoprotective activities.* J Thromb Haemost, 2020. **18**(5): p. 1027-1038.
79. Adams, M.N., et al., *Structure, function and pathophysiology of protease activated receptors.* Pharmacol Ther, 2011. **130**(3): p. 248-82.
80. Heuberger, D.M. and R.A. Schuepbach, *Correction to: protease-activated receptors (PARs): mechanisms of action and potential therapeutic modulators in PAR-driven inflammatory diseases.* Thromb J, 2019. **17**: p. 22.
81. Nieman, M.T., *Protease-activated receptors in hemostasis.* Blood, 2016. **128**(2): p. 169-77.
82. Coughlin, S.R., *Thrombin signalling and protease-activated receptors.* Nature, 2000. **407**(6801): p. 258-64.
83. Gieseler, F., et al., *Proteinase-activated receptors (PARs) - focus on receptor-receptor-interactions and their physiological and pathophysiological impact.* Cell Commun Signal, 2013. **11**: p. 86.
84. Gerszten, R.E., et al., *Specificity of the thrombin receptor for agonist peptide is defined by its extracellular surface.* Nature, 1994. **368**(6472): p. 648-51.
85. Ruf, W., *Proteases, Protease-Activated Receptors, and Atherosclerosis.* Arterioscler Thromb Vasc Biol, 2018. **38**(6): p. 1252-1254.
86. Shahzad, K., et al., *Nlrp3-inflammasome activation in non-myeloid-derived cells aggravates diabetic nephropathy.* Kidney Int, 2015. **87**(1): p. 74-84.
87. Feig, J.E. and E.A. Fisher, *Laser capture microdissection for analysis of macrophage gene expression from atherosclerotic lesions.* Methods Mol Biol, 2013. **1027**: p. 123-35.
88. Gadi, I., et al., *Different DOACs Control Inflammation in Cardiac Ischemia-Reperfusion Differently.* Circ Res, 2021. **128**(4): p. 513-529.
89. Shahzad, K., et al., *Caspase-1, but Not Caspase-3, Promotes Diabetic Nephropathy.* J Am Soc Nephrol, 2016. **27**(8): p. 2270-5.
90. Isermann, B., et al., *Autoantibodies in diabetes mellitus: current utility and perspectives.* Exp Clin Endocrinol Diabetes, 2007. **115**(8): p. 483-90.
91. Shahzad, K., et al., *Minocycline reduces plaque size in diet induced atherosclerosis via p27(Kip1).* Atherosclerosis, 2011. **219**(1): p. 74-83.
92. Lima-Junior, D.S., et al., *Inflammasome-derived IL-1beta production induces nitric oxide-mediated resistance to Leishmania.* Nat Med, 2013. **19**(7): p. 909-15.
93. Marim, F.M., et al., *A method for generation of bone marrow-derived macrophages from cryopreserved mouse bone marrow cells.* PLoS One, 2010. **5**(12): p. e15263.
94. Madhusudhan, T., et al., *Defective podocyte insulin signalling through p85-XBP1 promotes ATF6-dependent maladaptive ER-stress response in diabetic nephropathy.* Nat Commun, 2015. **6**: p. 6496.

95. Dong, W., et al., *Activated Protein C Ameliorates Renal Ischemia-Reperfusion Injury by Restricting Y-Box Binding Protein-1 Ubiquitination.* J Am Soc Nephrol, 2015. **26**(11): p. 2789-99.
96. *Report of the Expert Committee on the Diagnosis and Classification of Diabetes Mellitus.* Diabetes Care, 1997. **20**(7): p. 1183-97.
97. Association, A.D., *Report of the expert committee on the diagnosis and classification of diabetes mellitus.* Diabetes Care, 2003. **26 Suppl 1**: p. S5-20.
98. Li, W., et al., *Decreased activated protein C levels are inversely associated with the urinary albumin excretion rate in patients with type 2 diabetes.* Clin Lab, 2014. **60**(2): p. 261-6.
99. Matsumoto, K., et al., *Inverse correlation between activated protein C generation and carotid atherosclerosis in Type 2 diabetic patients.* Diabet Med, 2007. **24**(12): p. 1322-8.
100. Vukovich, T.C. and G. Schernthaner, *Decreased protein C levels in patients with insulin-dependent type I diabetes mellitus.* Diabetes, 1986. **35**(5): p. 617-9.
101. Gil-Bernabe, P., et al., *Exogenous activated protein C inhibits the progression of diabetic nephropathy.* J Thromb Haemost, 2012. **10**(3): p. 337-46.
102. Madhusudhan, T., et al., *Signal integration at the PI3K-p85-XBP1 hub endows coagulation protease activated protein C with insulin-like function.* Blood, 2017. **130**(12): p. 1445-1455.
103. Aisiku, O., et al., *Parmodulins inhibit thrombus formation without inducing endothelial injury caused by vorapaxar.* Blood, 2015. **125**(12): p. 1976-85.
104. Yamaji, K., et al., *Activated protein C, a natural anticoagulant protein, has antioxidant properties and inhibits lipid peroxidation and advanced glycation end products formation.* Thromb Res, 2005. **115**(4): p. 319-25.
105. Bornfeldt, K.E., *Uncomplicating the Macrovascular Complications of Diabetes: The 2014 Edwin Bierman Award Lecture.* Diabetes, 2015. **64**(8): p. 2689-97.
106. Martinez-Hervas, S., et al., *Insulin resistance aggravates atherosclerosis by reducing vascular smooth muscle cell survival and increasing CX3CL1/CX3CR1 axis.* Cardiovasc Res, 2014. **103**(2): p. 324-36.
107. Bornfeldt, K.E. and I. Tabas, *Insulin resistance, hyperglycemia, and atherosclerosis.* Cell Metab, 2011. **14**(5): p. 575-85.
108. Costantino, S., et al., *Interplay among H3K9-editing enzymes SUV39H1, JMJD2C and SRC-1 drives p66Shc transcription and vascular oxidative stress in obesity.* Eur Heart J, 2019. **40**(4): p. 383-391.
109. Macaluso, M., et al., *pRb2/p130-E2F4/5-HDAC1-SUV39H1-p300 and pRb2/p130-E2F4/5-HDAC1-SUV39H1-DNMT1 multimolecular complexes mediate the transcription of estrogen receptor-alpha in breast cancer.* Oncogene, 2003. **22**(23): p. 3511-7.
110. Costantino, S., et al., *Epigenetics and precision medicine in cardiovascular patients: from basic concepts to the clinical arena.* Eur Heart J, 2018. **39**(47): p. 4150-4158.
111. Bolzan, A.D. and M.S. Bianchi, *Genotoxicity of streptozotocin.* Mutat Res, 2002. **512**(2-3): p. 121-34.
112. Bekkering, S., et al., *Trained innate immunity and atherosclerosis.* Curr Opin Lipidol, 2013. **24**(6): p. 487-92.
113. Netea, M.G., et al., *Trained immunity: A program of innate immune memory in health and disease.* Science, 2016. **352**(6284): p. aaf1098.

114. Kong, L., et al., *PKCbeta promotes vascular inflammation and acceleration of atherosclerosis in diabetic ApoE null mice.* Arterioscler Thromb Vasc Biol, 2013. **33**(8): p. 1779-87.
115. Nagareddy, P.R., et al., *Hyperglycemia promotes myelopoiesis and impairs the resolution of atherosclerosis.* Cell Metab, 2013. **17**(5): p. 695-708.
116. Devaraj, S., et al., *Increased toll-like receptor (TLR) 2 and TLR4 expression in monocytes from patients with type 1 diabetes: further evidence of a proinflammatory state.* J Clin Endocrinol Metab, 2008. **93**(2): p. 578-83.
117. Camici, G.G., et al., *Genetic deletion of p66(Shc) adaptor protein prevents hyperglycemia- induced endothelial dysfunction and oxidative stress.* Proc Natl Acad Sci U S A, 2007. **104**(12): p. 5217-22.
118. Bornfeldt, K.E., *2013 Russell Ross memorial lecture in vascular biology: cellular and molecular mechanisms of diabetes mellitus-accelerated atherosclerosis.* Arterioscler Thromb Vasc Biol, 2014. **34**(4): p. 705-14.
119. Yu, E., et al., *Mitochondrial DNA damage can promote atherosclerosis independently of reactive oxygen species through effects on smooth muscle cells and monocytes and correlates with higher-risk plaques in humans.* Circulation, 2013. **128**(7): p. 702-12.
120. Zhou, S., et al., *Repression of P66Shc expression by SIRT1 contributes to the prevention of hyperglycemia-induced endothelial dysfunction.* Circ Res, 2011. **109**(6): p. 639-48.
121. Gorbacheva, L., et al., *Activated protein C prevents glutamate- and thrombin-induced activation of nuclear factor-kappaB in cultured hippocampal neurons.* Neuroscience, 2010. **165**(4): p. 1138-46.
122. Joyce, D.E., et al., *Gene expression profile of antithrombotic protein c defines new mechanisms modulating inflammation and apoptosis.* J Biol Chem, 2001. **276**(14): p. 11199-203.
123. Pollack, R.M., et al., *Anti-inflammatory Agents in the Treatment of Diabetes and Its Vascular Complications.* Diabetes Care, 2016. **39 Suppl 2**: p. S244-52.
124. Gray, S.P., et al., *NADPH oxidase 1 plays a key role in diabetes mellitus-accelerated atherosclerosis.* Circulation, 2013. **127**(18): p. 1888-902.
125. Paneni, F., et al., *Reprogramming ageing and longevity genes restores paracrine angiogenic properties of early outgrowth cells.* Eur Heart J, 2016. **37**(22): p. 1733-7.
126. Hsueh, W., et al., *Recipes for creating animal models of diabetic cardiovascular disease.* Circ Res, 2007. **100**(10): p. 1415-27.
127. Zeadin, M.G., C.I. Petlura, and G.H. Werstuck, *Molecular mechanisms linking diabetes to the accelerated development of atherosclerosis.* Can J Diabetes, 2013. **37**(5): p. 345-50.

9. Acknowledgement

In the name of God, who gives me the patience and potency in this life, who sends me very special and supportive people, all praises to you.

I express my sincere gratitude to my supervisor Prof. Dr. Berend Isermann for his continuous valuable support, guidance and encouragement during my Ph.D. study and related research. Without his moral support I would not have been able to finish this work. Thank you very much, Prof. Dr. Berend Isermann, I learnt more from you in the past 5 years than all my years of being in this field.

My special mention goes to Dr. Khurrum Shahzad for generous support, guidance and helpful suggestions during my research work all the times in the lab. Without his support, accomplishment of this work would not have been possible. Thank you to Dr. Shahzad who made it easier for me.

I am also very grateful to my colleagues for support, nice discussions and accompanying me during this time. I am thankful to Shrey kohly, Aldabet, Ahmad El-Wakiel, Jayakumar Manoharan, Rajiv Rana, Dheerendra Gupta, Shruthi Krishnan, Akash Mathew, Silke Zimmerman, Ronald Biemann, Anubhuti Gupta, Sameen Fatima, Hamzah Khawajah and Saira Ambreen.

Alongside I would like to extend my thanks for technical support to Ms. Kathrin Deneser, Julia Judine, Mr. Rene Rudat, Susann Lautenschläger, Silvana Müller, Rumiya Makarova, Lauf Johannis. Thanks for being with me behind my success and reaching this work in final shape.

Lastly, but no means the least, I am particularly indebted to Mom and Dad as well as my parents in Laws. A huge and special gratitude goes to my parents, who waited to see this day. You are the most valuable people in this world, without your prayers and blessings I would not reach here. I am also thankful to my brothers and sisters for continuous support throughout my life.

My beloved wife Saima, no words can reward you. You inspired me with the strength, with your supportive smile, warm words and true belief. Without your support, it would never have been possible to accomplish this. You lost your mom during this time. May Allah bless her soul in heaven. Through thick and thin, you gave me love and support. My adorable little Sons, Aizaz and Amr, I am pleased to be your father; I dedicate this work to my family.

10. Declaration

Ich erkläre, dass ich die der Medizinischen Fakultät der Otto-von-Guericke-Universität zur Promotion eingereichte Dissertation mit dem Titel

Activated protein C reverses epigenetically sustained p66^{Shc} expression in plaque-associated macrophages in diabetes.

im Institut für Klinische Chemie und Pathobiochemie der Medizinischen Fakultät der Otto-von-Guericke-Universität Magdeburg

mit Unterstützung durch Prof. Dr. med. Berend Isermann

ohne sonstige Hilfe durchgeführt und bei der Abfassung der Dissertation keine anderen, als die dort aufgeführten Hilfsmittel benutzt habe.

Bei der Abfassung der Dissertation sind Rechte Dritter nicht verletzt worden.

Ich habe diese Dissertation bisher an keiner in- und ausländischen Hochschule zur Promotion eingereicht. Ich übertrage der Medizinischen Fakultät das Recht, weitere Kopien meiner Dissertation herzustellen und zu vertreiben.

Leipzig, den 06.05.2021

Ihsan Gadi

11. List of publications

1. **Gadi I***, Fatima S*, Elwakiel A, Nazir S, Mohanad Al-Dabet M, Rana R, Bock F, Manoharan J, Gupta D, Biemann R, Nieswandt B, Braun-Dullaeus R, Besler C, Scholz M, Geffers R, Griffin JH, Esmon CT, Kohli S, Isermann B, Shahzad K. Different DOACs Control Inflammation in Cardiac Ischemia-Reperfusion Differently. Circ Res. 2021 Feb 19;128(4):513-529. PMID: 33353373. (* equal contribution) **IF: 15.86**

2. Madhusudhan T, Ghosh S, Wang H, Dong W, Gupta D, Elwakiel A, Stoyanov S, Al- Dabet MM, Krishnan S, Biemann R, Nazir S, Zimmermann S, Mathew A, **Gadi I**, Rana R, Zeng-Brouwers J, Moeller MJ, Schaefer L, Esmon CT, Kohli S, Reiser J, Rezaie AR, Ruf W, Isermann B. Podocyte Integrin-β 3 and Activated Protein C Coordinately Restrict RhoA Signaling and Ameliorate Diabetic Nephropathy. J Am Soc Nephrol. 2020 Aug;31(8):1762-1780 PMID: 32709711 **IF: 9.27**

3. Shahzad K*, **Gadi I***, Nazir S, Al-Dabet MM, Kohli S, Bock F, Breitenstein L, Ranjan S, Fuchs T, Halloul Z, Nawroth PP, Pelicci PG, Braun-Dullaeus RC, Camerer E, Esmon CT, Isermann B. Activated protein C reverses epigenetically sustained $p66^{Shc}$ expression in plaque-associated macrophages in diabetes. Commun Biol. 2018 Aug 6;1:104. doi: 10.1038/s42003-018-0108-5. PMID: 30271984. (* equal contribution) **IF: 4.04**

4. Nazir S, **Gadi I**, Al-Dabet MM, Elwakiel A, Kohli S, Ghosh S, Manoharan J, Ranjan S, Bock F, Braun-Dullaeus RC, Esmon CT, Huber TB, Camerer E, Dockendorff C, Griffin JH, Isermann B, Shahzad K. Cytoprotective activated protein C averts Nlrp3 inflammasome-induced ischemia-reperfusion injury via mTORC1 inhibition. Blood. 2017 Dec 14;130(24):2664-2677. PMID: 28882883. **IF: 17.54**

5. Ranjan S, Goihl A, Kohli S, **Gadi I**, Pierau M, Shahzad K, Gupta D, Bock F, Wang H, Shaikh H, Kähne T, Reinhold D, Bank U, Zenclussen AC, Niemz J, Schnöder TM, Brunner-Weinzierl M, Fischer T, Kalinski T, Schraven B, Luft T, Huehn J, Naumann M, Heidel FH, Isermann B. Activated protein C protects from GvHD via PAR2/PAR3 signalling in regulatory T-cells. Nat Commun. 2017 Aug 21;8(1):311. PMID: 28827518. **IF: 12.12**

6. Marquardt A, Al-Dabet MM, Ghosh S, Kohli S, Manoharan J, ElWakiel A, **Gadi I**, Bock F, Nazir S, Wang H, Lindquist JA, Nawroth PP, Madhusudhan T, Mertens PR, Shahzad K, Isermann B. Farnesoid X Receptor Agonism Protects against Diabetic Tubulopathy: Potential Add-On Therapy for Diabetic Nephropathy. J Am Soc Nephrol. 2017 Nov;28(11):3182-3189. PMID: 28696246. **IF: 9.27**

7. Kohli S, Hoffmann J, Lochmann F, Markmeyer P, Huebner H, Fahlbusch FB, Al- Dabet MM, **Gadi I**, Manoharan J, Löttge M, Zenclussen AC, Aharon A, Brenner B, Shahzad K, Ruebner M, Isermann B. p45 NF-E2 regulates syncytiotrophoblast differentiation by post-translational GCM1 modifications in human intrauterine growth restriction. Cell Death Dis. 2017 Apr 6;8(4):e2730. PMID: 28383551. **IF: 10.71**

8. Shahzad K, Bock F, Al-Dabet MM, **Gadi I**, Nazir S, Wang H, Kohli S, Ranjan S, Mertens PR, Nawroth PP, Isermann B. Stabilization of endogenous Nrf2 by minocycline protects against Nlrp3-inflammasome induced diabetic nephropathy. Sci Rep. 2016 Oct 10;6:34228. PMID: 27721446. **IF: 4.0**

9. Shahzad K, Bock F, Al-Dabet MM, **Gadi I**, Kohli S, Nazir S, Ghosh S, Ranjan S, Wang H, Madhusudhan T, Nawroth PP, Isermann B. Caspase-1, but Not Caspase-3, Promotes Diabetic Nephropathy. J Am Soc Nephrol. 2016 Aug;27(8):2270-5. PMID: 26832955. **IF: 9.27**